The Impact of Inhomogeneity on the Analysis of Cosmological Data

Alnadhief Hamed Ahmed Alfedeel
Supervisor: Charles Hellaby

Thesis Presented for the Degree of
DOCTOR OF PHILOSOPHY
in the Department of Applied Mathematics
UNIVERSITY OF CAPE TOWN

May 13, 2013

Abstract

We consider the Lemaître metric, which is the inhomogeneous, spherically symmetric metric, containing a non-static, comoving, perfect fluid with non-zero pressure. We use it to generalise the metric of the cosmos algorithm, first derived for the zero-pressure Lemaître-Tolman (LT) metric, to the case of non-zero pressure and non-zero cosmological constant. We present a method of integration with respect to the null coordinate w, instead of comoving t, and reduce the Einstein's Field Equation (EFEs) to a system of differential equations (DEs). We show that the non-zero pressure introduces new functions, and makes several functions depend on time that did not in the case of LT. We present clearly, step by step an algorithmic solution for determining the metric of the cosmos from cosmological data for the Lemaître model, on which a numerical implementation can be based.

In our numerical execution of the algorithm we have shown that there are some regions which need special treatment : the origin and the maximum in the diameter distance. We have coded a set of MATLAB programs for the numerical implementation of this algorithm, for the case of pressure with a barotropic equation of state and non-zero Λ. Initially, the computer code has been successfully tested using artificial and ideal cosmological data on the observer's past null cone, for homogeneous and non-homogeneous spacetimes. Then the program has also been generalized to handle realistic data, which has statistical fluctuations. A key step is the data smoothing process, which fits a smooth curve to discrete data with statistical fluctuations, so that the integration of the DEs can proceed. Since the algorithm is very sensitive to the second derivative of one of the data functions, this has required some experimentation with methods. Finally, we have successfully extracted the metric functions for the Lemaître model, and their evolution from the initial data on the past null cone.

Acknowledgements

I would like to take this chance and express my grateful and thanks to my supervisor Charles W. Hellaby who was very supportive in many occasions beyond the academic area. Hence, this work would not have been seen the light without his guidance and valuable suggestions towards completing my postgraduate studies.

I also extend my thanks to my wife Sonia Abdelfatah Babeker Ahmed for standing behind me during the time of my study, and for her unlimited patience when sometimes i come home late. I do not forget that she looked after our lovely Baby Ahmed so that an extra of love, thanks and grateful goes to here. I also thanks my father, mother, sisters and brothers whom I almost left for seven years.

I also thanks the DAAD, the University of Cape Town (UCT), and the African Institute for Mathematical Sciences (AIMS) for their financial support during my post graduate studies.

Contents

List of Figures

Chapter 1

Introduction

Cosmology is the study of the structure, formation and evolution of the universe that we live in. In order to come up with a model that describes the cosmic dynamics and has good agreement with its observations, we need a working theoretical framework and some assumptions or principles. Many assumptions and models have been considered for describing the universe [78]. For instance, according to the ancient Indian overview the universe is assumed to be infinite and heterogeneous in space and time. The ancient Greek (Ptolemaic) view also states that the earth is the center of the universe. These ancient cosmologies reflect the unstoppable human attempt to understand the universe, but most of them did not gain scientific attention, because they were based on philosophical thought instead of a physical framework. Even more, they did not meet any kind of observational tests.

In the modern age, in contrast, we prefer the Copernican Principle, which asserts that the earth is not the center of the universe, nor is it in a special or unique location. A much stronger statement is the Cosmological Principle (CP), which states that the universe looks (almost) the same when viewed by an observer in any location. Consequently the universe looks homogeneous and isotropic, at least on the very large scale.

In the year 1916, Einstein discovered the revolutionary theory of General Relativity (GR) which is now regarded as the best candidate for describing the force of gravity [40, 71]. In his theory, the source of gravity was interpreted as an interaction between the matter content of the universe and its geometry, i.e, the matter in the universe makes the spacetime curved and the curvature tells the matter how to move. In the beginning Einstein, like many in his day, was assuming that the universe is static, thus he modified his theory by adding the Cosmological constant to his equations, to permit a static solution for the universe. The cosmological constant acts like a global repulsion, or like matter with negative pressure equal to its density. Beyond doubt, GR has proved useful because it has successfully passed a number of observational tests [12, 48, 73, 80, 94].

A Few years later Edwin Hubble and Milton Humason discovered that the universe is expanding, through the analysis of the redshift, or "Doppler effect", of receding galaxies [42], meaning the universe is not static. Therefore the cosmological constant was not actually needed. Although Einstein considered the cosmological constant his greatest mistake, it has become, 80 years later, a central component of the current "standard model". That model interprets the dimming of the supernovae as evidence for acceleration of the cosmic expansion.

Since GR is a geometrical theory, and the Einstein field equations (EFEs) are a set of 10 partial differential equations which cannot be solved as is, without making strong assumptions, hence, Friedman [29, 30], Lemaître [56], Robertson [77] and Walker [93] (FLRW) solved the EFEs by considering that the matter content of the universe is homogeneously and isotropically distributed. They obtained the fundamental Cosmological model of today — the FLRW model. Since then, the Cosmological Principle has played a major role in the development of the modern theory of cosmology. The FLRW model is a spatially homogeneous and isotropic exact solution of the EFEs for a perfect fluid, and its metric (which is the distance between two events in the spacetime) is characterized by two variables; the scale factor which is a time dependent function that measures the expansion of the universe, and the curvature constant k which takes the values $0, -1$ and 1 indicating flat, negative, and positive curvature respectively of the 3-dimensional spatial sections. The value of k also controls the time evolution of the expansion, so it has both a dynamic and a geometric role. However, exact homogeneity cannot account for all the stars, galaxies, galaxy clusters, etc we observe. Hence the FLRW model must be complemented with a theory of structure formation. These include linear perturbation theory, N-body Newtonian simulations, and studies of exact inhomogeneous solutions of the EFEs.

1.1 The Homogeneous Model

The FLRW model forms the core of our present understanding of early universe cosmology [57], or "hot big bang cosmology" as it is popularly known. According to this model the universe has passed through different phases, and its expansion rate is controlled or determined by the dominant matter components at that time. A number of evolution epochs, have been identified, during which distinctive processes occur. The main ones are as follows. The Big Bang singularity (BBs) is regarded as the origin of the universe or the start of both space and time. Since the mathematics breaks down at a singularity, we can't say for sure what happened at the very "beginning". The Baryogenesis era is

the time during which the fundamental constituents of the universe froze out, and matter came to dominate over antimatter, but the underlying processes of particle physics are poorly understood. In the inflation phase, a "false vacuum" state caused exponential expansion of space by about 60 e-foldings.[1] Again, the fundamental fields that are responsible for inflation have yet to be established — for inflation to start and stop correctly, considerable fine tuning of the field potential is required. During the era of Big Bang Nucleosynthesis (BBN), neutrons are both combining with protons to form nuclei, and also decaying into protons. Only very light elements are formed — Hydrogen (H), Helium (He), some Lithium (Li), and almost nothing else. The exact neutron/proton balance and the proportions of He and Li depend sensitively on the expansion rate at that time. During the acoustic oscillation phase between inflation and recombination, the hot baryonic plasma underwent oscillations, and as the horizon size expanded, successively larger wavelengths "entered" the horizon and began oscillating until recombination, at which time pressure vanished, oscillation stopped, and the CMB was formed. This is complemented by the essentially pressureless "dark matter", which did not oscillate, but gradually formed density concentrations which then became the seeds of baryon structure formation after recombination. Recombination, or last scattering, is the process of electrons and ions forming neutral atoms, and emitting photons, and it happens as the temperature drops to about 1000° Kelvin. Once the plasma disappears, light hardly interacts with matter, and it free-streams across the universe to form the CMB we observe today. The measured power spectrum of perturbations in the CMB is the imprint of the oscillation state of the plasma at recombination [52, 79]. The structure growth phase is the period from recombination to now during which the tiny perturbations present at recombination grow into superclusters, voids, walls and filaments, and collapse into stars and galaxies. The cosmological constant domination era, which is just starting now, occurs when the dark and baryonic matter density has dropped so low that the cosmological constant takes over and causes an accelerated expansion of the universe. The old ideas of an early radiation domination era, followed by a matter domination era have been superseded by the addition of "dark matter", and the inclusion of inflation.

The modern formulation of the FLRW model uses the density parameter Ω, which is

[1] Inflation was suggested by Guth [32] to solve the flatness problem, the horizon problem, and the monopole problem in FLRW models. The flatness problem is as follows: the universe is not strongly curved today, which means that at early times it was very close to flat — how did that happen? The horizon problem is the difficulty of explaining how the CMB is so uniform when opposite sides of the CMB sky have never been in causal contact; inflation takes a tiny region of the early universe that has already been in causal contact, and inflates it to cosmological size. The monopole problem is the observation of no monopoles when particle physics suggests they should be plentiful; and it is the enormous expansion of inflation, after monopole production has occurred, that accounts for their rarity.

the ratio of the mass density ρ to the critical density of the universe ρ_c. The critical density is the density that a $k = 0$ model has, so Ω is related to the spatial curvature of universe. Assuming the FLRW model and linear perturbation theory, analysis of observational data from the Wilkinson Microwave Anisotropy Probe (WMAP) [46, 47, 81], Baryon Acoustic Oscillations (BAO) [70] and Type Ia supernovas (SNIa) [75] have shown that $0.728^{+0.015}_{-0.016}\%$ of the constituents of the universe is cosmological constant or "dark energy" (Ω_Λ), $0.227 \pm 0.014\%$ is "dark matter" (Ω_c), $0.0456 \pm 0.0016\%$ is baryonic matter (Ω_m) and 0.001% is radiation (Ω_r). The baryonic matter and the radiation are the familiar components whose physics we understand, but the dark matter and dark energy components are exotic new forms of matter that pose a challenge to present-day physics. This "ΛCDM" model or "standard model", is the prevalent view of cosmology. The discovery of the CMB has provided the strongest evidence for one of the fundamental assumptions of the FLRW model, isotropy. Apart from the uniform CMB temperature, the X-ray Background (XRB), the distribution of radio sources and the Lyman-α absorption of the photons by neutral hydrogen [53, 54] support isotropy.

1.2 Limitations

Although this model is an exact solution of EFEs and has successfully described many of the bulk phenomena in the observable universe, it has a problem when we come to structure formation — the study of how the galaxy clusters, super-clusters and voids emerged with time. On all scales less than 100 Mpc the universe is distinctly inhomogeneous. To understand this puzzle we must explain the origin of density fluctuations, and what makes them grow with time. It has been suggested that density fluctuations are either caused by some topological defects such as cosmic strings, or by the amplification of quantum fluctuations during inflation. The inflation scenario is widely accepted because of its consistency with CMB calculations.[2] This results in a power law fluctuation spectrum, from which the acoustic oscillations grow. Following recombination, the gravitational self force produced by these density fluctuations in time forms the large scale structure seen today. With regards to the post-recombination evolution of the structure, two approaches are commonly used, the N-body simulation and the perturbation theory. Each approach has its problems when describing the evolution of the structure formation in reality. For instance, there are two approaches of perturbation theory; the Newtonian perturbations which are only valid for weak fields at sub-horizon scales, and the relativistic

[2]To fully understand the origin of these quantum fluctuations we need a quantum gravity theory, which we do not yet have.

or cosmological perturbations which require GR and are also applicable to super-horizon scales. According to the cosmological perturbation approach, the density fluctuations must always remain $\delta \ll 1$ for the perturbations to be linear. But once $\delta \sim 1$, the first order perturbation beaks down, because the perturbations are large, in other words the perturbations are non-linear. However, since the present day universe is very lumpy or inhomogeneous on many scales, we should look at alternative models that can deal with the non-linear structure formation, such as exact solutions of EFEs. Although it is sometimes claimed that perturbation theory is sufficient for cosmology, there are solid reasons to question this [16]. Briefly these reasons are as follows. (i) Both the density contrast and the curvature contrast must always be less than one for the perturbations to be within the limit of the linear mode. The density contrast is well above 1 in present-day galaxy clusters. Also, in negative curvature LT models, the curvature contrast decreases with time while the density contrast increases, which means the curvature contrast is not a good enough measure of linearity. (ii) Higher-order perturbations can only improve the result achieved by the first order, when the model is still in the above linear limit, so that there can be convergence. Further, there are various studies showing linearisation instability in some important classes of cosmological models. For more details about such problems, see [16], pp 2-3. Similarly, the N-body approach, being based on Newtonian gravity, is not relativistic, even if it is non-linear. Thus it is important to compare these approaches with exact inhomogeneous solutions of the EFEs.

Apart from this, there is a fundamental scientific imperative — don't just assume something if you can test it — we should test our theories in whatever way we can. While isotropy is relatively easy to check, there are so many factors that affect the variation of observations with distance, that it is not at all easy to verify radial homogeneity without assuming it! For example [69], if the observed luminosity-redshift plot deviates from that expected in an FLRW model, is it due to a different equation of state, or to evolution of the sources, or to inhomogeneity. As the collection of cosmological observations grows, we are reaching the stage when we can test for homogeneity. Thus in this thesis we analyse observations in a general framework. One of the long term goals is to see if the results support homogeneity, but the available data is not yet good enough. Therefore this thesis is a contribution to developing the theory and numerics that will be needed.

1.3 Inhomogeneous Models

There are several exact solutions of EFEs that have been used to study inhomogeneity in the universe. These include: the spherically symmetric Lemaître-Tolman (LT) model

[56, 91] sometimes refereed to as the Lemaître-Tolman-Bondi (LTB) model [17] which is pure dust, and it is the simplest one; the spherically symmetric Lemaître model [56] which allows non-zero pressure; the non-symmetric Szekeres model [13, 14, 38, 87, 88] which is also pure dust, and its non-zero pressure version, the Szafron model [86]. The Stephani [21–23, 31] model which is also a generalisation of FLRW model and the Szafron metrics [67]. However, the Stephani model does not have a realistic equation of state; none is imposed and unphysical behaviour can easily occur. These models have been differently used according to their properties to explain some challenging problems in cosmology today without need of dark energy. For example, they can be used to study the evolution of cosmic structure, structure formation around central black hole, the dimming of Ia type supernovae (SNIa), and the geometry of the universe. Most of these topics are well addressed in [16]. Unfortunately most of these topics are not in the scope of this thesis, so that we will only pay attention to the last one which is determining the geometry of the universe that we live in, without assuming homogeneity. For further information, there is an excellent review of inhomogeneous cosmologies by Krasinski [49], a more recent summary of developments in [16], and a well illustrated description of Lemaître-Tolman and Szekeres models and some of the work done with them is given in [36].

1.4 Deducing the Metric from Observations

The idea of calculating observational relations in a given spacetime geometry was firstly suggested by Temple [90], then reviewed by McCrea [64, 65]. McCrea made the assumption that the dynamics of the universe is governed by the theory of GR, then he studied the observational relations for anisotropic and homogeneous matter distribution. In his second paper, he derived these quantities without assuming isotropic and homogeneous matter distribution. His result was presented as a series approximation solution up to the first order term.

25 years later, Kristian and Sachs [51] were the first to consider determining the spacetime metric from cosmological data. They made three assumptions to obtain their solution, these are: (i) The geometry of the spacetime is pseudo Riemannian, (ii) Light travels along null geodesics, (iii) the source of gravitational fields is pure matter, i.e. "dust". They also did power series approximation to the EFEs near our present position, and derived expressions for the redshift, the area distance, the image distortion, the number density, and the proper motion in terms of the corrected luminosity distance. These five quantities were represented as series coefficients, where their values can be numerically calculated. They concluded at that time that the assumption of homogeneity

cannot be proven.

Following the Kristian and Sachs approach, Ellis, Stoeger, Maartens, Whitman and others, decided to determine the spacetime geometry from ideal Cosmological data, but in a different way. Their main idea was to determine the spacetime metric away from the observer's position more generally and not merely as a series approximation around the observer. They considered general inhomogeneous models for developing the observational cosmology program (OC) [3–8, 10, 25, 61, 62, 74, 82–85]. In that program, they introduced a new set of coordinates, the observer coordinate system, which is different from the usual space and time coordinates. These coordinates are centered on the observer's worldline (that is, our worldline) and aligned with the incoming light rays. In other words, the observer is moving on his worldline, and at each time (observation event), the set of received light rays form a past null cone (PNC). These PNCs foliate the spacetime, just as the constant time surfaces do for time-space coordinates. *The* PNC is the one centered on us at the present day; the history of extra-galactic observations is very nearly a single moment in time. Note that these coordinates do not describe all the universe, but rather they describe what we can see of the universe. Firstly they considered a cosmographic analysis, which is the analysis of the cosmological observational data without taking the field equations into account, and they showed that it is not possible to determine the spacetime geometry from the data on the PNC. Secondly, they considered the theory of GR as a dynamical physical description of the universe, and the matter composed of dust particles as the source of the gravitational field. Then they showed that it is possible to determine the spacetime geometry on the PNC, and off the PNC. The observer coordinates provide a highly flexibility way of solving the EFEs on the PNC, and then evolving the solution off the PNC to the future or to the past. The solution process directly uses the observational data on an initial PNC to solve for metric functions along that surface, and this PNC data is viewed as initial conditions for deriving the subsequent model evolution. Also, as a more general alternative, they introduced the fluid-ray tetrad formalism, calculating the "spin coefficients" plus some constraints to derive their basic mathematical equations. In addition to the procedure of the exact solution of the EFEs, Hellaby & Alfedeel [37], reviewed earlier work, and presented a complete analysis of the solution process in observer coordinates approach in the spherically symmetric dust case. Previous papers on this case tended to refer to each other for part of the solution, or used a less than ideal method, or glossed over important details.

The OC approach is not the only one that was used to tackle this problem. A parallel research program by Hellaby and others aims to develop this idea into viable numeri-

cal procedures that input actual observational data. Mustafa, Hellaby and Ellis (MHE) [69], assumed the universe is a spherically symmetric, inhomogeneous Lemaître-Tolman model, and considered how to deduce the model's 3 arbitrary functions — which define spacetime metric — from given cosmological data on the PNC. Given the luminosity distance or angular diameter distance, and the number count density as functions of redshift, coupled with their evolution functions, the absolute luminosity or the true diameter, and the average mass per source, MHE outlined a theoretical algorithm that would allow one to determine the Lemaître-Tolman metric functions. They showed an FLRW model can be fitted to any reasonable data, if you fiddle the evolution functions, and conversely, if the evolution functions are fixed an LT model will fit the data. A method for testing for source evolution functions independently of inhomogeneity, using multicolour observavtions was proposed by Hellaby in [34]. A serious attempt at eventually extracting metric functions from cosmological data, the Metric of the Cosmos (MoC) project, was initiated by Hellaby, Lu and McClure [35, 36, 58, 59, 63]. Lu & Hellaby reformulated the MHE algorithm in terms of differential equations (DEs) for the Lemaître-Tolman arbitrary functions, and they wrote Matlab programs to integrate them numerically. They showed that when the diameter distance reaches it maximum value, the "apparent horizon", the DEs become singular, which leads to a numerical problem. This is true both for homogeneous FLRW cosmologies and for inhomogeneous ones. They overcame this difficulty by showing a Taylor series solution near the maximum point is well behaved. Similarly, the origin needed special treatment. They tested their numerical program with fake observational data generated from a selection of models, and in each case successfully recovered the correct Lemaître-Tolman metric functions. It has been pointed out by Hellaby [35] that, at the maximum in the diameter distance, and only there, there is a simple relation between the diameter distance, the net mass within that radius, and the cosmological constant. Thus a measurement of this maximum diameter distance tells us the total mass present. Further, it can be used as a consistency check in these numerical schemes — if the integrated total mass is not consistent with the mass calculated from this relation, there are errors in the given data. This relation at the apparent horizon was generalised to the case of non-zero pressure, i.e. the Lemaître metric, by Alfedeel & Hellaby [2]. This paper also showed that the concept of mass cannot be well separated from other variables when both pressure and cosmological constant Λ are non-zero, as well as outlining a numerical algorithm for generating Lemaître models. McClure & Hellaby [63] extended the original code of Lu in several ways, writing a C++ program that can determine the Lemaître-Tolman arbitrary functions from simulated observational data

that has statistical and/or systematic errors. Their implementation smoothed the data by means of a moving average, and showed good approximations to the correct Lemaître-Tolman functions can be obtained even if the data has significant statistical errors. They also analysed the stability of the DEs with respect to small data errors, and found that the DEs are stable, except for the DE for the mass function after the maximum in the diameter distance. Importantly, they used data with systematic errors, and showed how the above apparent horizon relation can be used to detect the inconsistency and correct for it. Although the correction is not unique, it is a great improvement on not knowing the data is systematically off. More recently, Bolejko, Hellaby & Alfedeel [15], showed that one can use the luminosity and galaxy cluster age data (against redshift) to reconstruct the Lemaître-Tolman metric functions instead of using the luminosity and number count data (against redshift).

The first numerical treatment of this problem, often called the 'inverse problem', was by Bishop and Haines [11]. They realised it is a kind of time-reverse of the characteristic initial value problem used in numerical relativity. However, their code blew up at the apparent horizon (this problem is explained and solved in chapter 5). In fact it was suggested by Vanderveld, Flanagan and Wasserman [92] that the inverse problem could not be solved for a non-FLRW model, because they did not understand the properties of the apparent horizon. This was clarified in [50]. Soon after the dimming of the they Ia supernovae was discovered Celerier [19] used a parabolic LT model, expanding functions in powers of z, to show that inhomogeneity could explain this effect without the need for acclerating expansion. This was generalised to all LT models by Tanimoto and Nambu [89]. Papers by Rindler and Suson [76] and by Ishak [44] contain some general discussions of the problem. Chung and Romano [20] also tried to reproduce the ΛCDM distance-redshift relation, but encountered difficulties.

Iguchi, Nakamura and Nakao [43] fitted the luminosity distance-redshift relation of the ΛCDM model with an LT model. This was not the full 'inverse problem', as only one observational function was used. Therefore it was necessary to assume another physical relationship. They tried two possibilites: constant bang time, and spatial flatness. They were able to find some reasonable models. However they got stuck at the apparent horizon. Later Yoo, Kai and Nakao [96] considered the effect of the Dyer-Roeder clumpiness parameter, and they concluded that it could reduce the amount of inhomogeneity needed to fit observations. They seem to have solved the apparent horizon problem with some kind of shooting method. In [95] Yoo discussed the full inverse problem for LT models, where the diameter distance and the redshift space mass density are given as functions of

z, especially the solution at the apparent horizon, and derived the necessary and sufficient conditions for a solution to exist. The results were expressed in terms of the notation of [89] for the LT evolution equations. However they support the point made in [35] and [69] that arbitrary choices for the observational data functions will not satisfy the AH conditions.[3] A numerical example was calculated, in which the observational relations of an FLRW universe with baryonic matter ($p = 0$) and dark energy ($p = w\rho$), were mimicked by an LT model, which was constructed by proposing "fitting functions" for the 3 arbitrary functions of the LT model. The difference was a few percent.

A very interesting issue that we don't consider here is how the redshift of sources evolves with time, as it is believed this may be able to distinguish universe models [9, 26, 45, 55, 96].

1.5 The Present Work

In this thesis, we will generalise the MoC algorithm to the case of non-zero pressure and Λ, i.e the Lemaître model. That is, we will develop theoretically the procudure for determining the functions of the Lemaître metric from observational data on the past null cone, obtaining the differential equations that need to be solved, and then code this algorithm in a set of Matlab programs and test them. The structure of this thesis is as follows. In chapter 2, we will present a fairly general, spherically symmetric inhomogeneous cosmological model, the Lemaître model, and its EFE solution. Then, we will present a clear description of the cosmological source observations, and discuss how to generalise the MoC algorithm. In chapter 3, we will review the basic concept of the observer coordinates and observer metric. In chapter 4, we will present the full solution procedure for the Lemaître metric in observer coordinates, and then the algorithm for obtaining the solution from the data will also be presented. In chapter 5, we will study the origin limits of the DEs, and their behavior at the apparent horizon, followed by approximate solutions of the DEs at those regions. The data smoothing procedure will be discussed in detail in chapter 6. In chapter 7, our numerical implementation scheme will be clearly addressed. In chapter 8, we will present our numerical integration results, and finally, we will end the thesis with our conclusions.

[3] This way of making the statement is deceptive. Every single PNC in every single (well-behaved) LT model generates observational functions that satisfy the AH conditions. This was shown in [50] and in corollary 1 of [95].

Chapter 2

The Lemaître Model

As introduced in chapter 1, the broad-brush homogeneous cosmology of the FLRW model needs to be complemented by a theory of structure formation, and further, the assumption of homogeneity needs to be tested. For this purpose we need an inhomogeneous cosmology, so that we don't assume homogeneity ab initio. To be a cosmology, a solution of the EFEs must allow non-zero density everywhere. Krasinski [49] defined an inhomogeneous cosmology as one that contains the RW metric as a special case. Here we introduce the Lemaître (L) metric, which will be central to the rest of the thesis.

The study of inhomogeneous solutions of the EFEs began quite early on. The L model [56] was firstly presented by Abbé Georges Lemaître in 1933, the same paper that introduced the Lemaître-Tolman model, and it is a fairly general spherically symmetric model that has a non-zero pressure. In the literature, the later work of Misner and Sharp [66], and to a lesser extent that of Podurets [72] are more often cited, though Lemaître's description was clearly the first, and is in fact more general. In fact Lemaître allowed the radial and tangential pressures to be different, while most other treatments assume an isotropic pressure. In the following, we also assume the pressure to be isotropic. This metric was also considered in [18, 33]. The L model can be thought of as a generalisation of the FLRW model, that represents a spherically symmetric matter distribution that is inhomogeneous in the radial direction, and has non-zero pressure p and non-zero cosmological constant Λ. The standard coordinates $x^a = (t, r, \theta, \phi)$ are synchronous and comoving with the matter flow, while the fluid 4-velocity u^a is a timelike quantity that satisfies $u^a u_a = -1$. With these assumptions, Lemaître solved the EFEs and reduced them to a system of first order differential equations (DEs), and also he obtained an expression for the total gravitational mass from the conservation equation of the energy momentum tensor. Throughout this chapter and in the rest of this thesis, we will use geometric units $G = c = 1$.

2.1 The Metric and the Matter

With the assumptions mentioned above, the diagonal, spherically symmetric spacetime metric, may be written as

$$ds^2 = -e^{2\sigma}\,dt^2 + e^{\lambda}\,dr^2 + R^2\,(d\theta^2 + \sin^2\theta\,d\phi^2)\ , \tag{2.1}$$

where $\sigma = \sigma(t,r)$, $\lambda = \lambda(t,r)$ are functions to be determined, and $R = R(t,r)$ corresponds to the areal radius. Since the metric form is unchanged by the coordinate transformations

$$\overline{t} = \overline{t}(t)\ , \qquad \overline{r} = \overline{r}(r)$$

there is a gauge freedom in each of the t and r coordinates. The energy momentum tensor is given by

$$T^{ab} = (\rho + p)\,u^a\,u^b + g^{ab}p\ , \tag{2.2}$$

where $\rho = \rho(t,r)$ is the mass-energy density of the perfect fluid, and $p = p(t,r)$ is the matter pressure, and $u^a = (e^{-\sigma},0,0,0)$ is the matter 4-velocity, assumed to be comoving. This equation of state is less general than the full Lemaître metric, as we assume isotropic pressure, and thus we only need one equation of state.

2.2 The Field Equations

The EFEs, $G^{ab} = \kappa\,T^{ab} - g^{ab}\Lambda$, can be reduced to the following set of equations

$$e^{2\sigma}\,G^{tt} = -\left(\frac{2R''}{R} + \frac{R'^2}{R^2} - \frac{R'}{R}\,\lambda'\right)\,e^{-\lambda} + \left(\frac{\dot{R}^2}{R^2} + \frac{\dot{R}}{R}\,\dot{\lambda}\right)\,e^{-2\sigma} + \frac{1}{R^2} = \kappa\rho + \Lambda\ , \tag{2.3}$$

$$e^{\lambda}\,G^{tr} = \left(\frac{2\dot{R}'}{R} - \frac{2\dot{R}}{R}\,\sigma' - \frac{R'}{R}\,\dot{\lambda}\right)\,e^{-2\sigma} = 0\ , \tag{2.4}$$

$$e^{\lambda}\,G^{rr} = \left(\frac{R'^2}{R^2} + \frac{2R'}{R}\,\sigma'\right)\,e^{-\lambda} - \left(\frac{2\ddot{R}}{R} + \frac{\dot{R}^2}{R^2} - \frac{2\dot{R}}{R}\,\dot{\sigma}\right)\,e^{-2\sigma} - \frac{1}{R^2} = \kappa p - \Lambda\ , \tag{2.5}$$

$$\begin{aligned} R^2\,G^{\theta\theta} = &\left(\frac{R''}{R} + \frac{R'}{R}\,\sigma' + \sigma'' + \sigma'^2 - \frac{R'}{2R}\,\lambda' - \frac{1}{2}\,\sigma'\,\lambda'\right)\,e^{-\lambda} \\ &+ \left(\frac{\dot{R}}{R}\,\dot{\sigma} - \frac{\ddot{R}}{R} - \frac{1}{2}\,\ddot{\lambda} + \frac{1}{2}\dot{\lambda}\,\dot{\sigma} - \frac{\dot{R}}{2R}\dot{\lambda} - \frac{1}{4}\,\dot{\lambda}^2\right)\,e^{-2\sigma} = \kappa p - \Lambda\ , \end{aligned} \tag{2.6}$$

where the dot means a derivative with respect to t, and the prime means a derivative with respect to r. Since geometric units areused we have $\kappa = 8\pi$. The conservation equations $\nabla_a T^{ab} = 0$ are

$$\frac{2e^{2\sigma}}{(\rho+p)}\,\nabla_a T^{ta} = \dot{\lambda} + \frac{2\dot{\rho}}{(\rho+p)} + \frac{4\dot{R}}{R}\ = 0 \tag{2.7}$$

$$\frac{e^{\lambda}}{(\rho+p)}\nabla_a T^{ra} = \sigma' + \frac{p'}{p+\rho} = 0\ . \tag{2.8}$$

Since pressure gradients are expected, the matter flow lines are not in general geodesic, and the acceleration of the worldlines is

$$a^b = u^c\nabla_c u^b = \left(0, \sigma' e^{-\lambda}, 0, 0\right)\ . \tag{2.9}$$

However, it is clear from (2.8) and (2.9) that $p' = 0$ implies $\sigma' = 0$, which implies geodesic matter flow.

To solve these equations, we multiply (2.3) by R^2R' and use (2.4) to eliminate the term that contains $\dot{\lambda}$, which produces

$$\frac{\partial}{\partial r}\left[R + R\dot{R}^2e^{-2\sigma} - RR'^2e^{-\lambda} - \frac{1}{3}\Lambda R^3\right] = \kappa\rho R^2R'\ . \tag{2.10}$$

Multiplying (2.5) by $R^2\dot{R}$ and using (2.4) to eliminate the term that contains σ', shows (2.5) can be rewritten as

$$\frac{\partial}{\partial t}\left[R + R\dot{R}^2e^{-2\sigma} - RR'^2e^{-\lambda} - \frac{1}{3}\Lambda R^3\right] = -\kappa p R^2\dot{R}\ . \tag{2.11}$$

The term in square brackets is related to the total mass-energy of the system, $2M$, interior to a comoving shell of constant r, which is normally defined by

$$\frac{2M}{R} = \dot{R}^2e^{-2\sigma} - R'^2e^{-\lambda} + 1 - \frac{1}{3}\Lambda R^2\ . \tag{2.12}$$

For more details about the justification for calling this the mass, the reader is referred to [1, 56]. With this definition, equations (2.10) and (2.11) give expressions for the density and the pressure

$$\kappa\rho = \frac{2M'}{R^2R'}\ , \tag{2.13}$$

$$\kappa p = -\frac{2\dot{M}}{R^2\dot{R}}\ . \tag{2.14}$$

Here $M = M(t,r)$, and (2.14) ensures that the mass will decrease with time as the Universe expands, assuming p is positive. Equation (2.12) may be rearranged as an evolution equation for the model,

$$\dot{R} = \pm e^{\sigma}\sqrt{\frac{2M}{R} + f + \frac{\Lambda R^2}{3}}\ , \tag{2.15}$$

where

$$f(t,r) = R'^2e^{-\lambda} - 1 \tag{2.16}$$

acts as the curvature term, or twice the total energy per unit mass of the particles at r (analogous to f in the LT model). We also define

$$W(t,r) = \sqrt{1+f} \tag{2.17}$$

and we will often change between f and W in our working. Equation (2.15) is the analogue of the Friedman Equation in FLRW models, describing the evolution of the areal radius of each worldline, $R(t,r)$, instead of the scale factor $a(t)$ as in FLRW models. The $\pm$ signs indicate whether the universe expands or contracts with time.

The metric variables g_{tt} and g_{rr} can be obtained by integrating (2.8) and (2.7) as follows,

$$\sigma = \sigma_0(t) - \int_{r_0}^{r}{}^{\text{const } t} \frac{p'\,\mathrm{d}r}{(\rho+p)} = \sigma_0 - \int_{\rho_0}^{\rho}{}^{\text{const } t} \frac{(\partial p/\partial\rho)}{(\rho+p(\rho))}\,\mathrm{d}\rho\ , \tag{2.18}$$

and

$$\lambda = \lambda_0(r) - 2\int_{\rho_0}^{\rho}{}^{\text{const } r} \frac{\mathrm{d}\rho}{(\rho+p(\rho))} - 4\ln\left(\frac{R}{R_0}\right)\ , \tag{2.19}$$

where $\sigma_0(t)$ and $\lambda_0(r)$ are arbitrary functions of integration. Typically, we would choose $r_0 = 0$ to be the origin, where $R(t,0) = 0$. Having solved (2.3)-(2.5) and (2.7)-(2.8), the θ-θ field equation (2.6) is now satisfied, since

$$\begin{aligned} R^2\,G^{\theta\theta} = &\left(R\left(\frac{\sigma'}{4R'} - \frac{\dot\lambda}{8\dot R}\right) - \frac{1}{2}\right)e^{2\sigma}\,G^{tt} - \left(\frac{R}{4\dot R}\right)\partial_t\left(G^{tt}e^{2\sigma}\right) \\ &+ \left(R\left(\frac{\sigma'}{4R'} - \frac{\dot\lambda}{8\dot R}\right) + \frac{1}{2}\right)e^{\lambda}\,G^{rr} + \left(\frac{R}{4R'}\right)\partial_r\left(G^{rr}e^{\lambda}\right) \\ &+ \left(\frac{e^{2\sigma}}{2\dot R}\left(\frac{R\lambda'}{4} - \frac{R\sigma'}{2} - R'\right) + \frac{e^{\lambda}}{2R'}\left(\frac{R\dot\lambda}{4} - \frac{R\dot\sigma}{2} + \dot R\right)\right)G^{tr} \\ &+ \left(\frac{R}{4R'e^{2\sigma}}\right)\partial_t\left(G^{tr}e^{2\sigma+\lambda}\right) - \left(\frac{R}{4\dot R e^{\lambda}}\right)\partial_r\left(G^{tr}e^{2\sigma+\lambda}\right)\ , \end{aligned} \tag{2.20}$$

and to get the right hand side of (2.6) we also add

$$0 = \frac{\kappa R e^{2\sigma}}{4\dot R}\,\nabla_b T^{tb} - \frac{\kappa R e^{\lambda}}{4R'}\,\nabla_b T^{rb}\ . \tag{2.21}$$

Equation (2.15) does not solve as given, since we do not yet know the value of λ, σ and M. However by defining the proper time τ of comoving observers as

$$\tau = \int_{a(r)}^{t} e^{\sigma}\,dt\ , \tag{2.22}$$

we can write

$$\tau = \int_0^R \frac{dR}{\pm\sqrt{\frac{2M}{R} + f + \frac{\Lambda R^2}{3}}} \,, \tag{2.23}$$

$$\tag{2.24}$$

where $a(r)$ is an arbitrary function of integration that describes the bang time as a function of the r coordinate Here the Big Bang, where $R = 0$, occurs at $t = a$, and it does not happen simultaneously as in the FLRW model, but it occurs at different times on each r worldline.

Equation (2.4) provides a constraint equation for the metric variable λ, which we will make use of later on,

$$\dot{\lambda} = \frac{\dot{R}'}{R'} - \frac{\dot{R}}{R'}\sigma' \,. \tag{2.25}$$

The simpler LT model can be obtained directly by setting $p = 0$ in (2.18) and (2.14), so that the metric components in (2.1) become $e^{\sigma} = 1$ and $e^{\lambda} = R'^2/\sqrt{1 + f(r)}$.

2.3 The Past Null Cone (PNC)

The Lemaître model contains 5 free functions: the equation of state $p(\rho)$, a coordinate freedom in each of t and r, and two that fix physical properties [2]. In the following we will also make two gauge choices. The observational data will determine the two physical functions, but the equation of state must be chosen by the user.

As we know, all the cosmological information we receive, is transmitted by light rays, and light rays travel along the past null cone (PNC). Therefore, we first need to set up the PNC of an observing event, $t = t_o$, $r = r_o = 0$. Hereafter, each quantity $Q(t, r)$, when evaluated on the PNC, will be indicated with a hat on top or as subscript, for example $\hat{Q} = Q(\hat{t}(r), r) = [Q]_{\wedge}$.

Thus, for the incoming radial null geodesics, $ds^2 = 0 = d\theta^2 = d\phi^2$, the metric in (2.1) implies

$$\frac{\mathrm{d}\hat{t}}{\mathrm{d}r} = -\frac{e^{\hat{\lambda}/2}}{e^{\hat{\sigma}}} \,. \tag{2.26}$$

Because of the coordinate freedom in (2.1), we can use a radial coordinate choice to simplify the solution. We write

$$\frac{\mathrm{d}\hat{t}}{\mathrm{d}r} = -e^{\zeta} = -\frac{e^{\hat{\lambda}/2}}{e^{\hat{\sigma}}} \quad \rightarrow \quad \hat{\lambda} = 2\hat{\sigma} + 2\zeta \quad \rightarrow \quad \widehat{R}' = e^{\hat{\sigma}+\zeta}\sqrt{1 + \hat{f}} \,. \tag{2.27}$$

The gauge function $\zeta(r) = \hat{\lambda}/2 - \hat{\sigma}$ is only defined on the PNC, and it will be set later. Then the observer's PNC (2.26) has the simple solution

$$\hat{t}(r) = t_o - \int_0^r e^{\zeta}\, dr \ , \tag{2.28}$$

where t_o is a constant of integration which we can take to be the current age of the Universe at the observing event.

2.4 Observables

Generally cosmological sources are characterised by a set of observational quantities, the redshift z, the angular diameter δ, the apparent luminosity ℓ and the number count density n in redshift space. With each one of them, there are associated time dependent functions, the true diameter D, the absolute luminosity L and the average mass per source μ, that characterise the evolution of the source properties, and which are needed to relate the theoretical model to observational data.

2.4.1 The Redshift

In Cosmology, the redshift is the measurement of the relative shift spectral lines between an observer and the cosmological objects or sources. While the Universe is expanding, the redshift is connected to the comoving distance in the following way. Consider a cosmological source such as a "galaxy", that emits two light rays at proper times τ_e and $\tau_e + T_e$, which are passing through the world lines of constant r and $r + \mathrm{d}r$, and are received by an observer at times τ_o and $\tau_o + T_o$ (see figure (2.1)). Here T_e and T_o are the light oscillation periods, measured in terms of local proper time τ. The redshift is given by

$$(1 + z) = \frac{T_o}{T_e} \ . \tag{2.29}$$

For the two successive wavefronts passing through the events B and A or D and C respectively on those neighboring worldlines, Taylor expansions along the curves AB and CD give the change in time $\hat{t}$ between those points as,

$$\tau_B = \tau_A + \left.\frac{d\hat{\tau}}{dr}\right|_A dr + \mathcal{O}(dr^2) \ , \tag{2.30}$$

$$\tau_D = \tau_C + \left.\frac{d\hat{\tau}}{dr}\right|_C dr + \mathcal{O}(dr^2) \ . \tag{2.31}$$

the change in the light oscillation period T over a distance $\mathrm{d}r$ is given by

$$\mathrm{d}T = T_{BD} - T_{AC} = \Big(\tau_D - \tau_B\Big) - \Big(\tau_C - \tau_A\Big) = \Big(\tau_D - \tau_C\Big) - \Big(\tau_B - \tau_A\Big) \ , \tag{2.32}$$

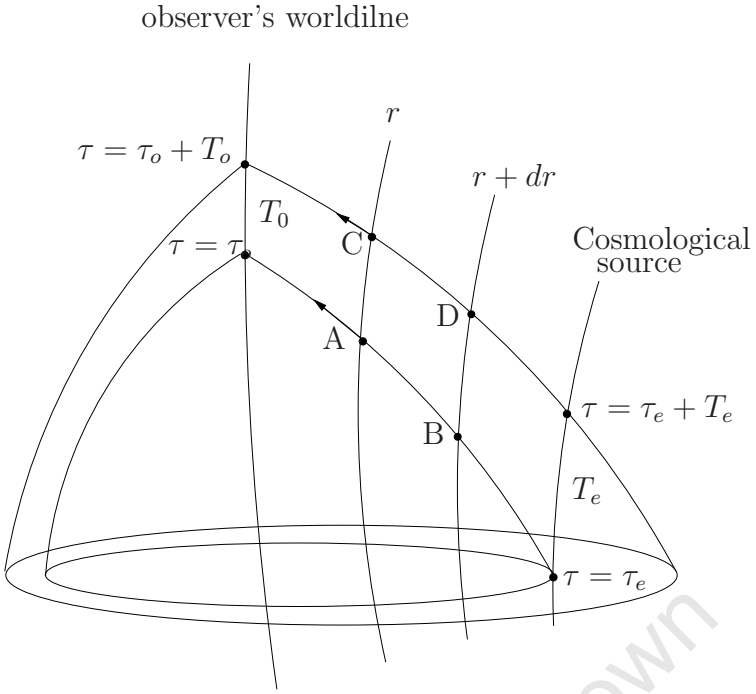

Figure 2.1: The path of the light rays from the source to observer

Substituting from (2.30), (2.31) and neglecting the higher order terms because the change in the light oscillation period is very small, we have

$$\mathrm{d}T = \left.\frac{\mathrm{d}\hat{\tau}}{\mathrm{d}r}\right|_C \mathrm{d}r - \left.\frac{\mathrm{d}\hat{\tau}}{\mathrm{d}r}\right|_A \mathrm{d}r \ . \tag{2.33}$$

Again, doing a Taylor expansion about A for the first term on the right of (2.33), we find

$$\begin{aligned} \mathrm{d}T &= \left(\left.\frac{\mathrm{d}\hat{\tau}}{\mathrm{d}r}\right|_A + \frac{\partial}{\partial\tau}\left(\frac{\mathrm{d}\hat{\tau}}{\mathrm{d}r}\right)\Big|_A T \right) \mathrm{d}r - \left.\frac{\mathrm{d}\hat{\tau}}{\mathrm{d}r}\right|_A \mathrm{d}r \ , \\ \frac{\mathrm{d}T}{T} &= \frac{\partial}{\partial\tau}\left(\frac{\mathrm{d}\hat{\tau}}{\mathrm{d}r}\right)\Big|_A \mathrm{d}r \ . \end{aligned} \tag{2.34}$$

where $\partial/\partial\tau$ is along the comoving worldlines of constant r. By (2.22) and (2.26) we have

$$\frac{\mathrm{d}\hat{\tau}}{\mathrm{d}r} = \frac{\partial\tau}{\partial t}\frac{\mathrm{d}\hat{t}}{\mathrm{d}r} + \frac{\partial\tau}{\partial r} \tag{2.35}$$

$$= e^{\sigma}\left(-\frac{e^{\lambda/2}}{e^{\sigma}}\right) + \int_a^t e^{\sigma}\sigma'\,dt - a'\left[e^{\sigma}\right]_{t=a} \tag{2.36}$$

so that

$$\frac{\partial}{\partial\tau}\left(\frac{\mathrm{d}\hat{\tau}}{\mathrm{d}r}\right) = \left[\frac{1}{e^{\sigma}}\frac{\partial}{\partial t}\left(\frac{\mathrm{d}\hat{\tau}}{\mathrm{d}r}\right)\right]_{\wedge} \tag{2.37}$$

$$= \left[-\frac{\dot{\lambda}}{2}\frac{e^{\lambda/2}}{e^{\sigma}} + \sigma'\right]_{\wedge} \tag{2.38}$$

Therefore, (2.34) can be integrated down the PNC to give

$$\ln\left(\frac{T_o}{T_e}\right) = \int_0^{r_e} \left[\frac{\dot{\lambda}}{2}\frac{e^{\lambda/2}}{e^{\sigma}} - \sigma'\right]_{\wedge} \mathrm{d}r \ , \tag{2.39}$$

which leads to the following

$$\ln(1+z) = \int_0^{r_e} \left[\frac{\dot{\lambda}}{2}e^{\zeta} - \sigma'\right]_{\wedge} \mathrm{d}r \ . \tag{2.40}$$

This gives the redshift for the central observer at $r = 0$, receiving signals from a source at $r = r_e$. This is where a second gauge choice can be made. We write

$$\ln(1+z) = \int_0^{r_e} \left[Z\, e^{\zeta}\right] \mathrm{d}r \ . \tag{2.41}$$

and, as with ζ, $Z(r) = \left[\dot{\lambda}/2 - \sigma' e^{-\zeta}\right]_{\wedge}$ exists only on the PNC and it will be specified later. Written as a differential equation this is

$$\varphi = \left.\frac{\mathrm{d}r}{\mathrm{d}z}\right|_{\wedge} = \frac{1}{e^{\zeta} Z(1+z)} \ . \tag{2.42}$$

2.4.2 The Angular Diameter Distance

The angular diameter distance is one way of measuring how far away a cosmological source of known size is, or rather appears to be. Working in Euclidean flat spacetime, suppose we have a cosmological source or "galaxy" with a given true diameter D, and a measured angular diameter δ (see Fig (2.2)). Assuming that the measurement of the two ends of the diameter was at the same time t, then its angular diameter distance d_D is the ratio between the true diameter D ("proper diameter") and the measured angular diameter δ [25, 40, 83],

$$d_D = \frac{D}{\delta} \ . \tag{2.43}$$

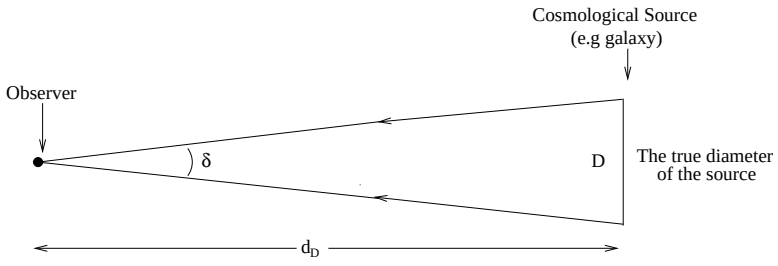

Figure 2.2: The Diameter distance between the observer and a the cosmological source (galaxy) in flat space.

Now, in a curved spacetime whose geometry is described by the Lemaître metric, suppose we have two radial null geodesics propagating along constant θ and ϕ directions

meeting at the central observer at time t_o with angular separation δ, having been emitted at time t_e from the source of true diameter D at comoving coordinate r_e (see Fig (2.3)). Then the metric in (2.1) relates the angular displacement δ (at constant r_e) to the physical size D, i.e

$$D = \hat{R}(t_e, r)\,\delta. \tag{2.44}$$

Substituting (2.44) into (2.43) and noting $t_e = \hat{t}(r_e)$, the angular diameter distance is

$$d_D = \hat{R}_e\ . \tag{2.45}$$

Equation (2.45) shows that the angular diameter distance in the Lemaître metric corresponds to the areal radius evaluated on the PNC.

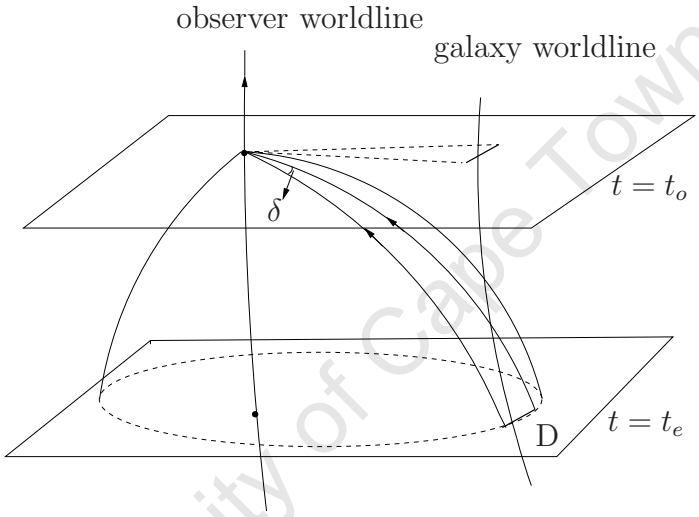

Figure 2.3: Shows how we measure the diameter distance between the observer and the cosmological source (galaxy) in 4-d spacetime, when the light rays are emitted at time t_e and received by an observer at time t_o.

2.4.3 The Luminosity Distance

The luminosity distance is based on measuring the amount of light that we receive from a faraway cosmological object. In Euclidean flat spacetime, imagine that we have a source located at distance d_L that emits energy J_e per unit time measured in Js^{-1}. Then the flux that is received by an observer located at $r = 0$ (see Fig (2.4)) is,

$$\ell = \frac{J_e}{4\pi d_L^2}\ , \tag{2.46}$$

where ℓ is apparent luminosity of the source measured in $Js^{-1}m^{-2}$. The absolute luminosity L is what would be measured at 10 parsecs,

$$L = \frac{J_e}{4\pi d_{10}^2}\ , \tag{2.47}$$

where $d_{10} = 10$ pc. Eliminating the term $J_e/4\pi$ by dividing (2.46) and (2.47) the luminosity distance d_L for any cosmological source is defined in terms of the ratio between apparent luminosity ℓ and absolute luminosity L, see Fig (2.4). It is given by

$$d_L = \sqrt{\frac{L}{\ell}}\; d_{10} = 10^{(m-\tilde{m})/5}\, d_{10}\ . \tag{2.48}$$

Here, m and $\tilde{m}$ are the apparent and absolute magnitude of the cosmological source.

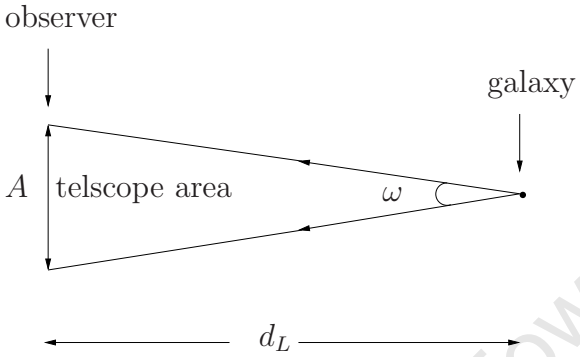

Figure 2.4: The Luminosity distance between the observer and the cosmological source (galaxy) in flat spacetime. The telescope area A subtends solid angle ω at the source and collects a small part of the emitted wavefront.

In our curved spacetime, the luminosity distance is very hard to calculate, but the reciprocity theorem gives the relationship between the luminosity distance d_L and the diameter distance d_D in terms of the redshift z (see Fig (2.5)), and it holds in any 4-dimensional spacetime under very general conditions,

$$d_L = (1+z)^2 d_D\ . \tag{2.49}$$

Equation (2.49) was first introduced by Etherington and then shown more generally by Penrose (for more details see [24, 27, 41]).

2.4.4 The 3-d Volume & the Mass Density

The number count density or the mass density is an essential quantity in observational Cosmology. In order to calculate the number of sources in an expanding region, we need to compute the physical volume dV^3 that contains these sources, and the number of sources inside this volume. Suppose we have N sources, distributed between sphere r and $r + dr$ and within the solid angle $d\omega = \sin\theta\, d\theta d\phi$, then the proper 3-volume enclosing these sources at the time of emission, as measured by comoving observers with velocity u^a (see Figure (2.6) and [40]), is given by

$$dV^3 = \sqrt{|-g|}\epsilon_{0123}\, u^0\, dx^1\, dx^2\, dx^3 = \sqrt{|-e^{2\sigma}e^{\lambda}R^4\sin^2\theta|}e^{-\sigma}\, dr\, d\theta\, d\phi = e^{\lambda/2}\, R^2\, d\omega\, dr\ , \tag{2.50}$$

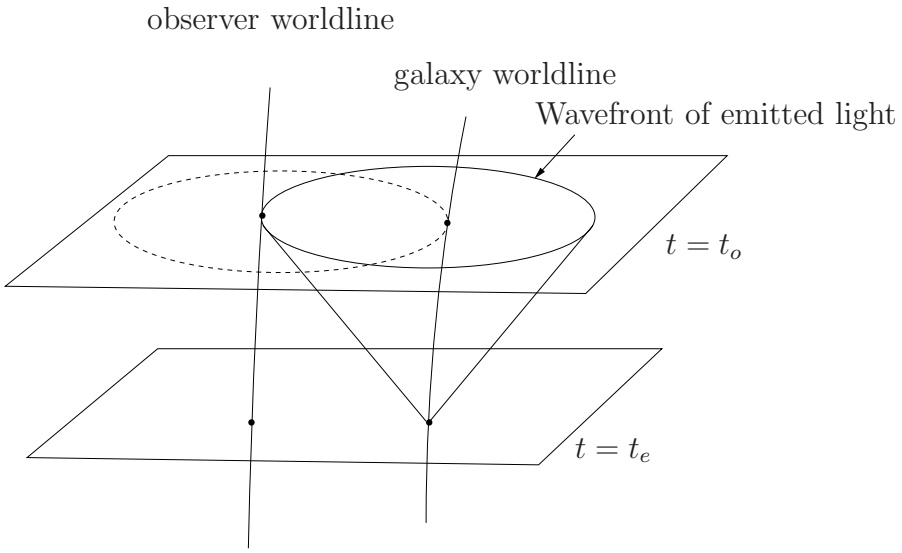

Figure 2.5: A graphical illustration showing how the observer sitting at center of his worldline will measure the luminosity distance at time t_o using light from the cosmological source (galaxy) at time of emission t_e while the Universe is expanding.

and the corresponding total mass energy in this volume element, is

$$d\mathcal{M} = \rho\, e^{\lambda/2}\, R^2\, d\omega\, dr\ . \tag{2.51}$$

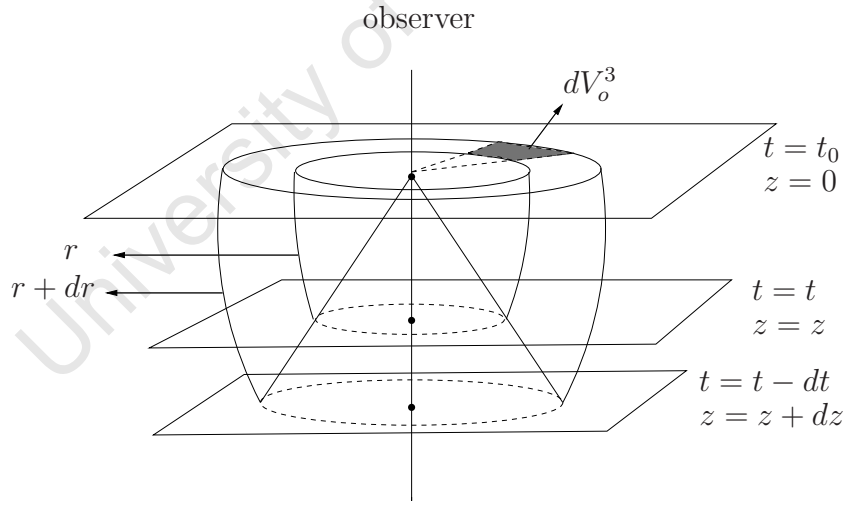

Figure 2.6: The geometry associated with a comoving volume dV_o^3, and the number count density of the galaxies inside that volume, as measured by an observer sitting at t_o.

On the other hand, working in redshift space, (z, θ, ϕ), let $n(z)$ stand for the observed number density of sources, that is the number per steradian per unit redshift interval, then the total rest mass between redshift z and $z + dz$, is

$$d\mathcal{M} = \mu\, n\, d\omega\, dz\ , \tag{2.52}$$

where $\mu = \mu(z)$ is the average mass per source. Equating (2.51) & (2.52), the relationship between n and $\hat{\rho}$ is given by

$$\mu n = \hat{\rho} e^{\hat{\lambda}/2} \hat{R}^2 \frac{\mathrm{d}r}{\mathrm{d}z} \,, \tag{2.53}$$

where $\hat{\rho} = \rho(t, r)$ is the density evaluated on the PNC.

2.5 The Solution from the Data

The given set of cosmological data include the direct observations, z, δ, ℓ, n, as well as the evolution functions, D, L and μ. These are combined to give the input functions for our problem, the redshift z, the luminosisty and diameter distances $d_D = \hat{R} = d_L(1+z)^2$, and the redshift space density $\kappa\mu n$ (2.53). With these, we should be able to determine the functions of the Lemaître model on the PNC.

The PNC equations can be found from the total derivatives of $\hat{R}$, $\hat{M}$, $\hat{W}$ and $\hat{\sigma}$ along the PNC as follows,

$$\frac{\mathrm{d}\hat{R}}{\mathrm{d}r} = \left[R' + \dot{R} \frac{\mathrm{d}\hat{t}}{\mathrm{d}r} \right]_\wedge \,, \tag{2.54}$$

and using (2.27) and (2.15), to eliminate the terms $\mathrm{d}\hat{t}/\mathrm{d}r$, $\widehat{R'}$ & $\widehat{\dot{R}}$, gives

$$e^{-\zeta} \left(\frac{\mathrm{d}\hat{R}}{\mathrm{d}r} \right) - e^{\hat{\sigma}} \sqrt{1 + \hat{f}} = -\widehat{\dot{R}} = \mp e^{\hat{\sigma}} \sqrt{\frac{2\hat{M}}{\hat{R}} + \hat{f} + \frac{\Lambda \hat{R}^2}{3}} \,. \tag{2.55}$$

Using (2.27), and re-arranging (2.55), the curvature function W, is given by

$$\hat{W} = \sqrt{1 + \hat{f}} = \frac{1}{2} \left[\frac{\left(\frac{\mathrm{d}\hat{R}}{\mathrm{d}r} \right)}{e^{\hat{\sigma}+\zeta}} + \frac{e^{\hat{\sigma}+\zeta} \left(1 - \frac{2\hat{M}}{\hat{R}} - \frac{\Lambda \hat{R}^2}{3} \right)}{\left(\frac{\mathrm{d}\hat{R}}{\mathrm{d}r} \right)} \right] . \tag{2.56}$$

Equation (2.56) tells us which regions of the spatial sections are hyperbolic $1 + f > 1$, parabolic $1 + f = 1$, or elliptic $1 + f < 1$, depending on the data that is obtained from the PNC. Also the total derivative of $\hat{M}$ on the PNC is

$$\frac{\mathrm{d}\hat{M}}{\mathrm{d}r} = \left[M' + \dot{M} \frac{\mathrm{d}t}{\mathrm{d}r} \right]_\wedge \,, \tag{2.57}$$

and using (2.13), (2.14) and (2.27) to eliminate the terms $\dot{M}$, M' and $\mathrm{d}\hat{t}/\mathrm{d}r$, followed by the left equality of (2.55) and (2.27) to replace $\hat{\dot{R}}$ and $\widehat{R'}$ in (2.57), shows

$$\frac{\mathrm{d}\hat{M}}{\mathrm{d}r} = \frac{\kappa}{2} \hat{R}^2 \left[\hat{\rho} \widehat{R'} + \hat{p} \widehat{\dot{R}} e^{\zeta} \right] \tag{2.58}$$

$$= \frac{\kappa(\hat{\rho} + \hat{p})}{2} \hat{R}^2 e^{\hat{\sigma}+\zeta} \hat{W} - \frac{\kappa \hat{p}}{2} \hat{R}^2 \frac{\mathrm{d}\hat{R}}{\mathrm{d}r} \,, \tag{2.59}$$

and substituting (2.56) into (2.59) gives

$$\frac{\mathrm{d}\hat{M}}{\mathrm{d}r}+\left[\frac{\kappa(\hat{\rho}+\hat{p})\hat{R}\,e^{2(\hat{\sigma}+\zeta)}}{2\left(\frac{\mathrm{d}\hat{R}}{\mathrm{d}r}\right)}\right]M=\frac{\kappa(\hat{\rho}+\hat{p})\,\hat{R}^2e^{2(\hat{\sigma}+\zeta)}\left(1-\frac{\Lambda R^2}{3}\right)}{4\left(\frac{\mathrm{d}\hat{R}}{\mathrm{d}r}\right)}+\frac{\kappa(\hat{\rho}-\hat{p})R^2\left(\frac{\mathrm{d}\hat{R}}{\mathrm{d}r}\right)}{4}\ . \tag{2.60}$$

Superficially this a first order, inhomogeneous differential equation for the total gravitational mass M, but it also depends on the functions $\hat{R}$, $\hat{\sigma}$, $\hat{\rho}$ & $\hat{p}$.

At this point in the working with the LT model, [59, 63, 69] used the fact that M, W & f were functions of r only, so $\partial M/\partial r=\mathrm{d}\hat{M}/\mathrm{d}r$, etc. This is not true for the L model. The method of taking the null cone derivative in all cases, and of using generalised gauge choices in (2.27) and (2.41) is due to C Hellaby. We take the null cone derivative of (2.15) and of (2.55), using (2.17) where necessary; that is, we evaluate them on the PNC and then take the derivative with respect to r,

$$2\hat{\dot{R}}\frac{\mathrm{d}\hat{\dot{R}}}{\mathrm{d}r}=e^{2\sigma}\left[2\left(\frac{2M}{R}+f+\frac{\Lambda R^2}{3}\right)\frac{\mathrm{d}\hat{\sigma}}{\mathrm{d}r}+\frac{2}{R}\frac{\mathrm{d}\hat{M}}{\mathrm{d}r}+\frac{\mathrm{d}\hat{f}}{\mathrm{d}r}+2\left(-\frac{M}{\hat{R}^2}+\frac{\Lambda R}{3}\right)\frac{\mathrm{d}\hat{R}}{\mathrm{d}r}\right]\ , \tag{2.61}$$

$$\frac{\mathrm{d}\hat{\dot{R}}}{\mathrm{d}r}=e^{-\zeta}\left(\frac{\mathrm{d}\hat{R}}{\mathrm{d}r}\frac{\mathrm{d}\zeta}{\mathrm{d}r}-\frac{\mathrm{d}^2\hat{R}}{\mathrm{d}r^2}\right)+e^{\hat{\sigma}}\left(\frac{\mathrm{d}\hat{W}}{\mathrm{d}r}+W\frac{\mathrm{d}\hat{\sigma}}{\mathrm{d}r}\right), \tag{2.62}$$

and we solve for $\mathrm{d}\hat{W}/\mathrm{d}r$ by eliminating $\mathrm{d}\hat{\dot{R}}/\mathrm{d}r$ between (2.61) and (2.62),

$$\begin{aligned}\frac{\mathrm{d}\hat{W}}{\mathrm{d}r}=&\left(\frac{\left(1-\frac{2\hat{M}}{\hat{R}}-\frac{\Lambda\hat{R}^2}{3}\right)\frac{\mathrm{d}\hat{\sigma}}{\mathrm{d}r}}{\frac{\mathrm{d}\hat{R}}{\mathrm{d}r}}-\frac{\frac{\mathrm{d}\hat{M}}{\mathrm{d}r}}{R\frac{\mathrm{d}\hat{R}}{\mathrm{d}r}}+\frac{\hat{M}}{\hat{R}^2}-\frac{\Lambda\hat{R}}{3}\right)e^{\hat{\sigma}+\zeta}\\&+\frac{\left(\frac{\mathrm{d}^2\hat{R}}{\mathrm{d}r^2}-\frac{\mathrm{d}\zeta}{\mathrm{d}r}\frac{\mathrm{d}\hat{R}}{\mathrm{d}r}\right)}{e^{\hat{\sigma}+\zeta}}+\left(\frac{\mathrm{d}\zeta}{\mathrm{d}r}-\frac{\mathrm{d}\hat{\sigma}}{\mathrm{d}r}-\frac{\frac{\mathrm{d}^2\hat{R}}{\mathrm{d}r^2}}{\frac{\mathrm{d}\hat{R}}{\mathrm{d}r}}\right)\hat{W}\ .\end{aligned} \tag{2.63}$$

Another expression for $\mathrm{d}\hat{W}/\mathrm{d}r$ comes from the PNC derivative of (2.56),

$$\begin{aligned}\frac{\mathrm{d}\hat{W}}{\mathrm{d}r}=&\left(\frac{\left(1-\frac{2\hat{M}}{\hat{R}}-\frac{\Lambda\hat{R}^2}{3}\right)}{2\frac{\mathrm{d}\hat{R}}{\mathrm{d}r}}\left(\frac{\mathrm{d}\hat{\sigma}}{\mathrm{d}r}+\frac{\mathrm{d}\zeta}{\mathrm{d}r}-\frac{\frac{\mathrm{d}^2\hat{R}}{\mathrm{d}r^2}}{\frac{\mathrm{d}\hat{R}}{\mathrm{d}r}}\right)-\frac{\frac{\mathrm{d}\hat{M}}{\mathrm{d}r}}{R\frac{\mathrm{d}\hat{R}}{\mathrm{d}r}}+\frac{\hat{M}}{\hat{R}^2}-\frac{\Lambda\hat{R}}{3}\right)e^{\hat{\sigma}+\zeta}\\&+\frac{\left(\frac{\mathrm{d}^2\hat{R}}{\mathrm{d}r^2}-\left(\frac{\mathrm{d}\hat{\sigma}}{\mathrm{d}r}+\frac{\mathrm{d}\zeta}{\mathrm{d}r}\right)\frac{\mathrm{d}\hat{R}}{\mathrm{d}r}\right)}{2e^{\hat{\sigma}+\zeta}}\ .\end{aligned} \tag{2.64}$$

Setting these two equal, we find

$$\left(\frac{\mathrm{d}\hat{\sigma}}{\mathrm{d}r}-\frac{\mathrm{d}\zeta}{\mathrm{d}r}+\frac{\frac{\mathrm{d}^2\hat{R}}{\mathrm{d}r^2}}{\frac{\mathrm{d}\hat{R}}{\mathrm{d}r}}\right)\left(\frac{1}{2}\left(1-\frac{2\hat{M}}{\hat{R}}-\frac{\Lambda\hat{R}^2}{3}\right)e^{\hat{\sigma}+\zeta}+\frac{1}{2e^{\hat{\sigma}+\zeta}}-\hat{W}\right)=0\ , \tag{2.65}$$

so clearly[1]

$$\frac{\mathrm{d}\hat{\sigma}}{\mathrm{d}r}=\frac{\mathrm{d}\zeta}{\mathrm{d}r}-\frac{\frac{\mathrm{d}^2\hat{R}}{\mathrm{d}r^2}}{\frac{\mathrm{d}\hat{R}}{\mathrm{d}r}}\ . \tag{2.66}$$

[1]Putting the second bracket in (2.65) to zero does not give a PNC derivative.

We next want to convert our DEs to z derivatives, because the comoving coordinate r is not observable on the PNC. This requires a new function φ, that links r and z, which we define as

$$\frac{dr}{dz} = \varphi \ . \tag{2.67}$$

For any quantity Q on the PNC, we transform its derivatives using

$$\frac{\mathrm{d}\hat{Q}}{\mathrm{d}r} = \frac{\frac{\mathrm{d}\hat{Q}}{\mathrm{d}z}}{\varphi} \ , \qquad \frac{\mathrm{d}^2\hat{Q}}{\mathrm{d}r^2} = \frac{\frac{\mathrm{d}^2\hat{Q}}{\mathrm{d}z^2}}{\varphi^2} - \frac{\frac{\mathrm{d}\hat{Q}}{\mathrm{d}z}\varphi_z}{\varphi^3} \ , \tag{2.68}$$

where $\varphi_z = \mathrm{d}\varphi/\mathrm{d}z$, so we will need (2.42) and its derivative,

$$\frac{\mathrm{d}\hat{r}}{\mathrm{d}z} = \varphi = \left.\frac{\mathrm{d}r}{\mathrm{d}z}\right|_{\wedge} = \frac{1}{e^{\zeta}Z(1+z)} \tag{2.69}$$

$$\frac{\mathrm{d}^2\hat{r}}{\mathrm{d}z^2} = \varphi_z = -\frac{1}{(1+z)Ze^{\zeta}}\left(\frac{\mathrm{d}\zeta}{\mathrm{d}z} + \frac{\left(\frac{\mathrm{d}Z}{\mathrm{d}z}\right)}{Z} + \frac{1}{(1+z)}\right) . \tag{2.70}$$

We also re-express the matter density in terms of the observed redshift-space density of sources using (2.53). Thus (2.66), (2.59), (2.53), (2.56) and (2.27) become

$$\varphi = \frac{\mathrm{d}\hat{r}}{\mathrm{d}z} = \frac{1}{e^{\zeta}Z(1+z)} \tag{2.71}$$

$$\frac{\mathrm{d}\hat{\sigma}}{\mathrm{d}z} = -\frac{\left(\frac{\mathrm{d}^2\hat{R}}{\mathrm{d}z^2}\right)}{\left(\frac{\mathrm{d}\hat{R}}{\mathrm{d}z}\right)} - \frac{\left(\frac{\mathrm{d}Z}{\mathrm{d}z}\right)}{Z} - \frac{1}{(1+z)} \ . \tag{2.72}$$

$$\frac{\mathrm{d}\hat{M}}{\mathrm{d}z} = \frac{\hat{R}^2}{2}\left(\frac{\kappa(\hat{\rho}+\hat{p})We^{\hat{\sigma}}}{(1+z)Z} - \kappa\hat{p}\left(\frac{\mathrm{d}\hat{R}}{\mathrm{d}z}\right)\right) \tag{2.73}$$

$$\hat{\rho} = \frac{\mu n}{\hat{R}^2 e^{\hat{\sigma}+\zeta}\varphi} = \frac{\mu n Z(1+z)}{\hat{R}^2 e^{\hat{\sigma}}} \ , \qquad \hat{p} = p(\hat{\rho}) \tag{2.74}$$

$$\hat{W} = \frac{\left(1 - \frac{2\hat{M}}{\hat{R}} - \frac{\Lambda\hat{R}^2}{3}\right)e^{\hat{\sigma}}}{(1+z)Z\left(\frac{\mathrm{d}\hat{R}}{\mathrm{d}z}\right)} + \frac{(1+z)Z\left(\frac{\mathrm{d}\hat{R}}{\mathrm{d}z}\right)}{2e^{\hat{\sigma}}} \tag{2.75}$$

$$\frac{\mathrm{d}\hat{t}}{\mathrm{d}z} = -\frac{1}{Z(1+z)} \ . \tag{2.76}$$

Note that the two first order DEs (2.71) and (2.72) replace the single second order DE for φ_z that appeared in the LT case, and also that $\mathrm{d}\zeta/\mathrm{d}z$ vanishes from these DEs. We now have a connected set of DEs, and we can make the gauge choices. We have the following combinations:

$$Z \ , \qquad Ze^{\zeta} \ , \qquad Ze^{-\hat{\sigma}} \ , \qquad \frac{\frac{\mathrm{d}Z}{\mathrm{d}z}}{Z} \ . \tag{2.77}$$

It is most important to make (2.71) and (2.72) integrable, then the rest will be integrable too. Therefore the most obvious choices are

$$e^{\zeta} = 1 \quad \rightarrow \quad \zeta = 0 \ , \quad \hat{\lambda} = 2\hat{\sigma} \ , \tag{2.78}$$

$$Z = Y(z) \quad \rightarrow \quad \hat{\dot{\lambda}} = 2(Y + \widehat{\sigma'} e^{-\zeta}) \ . \tag{2.79}$$

The first fixes the r coordinate relative to the metric functions, and the second fixes t relative to the rate of change of λ. Setting $Z = [\dot{\lambda}/2 - \sigma' e^{-\zeta}]_\wedge > 0$ is an assumption, equivalent to assuming the worldlines are expanding at every point on the PNC. Note that these choices do not extend beyond the top of the PNC. The purpose of $Y(z)$ is to keep $\hat{t}$ and $\hat{r}$ finite as the bang is approached and z diverges, as is the case in the FLRW models. For example, if $Y(z) = (1+z)$ then $t_o - \hat{t} = \hat{r} = z/(1+z)$, but if $Y(z) = 1$ then $t_o - \hat{t} = \hat{r} = \ln(1+z)$. If the numerical integration does not reach high z, then $Y = 1$ is simplest. For the choice (2.78) & (2.79), our DEs are

$$\varphi = \frac{\mathrm{d}\hat{r}}{\mathrm{d}z} = \frac{1}{Y(1+z)} \tag{2.80}$$

$$\frac{\mathrm{d}\hat{\sigma}}{\mathrm{d}z} = -\frac{\left(\frac{\mathrm{d}^2\hat{R}}{\mathrm{d}z^2}\right)}{\left(\frac{\mathrm{d}\hat{R}}{\mathrm{d}z}\right)} - \frac{Y_z}{Y} - \frac{1}{(1+z)} \tag{2.81}$$

$$\frac{\mathrm{d}\hat{M}}{\mathrm{d}z} = \frac{\hat{R}^2}{2}\left(\frac{\kappa(\hat{\rho}+\hat{p})We^{\hat{\sigma}}}{(1+z)Y} - \kappa\hat{p}\left(\frac{\mathrm{d}\hat{R}}{\mathrm{d}z}\right)\right) \tag{2.82}$$

$$\hat{\rho} = \frac{\mu n Y(1+z)}{\hat{R}^2 e^{\hat{\sigma}}} \ , \qquad \hat{p} = p(\hat{\rho}) \tag{2.83}$$

$$\hat{W} = \frac{\left(1 - \frac{2\hat{M}}{\hat{R}} - \frac{\Lambda\hat{R}^2}{3}\right)e^{\hat{\sigma}}}{2Y(1+z)\left(\frac{\mathrm{d}\hat{R}}{\mathrm{d}z}\right)} + \frac{Y(1+z)\left(\frac{\mathrm{d}\hat{R}}{\mathrm{d}z}\right)}{2e^{\hat{\sigma}}} \tag{2.84}$$

$$\frac{\mathrm{d}\hat{t}}{\mathrm{d}z} = -\frac{1}{Y(1+z)} \tag{2.85}$$

$$\frac{\mathrm{d}\hat{t}}{\mathrm{d}r} = -1 \ , \qquad \hat{t} = t_o - r \ . \tag{2.86}$$

Equations (2.80) to (2.85) are a system of DEs that can be integrated numerically in parallel to produce the metric and matter quantities $z(r)$, $\hat{\sigma}(r)$, $\hat{M}(r)$, $\hat{W}(r)$, $\hat{t}(r)$, $\hat{\rho}(r)$ and $\hat{p}(r)$ on the PNC, given the input functions $\hat{R}(z)$ and $\kappa\mu n(z)$. The last function $\hat{\lambda}(r)$ follows from the gauge choice. Since the observer coordinate approach of chapter 4 has been converted to a numerical procedure, this approach was not taken further.

Chapter 3

The Observer Coordinates

In this chapter we will review the basic concepts of the observational coordinate system as they were defined in many articles of the Observer Coordinates Program [3–5, 25, 61, 74, 82–85]. These coordinates are different from the usual spacetime coordinates and they have been set up by the authors to mirror the fact that observations provide a view of the universe down the past null cone, and not on a constant time slice. Solving the EFEs in these coordinates allows us to more easily relate real observations to the spacetime geometry on the PNC and its subsequent evolution.

3.1 The Coordinates and the Metric

The observer coordinates $x^a = (w, y, \theta, \phi) = (w, y, x^I)$ (where a ranges 0 - 3 and $I = 2, 3$) are centered on the observer's worldline $\mathcal{C}$ (see figure (3.1)), and they can be defined as follows:

(1) w is the observer's proper time, and it is used to label each past null cone along $\mathcal{C}$. For example, the surface of $w = constant$ specifies the set of light rays arriving at the observer ($\mathcal{C}$) at time w. Our principal PNC (that of the present time) is denoted as $w = w_0$. In general w will not be proper time for worldlines other than $\mathcal{C}$.

(2) y, is the radial coordinate along each light ray. It measures a kind of coordinate distance down each past null cone. It increases monotonically away from the central worldline $\mathcal{C}$, but is otherwise left flexible.

(3) θ and ϕ, are the longitude and latitude, the angles of the y lines as measured by the observer on $\mathcal{C}$. They are defined to be constant along each light ray. We write $x^I = (\theta, \phi)$, and although the 2-metric g_{IJ} would be that of a 2-sphere near $\mathcal{C}$, it would not retain this form further out.

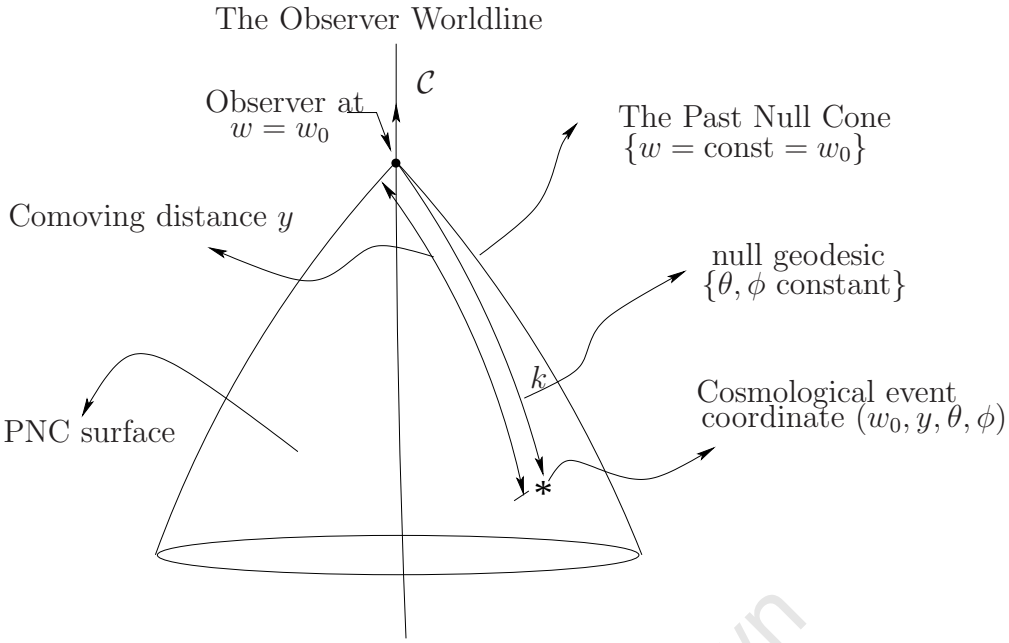

Figure 3.1: The observational coordinates (w, y, θ, ϕ) based on the observer event on the worldline $\mathcal{C}$

In this coordinate system, the observer's 4-velocity is $u^a = \mathrm{d}x^a/\mathrm{d}w|_{\mathcal{C}}$, and the tangent vector to the incoming light rays is $k^a = \mathrm{d}x^a/\mathrm{d}\nu$, where ν is an affine parameter along each light ray. The y coordinate lines are the incoming light rays — they follow constant w, θ and ϕ,

$$k^a \partial_a w = 0 \ , \qquad k^a \partial_a \theta = 0 \ , \qquad k^a \partial_a \phi = 0 \ , \tag{3.1}$$

and they are null

$$k^a k_a = 0 \ , \tag{3.2}$$

so

$$k^b = (1/\beta)\delta^b_1 \ , \tag{3.3}$$

where the function $\beta = \mathrm{d}\nu/\mathrm{d}y$ down the rays of the PNC, and it is non-vanishing for any well-behaved choice of y. Further, we normalise k^a such that

$$k_a = \partial_a w = \delta^0_a \ . \tag{3.4}$$

The property (3.2) allows us to deduce one of the metric tensor components,

$$k^a k_a = 0 \ , \quad \rightarrow \quad (k_c g^{ca})\, k_a = \delta^w_c \, g^{ca} \delta^w_a = g^{00} = 0 \ , \tag{3.5}$$

and similarly (3.3) and (3.4) give us

$$k^a = g^{ab} k_b \quad \rightarrow \quad (1/\beta)\delta^a_1 = g^{ab}\delta^0_b \quad \rightarrow \quad g^{a0} = (1/\beta)\delta^a_1 \ , \tag{3.6}$$

so that

$$g^{ab}g_{bc} = \delta^a_c \quad \rightarrow \quad g^{0b}g_{bc} = \delta^0_c \quad \rightarrow \quad g_{1c} = \beta\delta^0_c \ . \tag{3.7}$$

From all this, the list of metric components reads

$$g_{ab} = \begin{pmatrix} \alpha & \beta & v_2 & v_3 \\ \beta & 0 & 0 & 0 \\ v_2 & 0 & g_{22} & g_{23} \\ v_3 & 0 & g_{23} & g_{33} \end{pmatrix} \ , \qquad g^{ab} = \begin{pmatrix} 0 & 1/\beta & 0 & 0 \\ 1/\beta & \delta & \sigma_2 & \sigma_3 \\ 0 & \sigma_2 & g_{33}/h & -g_{23}/h \\ 0 & \sigma_3 & -g_{23}/h & g_{22}/h \end{pmatrix} \ , \tag{3.8}$$

where

$$h = \det(g_{IJ}) = g_{22}g_{33} - (g_{23})^2 \ , \tag{3.9}$$

$$\delta = -\frac{\alpha + \beta(v_2\sigma_2 + v_3\sigma_3)}{\beta^2} \ , \tag{3.10}$$

$$\sigma_2 = -\frac{v_2 g_{33} - v_3 g_{23}}{\beta h} \ , \tag{3.11}$$

$$\sigma_3 = -\frac{v_3 g_{22} - v_2 g_{23}}{\beta h} \ . \tag{3.12}$$

In these coordinates, the non-vanishing Christoffel symbols are

$$\Gamma^a{}_{bc} = \frac{1}{2}g^{ad}\left(\frac{\partial g_{db}}{\partial x^c} + \frac{\partial g_{dc}}{\partial x^b} - \frac{\partial g_{bc}}{\partial x^d}\right), \tag{3.13}$$

are calculated as follows:

$$\Gamma^0{}_{00} = \left(\frac{\beta_{,0}}{\beta} - \frac{\alpha_{,1}}{2\beta}\right) ,$$

$$\Gamma^0{}_{0I} = \left(\frac{\beta_{,I}}{\beta} - \frac{v_{I,1}}{2\beta}\right) \ ,$$

$$\Gamma^0{}_{IJ} = \frac{g_{IJ,1}}{2\beta} \ ,$$

$$\Gamma^1{}_{00} = \frac{1}{2}\left(\frac{\alpha_{,0}}{\beta} + \delta(2\beta_{,0} - \alpha_{,1}) + \sigma^I(2v_{I,0} - \alpha_{,I})\right) \ ,$$

$$\Gamma^1{}_{01} = \frac{1}{2}\left(\frac{\alpha_{,1}}{\beta} + \sigma^I(v_{I,1} - \alpha_{,I})\right) \ ,$$

$$\Gamma^1{}_{11} = \frac{\beta_{,1}}{\beta} \ ,$$

$$\Gamma^J{}_{01} = \frac{1}{2}g^{JI}\left(v_{I,1} - \beta_{,I}\right) \ ,$$

$$\Gamma^k{}_{1I} = \frac{1}{2}g^{kJ}g_{IJ,1} \ ,$$

$$\Gamma^1{}_{02} = \frac{1}{2}\left(\frac{\alpha_{,2}}{\beta} + \delta(2\beta_{,2} - v_{2,1}) + \sigma^2 g_{22,0} + \sigma^3(h_{23,0} + v_{3,2} - v_{2,3})\right) \ ,$$

$$\Gamma^1{}_{03} = \frac{1}{2}\left(\frac{\alpha_{,3}}{\beta} + \delta(2\beta_{,3} - v_{3,1}) + \sigma^3 g_{33,0} + \sigma^2(h_{23,0} + v_{2,3} - v_{3,2})\right) \ ,$$

$$
\begin{aligned}
\Gamma^1{}_{1I} &= \frac{1}{2}\left(\frac{\beta_{,I}}{\beta} + \frac{v_{I,1}}{\beta} + \sigma^J g_{IJ,1}\right) \ , \\
\Gamma^1{}_{22} &= \frac{1}{2}\left(\frac{(2v_{2,2} - g_{22,0})}{\beta} - \delta g_{22,1} + \sigma^2 g_{22,2} + \sigma^3(2h_{23,2} - g_{22,3})\right) \ , \\
\Gamma^1{}_{33} &= \frac{1}{2}\left(\frac{(2v_{3,3} - g_{33,0})}{\beta} - \delta g_{33,1} + \sigma^3 g_{33,3} + \sigma^2(2h_{23,3} - g_{33,2})\right) \ , \\
\Gamma^1{}_{23} &= \frac{1}{2}\left(\frac{(v_{2,3} + v_{3,2} - h_{23,0})}{\beta} - \delta h_{23,1} + \sigma^2 g_{22,3} + \sigma^3 g_{33,2}\right) \ , \\
\Gamma^2{}_{00} &= \frac{1}{2}\left(\sigma^2(2\beta_{,0} - \alpha_{,1}) + g^{2I}(2v_{I,0} - \alpha_{,I})\right) \ , \\
\Gamma^2{}_{02} &= \frac{1}{2}\left(\sigma^2(\beta_{,2} - v_{2,1}) + g^{22}g_{22,0} + g^{23}(h_{23,0} + v_{3,2} - v_{2,3})\right) \ , \\
\Gamma^2{}_{03} &= \frac{1}{2}\left(\sigma^2(\beta_{,3} - v_{3,1}) + g^{23}g_{33,0} + g^{22}(h_{23,0} + v_{2,3} - v_{3,2})\right) \ , \\
\Gamma^3{}_{03} &= \frac{1}{2}\left(\sigma^3(\beta_{,3} - v_{3,1}) + g^{33}g_{33,0} + g^{23}(h_{23,0} + v_{2,3} - v_{3,2})\right) \ , \\
\Gamma^2{}_{22} &= \frac{1}{2}\left(g^{22}g_{22,2} - g^{23}(g_{22,3} - 2h_{23,2}) - \sigma^2 g_{22,1}\right) \ , \\
\Gamma^2{}_{23} &= \frac{1}{2}\left(g^{22}g_{22,3} + g^{23}g_{33,2} - \sigma^2 h_{23,1}\right) \ , \\
\Gamma^2{}_{33} &= \frac{1}{2}\left(g^{23}g_{33,3} - g^{22}(2h_{23,3} - g_{33,2}) - \sigma^2 g_{33,1}\right) \ , \\
\Gamma^3{}_{00} &= \frac{1}{2}\left(\sigma^3(2\beta_{,0} - \alpha_{,1}) + g^{3I}(2v_{I,0} - \alpha_{,I})\right) \ , \\
\Gamma^3{}_{02} &= \frac{1}{2}\left(\sigma^3(2\beta_{,2} - v_{2,1}) + g^{33}(h_{23,0} + v_{3,2} - v_{2,3}) + g^{23}g_{22,0}\right) \ , \\
\Gamma^3{}_{22} &= \frac{1}{2}\left(g^{33}(2h_{23,2} - g_{22,3}) + g^{23}g_{22,2} - \sigma^3 g_{22,1}\right) \ , \\
\Gamma^3{}_{33} &= \frac{1}{2}\left(g^{33}g_{33,3} - g^{23}(g_{33,2} - 2h_{23,3}) - \sigma^3 g_{33,1}\right) \ , \\
\Gamma^3{}_{23} &= \frac{1}{2}\left(g^{33}g_{33,2} + g^{23}g_{22,3} - \sigma^3 h_{23,1}\right) \ ,
\end{aligned}
\tag{3.14}
$$

where $h_{23} = g_{23}/h$. It may easily be verified that, given the above metric form, the null vector k^a defined in (3.3) and (3.4) is also geodesic,

$$
k^a \nabla_a k^b = \left[0,\ k^1\left(\partial_1 k^1 + \frac{\partial_1 \beta}{\beta} k^1\right),\ 0,\ 0\right] = 0 \ . \tag{3.15}
$$

Note that the above applies to any choice of the observer's worldline $\mathcal{C}$. A further condition would be needed to make $\mathcal{C}$ geodesic.

3.2 Gauge Freedoms

The coordinates so defined retain some gauge freedom, which should be fixed before carrying out explicit calculations. The freedoms are explained as follows:

- w: if we specify w on our worldline, then automatically it will be fixed on other worldlines. For example, the obvious choice of w is to represent the proper time on the observer's worldline.

- y: there are many options associated with choice of y, for instance, it can be chosen to represent the affine parameter ν, or the redshift z, or the luminosity distance d_L, or one of these can be used on an initial worldline and then propagated along the fluid flow lines. In general, this last is a good choice, if the observer and the sources are comoving with the fluid, and our observations occur at a single time relative to cosmic timescales. Thus, having constrained the PNC with observational data, the EFEs are used to evolve this initial data.

- Finally, θ and ϕ: these can be transformed by a rigid rotation about the center i.e. the observer's worldline.

3.3 The Matter and the EFEs

The standard assumption is that of a perfect fluid

$$T^{ab} = (\rho + p)u^a u^b + p g^{ab} \ , \tag{3.16}$$

where u^a is the fluid 4-velocity. If the fluid is comoving, then $u^a = (1/\sqrt{\alpha}, 0, 0, 0)$. At the time the main OC papers were written, a universe composed of dust and isotropic radiation seemed a good description, and dust ($p = 0$) with zero Λ was used for the post-recombination region.

3.4 Relation to Observables and Physical Quantities

In this section we will present a derivation of the cosmological source observable quantities, the redshift z, the angular diameter and luminosity distances d_D and d_L and the reshift-space density $\kappa\mu n$, similar to the one in section 2.4, but this time we use the observer coordinates. For figures see section 2.4.

The chosen form of the OC metric (3.8) ensures the equation of the past null cone is very simple

$$w = \text{constant} \ , \qquad dw = 0 \tag{3.17}$$

with the $w = w_0$ being the PNC of present day observations.

The Redshift We assume that both emitter and observer are comoving, following curves of constant (y, θ, ϕ). The redshift of a comoving cosmological source on the null cone can be defined as the ratio between the light oscillation periods T measured at the observer o and the emitter e,

$$T = \frac{\partial \tau}{\partial w}\bigg| \, dw = \tau_w \, dw = \sqrt{\alpha} \;\; dw \;\; , \tag{3.18}$$

where τ is the proper time along the constant y worldlines. Since w is constant along the PNC, we apply a Taylor expansion along the light paths AB and CD of figure 2.1,

$$\tau_B = \tau_A + \hat{\tau}_y|_A \, dy \;\; , \qquad\qquad \tau_D = \tau_C + \hat{\tau}_y|_C \, dy \;\; . \tag{3.19}$$

Note that $\hat{\tau}_y$ is negative, so the change in the light oscillation periods T, as measured by comoving observers, between the points AC and BD is

$$dT = T_{BD} - T_{AC} = (\tau_D - \tau_B) - (\tau_C - \tau_A) \;\; . \tag{3.20}$$

Substituting (3.19) into (3.20), produces

$$dT = (\hat{\tau}_y|_C - \hat{\tau}_y|_A) \, dy \;\; , \tag{3.21}$$

and doing another Taylor expansion along AC, a worldline of constant y, gives

$$\hat{\tau}_y|_C = \hat{\tau}_y|_A + \frac{\partial \hat{\tau}_y}{\partial \tau}\bigg|_A \, T \;\; . \tag{3.22}$$

Now, combining (3.21), (3.22) and (3.18),

$$\frac{dT}{T} = \frac{\partial \hat{\tau}_y}{\partial \tau} = \frac{1}{\sqrt{\alpha}} \frac{\partial}{\partial w} \left(\frac{\partial}{\partial y} \hat{\tau} \right) \, dy = \frac{1}{\sqrt{\alpha}} \left(\frac{\partial}{\partial y} \tau_w \right) \, dy \tag{3.23}$$

$$= \frac{1}{\sqrt{\alpha}} \left(\frac{\partial}{\partial y} \sqrt{\alpha} \right) \, dy \tag{3.24}$$

so integrating this equation along the surface of constant w, i.e down the PNC, yields

$$\ln \frac{T_e}{T_o} = \ln \frac{(\sqrt{\alpha}\,)_e}{(\sqrt{\alpha}\,)_o} \quad \rightarrow \quad \frac{T_e}{T_o} = \frac{(\sqrt{\alpha}\,)_e}{(\sqrt{\alpha}\,)_o} \;\; , \tag{3.25}$$

and, by the fact that $(1+z) = \frac{T_o}{T_e}$, (3.25) gives

$$(1+z) = \frac{(\sqrt{\alpha}\,)_o}{(\sqrt{\alpha}\,)_e} \;\; . \tag{3.26}$$

Diameter distance The areal radius R, and the "angular" 2-metric f_{IJ} can be defined by (see [25] for more information about the derivation of this formula)

$$R^4 \sin^2\theta = h \ , \qquad f_{IJ} = \frac{g_{IJ}}{R^2} \ . \tag{3.27}$$

and $R(w, y, \theta, \phi)$ is the diameter distance of a source at (y, θ, ϕ) measured by $\mathcal{C}$ at time w. If multiple measurements of the shape of a source could be made, and the source's orientation and size $d\ell$ in 3-d is known, then

$$d\ell^2 = h_{IJ}\big|_{source}\, dx^I\, dx^J \tag{3.28}$$

could in principle provide the 2-metric components in that vicinity. Considerable detail is provided in [25].

Angular Drift If the source proper time is τ, and its 4-velocity is $u^a = \frac{\mathrm{d}x^a}{\mathrm{d}\tau}$, then

$$\frac{\mathrm{d}w}{\mathrm{d}\tau} = u^0 = 1 + z \ , \tag{3.29}$$

so that u^0 is deducible from a redshift measurement. Similarly, if the angular drift of the sources $(\frac{\mathrm{d}\theta}{\mathrm{d}w}, \frac{\mathrm{d}\phi}{\mathrm{d}w})$ can be measured, then

$$u^2 = \frac{\mathrm{d}\theta}{\mathrm{d}\tau} = (1+z)\frac{\mathrm{d}\theta}{\mathrm{d}w} \ , \qquad u^3 = \frac{\mathrm{d}\phi}{\mathrm{d}\tau} = (1+z)\frac{\mathrm{d}\phi}{\mathrm{d}w} \tag{3.30}$$

and u^1 follows from $u^a u_a = -1$ and involves local metric components.

Number Counts We look along a pencil of rays of solid angle $d\omega$, and we count the number of sources dN between z and $z + dz$. Suppose the density of sources in redshift space is n per steradian per unit redshift interval, and the average mass per source is μ, then the mass in that volume element is

$$d\mathcal{M} = \mu dN = \mu n\, d\omega\, dz = \mu n\, \sin\theta\, d\theta\, d\phi\, dz \ . \tag{3.31}$$

On the other hand, if ρ is the proper density (relative to the comoving worldlines) then the mass in solid angle $d\omega$ between y and $y + dy$ is

$$d\mathcal{M} = \rho\, d^3\mathcal{V} \tag{3.32}$$

and the proper volume is [37]

$$d^3\mathcal{V} = \eta_{abcd}\, u^a\, dx_1^b\, dx_2^c\, dx_3^d \tag{3.33}$$

$$= \sqrt{|g|}\ \epsilon_{0123} \left(\frac{1}{\sqrt{|\alpha|}}\right) dy\, d\theta\, d\phi \tag{3.34}$$

$$= \frac{\beta\sqrt{h}}{\sqrt{|\alpha|}}\, dy\, d\theta\, d\phi \tag{3.35}$$

$$= \frac{\beta}{\sqrt{|\alpha|}}\, R^2\, \sin\theta\, dy\, d\theta\, d\phi \tag{3.36}$$

where (3.27) was used. Combining (3.31), (3.32) and (3.36) on the PNC we have

$$\mu n\, dz = \hat{\rho}\, \frac{\hat{\beta}\, \hat{R}^2}{\sqrt{|\hat{\alpha}|}}\, dy\ . \tag{3.37}$$

If $F(z)$ is the fraction of actual sources that is observed, then the number count $\tilde{N}$ derived from observations is given by

$$\frac{\mathrm{d}\tilde{N}}{\mathrm{d}z} = F\frac{\mathrm{d}N}{\mathrm{d}z} = F\, n\, d\omega \qquad \rightarrow \qquad n = \frac{d\tilde{N}}{F\, dz\, d\omega}\ . \tag{3.38}$$

3.5 Fermi Normal Coordinates and Null Geodesic Based Normal Coordinates

We here show how regularity conditions at the centre of spherical symmetry are established. First we show the connection the above OCs and Fermi normal coordinates (FNCs).

Let indices r, p, q and s run over $\{1, 2, 3\}$. FNCs $x^a = (\tau, x^p)$ [28] use the fact that for a given point P in spacetime it is always possible to find a coordinate system such that

$$g_{ab}(P) = \tilde{\eta}_{ab} \qquad\qquad \Gamma^a{}_{bc}(P) = 0\ . \tag{3.39}$$

Here $\tilde{\eta}_{ab}$ represents the metric in flat space, and the above equation is sometimes refered to as "the local flatness-therom". This theory may be extended to include an entire geodesic, and it has been shown that for a timelike geodesic the metric tensor can be written as

$$\begin{aligned} g_{00} &= -1 - R_{0p0q}(\tau)\, x^p\, x^q + O(x^3)\ , \\ g_{0r} &= -\frac{2}{3} R_{0prq}(\tau)\, x^p\, x^q + O(x^3)\ , \\ g_{rs} &= \delta_{rs} - \frac{1}{3} R_{rpsq}(\tau)\, x^p\, x^q + O(x^3)\ , \end{aligned} \tag{3.40}$$

where τ is the proper time along the geodesic, and R_{rpsq} is the curvature tensor and.

The concept of FNCs was adopted by [60] to find corresponding version of the metric expansion form of (3.40) near the central worldline $\mathcal{C}$. In doing so, they introduced a new set of coordinates called "null geodesic based normal coordinates" of a point p lying an

affine parameter distance ν from $\mathcal{C}$ on the null geodesic, with spatial direction ℓ^p on the PNC, such that

$$x^a(p) = (w - \nu, \ell^p\, \nu) \ ,$$

and

$$x^0(\nu) = w - \nu \ , \qquad\qquad x^p(\nu) = \ell^p\, \nu \ ,$$

are the components of the null geodesic through $w = w_0$ of $\mathcal{C}$ in the direction ℓ^p, and ν is related to the comoving coordinate y via β as mentioned earlier in this chapter. Here ℓ^p are the direction cosines that define the standard coordinates (θ, ϕ) of a unit 2-sphere,

$$\ell^p(\theta, \phi) = (\sin\theta \sin\phi, \sin\theta \cos\phi, \cos\theta) \ , \qquad\qquad \sum_{p=1}^{3} (\ell^p\, \ell^p) = 1 \ . \tag{3.41}$$

Using these coordinates, we can transform the metric components as

$$\begin{aligned} g_{ww} &= g_{00}\, \frac{\partial x^0}{\partial w}\, \frac{\partial x^0}{\partial w} = g_{00} \ , \\ g_{wI} &= g_{0p}\, \frac{\partial x^p}{\partial x^I} = \left(g_{0p}\, \frac{\partial \ell^p}{\partial x^I} \right) \nu \ , \\ g_{II} &= g_{pq}\, \frac{\partial x^p}{\partial x^I}\, \frac{\partial x^q}{\partial x^I} = \left(g_{pq}\, \frac{\partial \ell^p}{\partial x^I}\, \frac{\partial \ell^q}{\partial x^I} \right) \nu^2 \ . \end{aligned} \tag{3.42}$$

where $I = (\theta, \phi)$. On other hand, the rest of metric components are related to coordinates ν & w via

$$k^a = \delta^a_\nu \ , \qquad k_a = \delta^w_a \ , \qquad \delta^w_a = g_{ab} \delta^b_\nu = g_{\nu a} \ , \tag{3.43}$$

so substituting (3.43) and (3.40) into (3.42) produces

$$\begin{aligned} \alpha(w, \nu, x^I) &= -1 - \Big[R_{0p0q}(w, 0)\, \ell^p\, \ell^q \Big] \nu^2 + O(\nu^3) \ , \\ \beta(w, \nu, x^I) &= 1 \ , \\ v_I((w, \nu, x^I)) &= \left[R_{0piq}(w, 0)\, \ell^p\, \frac{\partial \ell^r}{\partial x^I} \ell^q \right] \nu^3 + O(\nu^4) \ , \\ g_{IJ}(w, \theta, \phi) &= \mathrm{diag}(1, \sin^2\theta) \nu^2 + \frac{1}{3} \Big[R_{rpsq}(w, 0)\, \frac{\partial \ell^r}{\partial x^I} \ell^p\, \frac{\partial \ell^s}{\partial x^J} \ell^q \Big] \nu^3 + O(\nu^4) \ . \end{aligned} \tag{3.44}$$

Remember that $\ell^p = \ell^p(\theta, \phi)$. Now, to find the origin behavior of Eq (3.44), we must take the limit as $y \to 0$, so when we use the gauge choice $y = \nu$, this is

$$\lim_{\nu \to 0} \alpha = -1 \ , \qquad \lim_{\nu \to 0} \beta = 1 \ , \qquad \lim_{\nu \to 0} \left(\frac{v_I}{\nu^2} \right) = 0 \ , \qquad \lim_{\nu \to 0} \left(\frac{g_{IJ}}{\nu^2} \right) = \mathrm{diag}(1, \sin^2\theta) \ . \tag{3.45}$$

It is obvious that the metric is regular at the central worldline $\mathcal{C}$, thus we say that the coordinates x^a are the observational coordinates if and only if the metric tensor can be written in the form of (3.8) and regular at the center.

Chapter 4

Observer Coordinates Solution for the Lemaître Model

In the previous chapter we have briefly introduced the basic concept of the observer coordinates, and their importance in the field of the observational cosmology program. We showed that these coordinates provide a good way of determining or studying the geometrical nature or matter content of the universe from the analysis of cosmological data.

Here we will use the observer coordinates mentioned above and solve for the metric functions, assuming a Lemaître model. This is the generalisation of the LT result [37] to the case of non-zero pressure and non-zero Cosmological constant. Broadly, this is a contribution to the Metric of the Cosmos project: given realistic observational data on our past null cone (PNC), and a minimal set of assumptions about the geometry and matter content of the universe, develop the equations and numerical codes that will enable us to extract the metric functions. This chapter will focus on deriving the equations and producing a theoretical algorithm. Two different approaches will be used. In the first approach, we will solve the EFEs directly in the observer coordinates, and reduce them to a system of differential Equations (DEs) plus arbitrary functions of integration. In the second one, we will use a coordinate transformation to convert the standard Lemaître solution, in (t, r) coordinates, into the observer coordinate form, in (w, y) coordinates. The introduction of non-zero pressure will make several quantities depend on time, that was not the case in the Lemaître-Tolman solution. Hence we must introduce an appropriate time definition to facilitate the solution process. Having obtained the necessary equations, there are two main parts to the solution process - the solution on the initial PNC, where the observational data are given, and the evolution of the spacetime metric to the future and past.

4.1 The Lemaître Metric in Observer Coordinates

If the general metric (3.8) of the OC coordinates of chapter 3 are specialised to the case of spherical symmetry, then the metric functions depend only on w and y, the 2-metric g_{IJ} becomes that of a 2-sphere, where the position of the observer coincides with the centre of the symmetry, and the components v_2 and v_3 can be set to zero. The remainder can be written [3–5, 10]:

$$ds^2 = -A^2\,dw^2 + 2AB\,dw\,dy + C^2\left(d\theta^2 + \sin^2\theta\,d\phi^2\right)\,, \tag{4.1}$$

where $C = C(w,y)$ is the areal radius, and $A = A(w,y)$, $B = B(w,y)$ are the other metric functions. The energy momentum tensor of the perfect fluid, which is comoving with the y coordinates, is given by

$$T^{ab} = (\rho + p)u^a u^b + g^{ab}p\,, \tag{4.2}$$

$$u^a = (A^{-1}, 0, 0, 0)\,, \qquad u_a = (-A, B, 0, 0)\,, \qquad u^a u_a = -1\,, \tag{4.3}$$

where $\rho = \rho(w,y)$ is the proper density and $p = p(w,y)$ is the fluid pressure relative to observers on the comoving worldlines u^a. This must be complemented by an equation of state

$$p = p(\rho)\,. \tag{4.4}$$

Unlike the zero-pressure Lemaître-Tolman case, we don't expect geodesic worldlines, as the pressure gradient will exert a net force on the fluid particles.

The most general w-y transformation that preserves this metric form, based on past null cones and fluid flow lines, is $w = w(\bar{w})$, $y = y(\bar{y})$ which gives $\bar{A} = A\,\partial w/\partial\bar{w}$, $\bar{B} = B\,\partial y/\partial\bar{y}$. Thus A could be set to a chosen value along just one worldline, and B along just one PNC.

4.2 Solving the EFEs

In the following, we will derive a set of constraint equations involving y derivatives, and a set of evolution equations involving w derivatives and sometimes y derivatives or integrals. The former are for the extraction of boundary conditions from PNC data, the latter are for evolving the model away from the PNC.

The Einstein Field equations (EFEs) $G^{ab} = \kappa T^{ab} - \Lambda g^{ab}$ for this metric are:

$$G^{ww} = \frac{2}{A^2B^2}\left(\frac{A_yC_y}{AC} + \frac{B_yC_y}{BC} - \frac{C_{yy}}{C}\right) = \frac{\kappa(\rho+p)}{A^2}\,, \tag{4.5}$$

$$G^{wy} = \frac{2}{A^2B^2}\left(\frac{C_{wy}}{C} + \frac{C_wC_y}{C^2} + \frac{AC_y^2}{2BC^2} + \frac{A_yC_y}{BC} - \frac{AB}{2C^2}\right) = \frac{\kappa p}{AB} - \frac{\Lambda}{AB}\ , \tag{4.6}$$

$$G^{yy} = \frac{2}{A^2B^2}\left(\frac{A_wC_w}{AC} + \frac{B_wC_w}{BC} - \frac{C_{ww}}{C} + \frac{A_yC_w}{BC} + \frac{AB_wC_y}{B^2C} + \frac{AC_wC_y}{BC^2} + \frac{AA_yC_y}{B^2C} + \frac{A^2C_y^2}{2B^2C^2} - \frac{A^2}{2C^2}\right) = \frac{\kappa p}{B^2} - \frac{\Lambda}{B^2}\ , \tag{4.7}$$

$$G^{\theta\theta} = \frac{1}{ABC^2}\left(\frac{2C_{wy}}{C} + \frac{A_{wy}}{A} + \frac{B_{wy}}{B} - \frac{A_wA_y}{A^2} - \frac{B_wB_y}{B^2} + \frac{AC_{yy}}{BC} + \frac{A_{yy}}{B} - \frac{A_yB_y}{B^2} + \frac{A_yC_y}{BC} - \frac{AB_yC_y}{B^2C}\right) = \frac{\kappa p}{C^2} - \frac{\Lambda}{C^2}\ , \tag{4.8}$$

where subscripts w and y indicate $\partial/\partial w$ and $\partial/\partial y$ respectively. The conservation equations, $\nabla_b T^{ab} = 0$ are:

$$\nabla_b T^{wb} = \frac{1}{A^2}\left\{\rho_w + p_w + p_y\frac{A}{B} + (\rho+p)\left(\frac{2C_w}{C} + \frac{2B_w}{B} + \frac{A_y}{B}\right)\right\} = 0\ , \tag{4.9}$$

$$\nabla_b T^{yb} = \frac{1}{B}\left\{\frac{p_w}{A} + \frac{p_y}{B} + (\rho+p)\left(\frac{B_w + A_y}{AB}\right)\right\} = 0\ . \tag{4.10}$$

In these coordinates the fluid acceleration is

$$a^c = u^b\nabla_b u^c = \frac{B_w + A_y}{A^2B^2}(B, A, 0, 0)\ , \tag{4.11}$$

and we see by comparing (4.11) with (4.10) that the particle worldlines would be geodesic if

$$Bp_w + Ap_y = 0\ . \tag{4.12}$$

The following subtraction of the conservation equations (4.9) and (4.10) gives

$$A^2\nabla_b T^{wb} - AB\nabla_b T^{yb} = \rho_w + (\rho+p)\left(\frac{2C_w}{C} + \frac{2B_w}{B} + \frac{A_y}{B}\right) - (\rho+p)\left(\frac{B_w + A_y}{B}\right) = 0\ , \tag{4.13}$$

which simplifies to

$$\frac{B_w}{B} = -\frac{\rho_w}{(p+\rho)} - 2\frac{C_w}{C}\ . \tag{4.14}$$

From (4.6) & (4.7) above we obtain

$$\frac{A^2BC}{2}G^{wy} - \frac{AB^2C}{2}G^{yy} = \frac{C_{wy}}{B} - \frac{B_wC_y}{B^2} + \frac{C_{ww}}{A} - \frac{A_wC_w}{A^2} - \frac{C_w}{AB}(A_y + B_w) = 0\ , \tag{4.15}$$

and this can be written as

$$\frac{\partial}{\partial w}\left(\frac{C_w}{A}+\frac{C_y}{B}\right)=\frac{C_w}{AB}\left(A_y+B_w\right)\ . \tag{4.16}$$

We choose the term in parentheses on the left hand side to be

$$\frac{C_w}{A}+\frac{C_y}{B}=W\ , \tag{4.17}$$

where $W=W(w,y)$ is an undetermined function, which, we shall see, describes the curvature of the spacetime. Clearly, equation (4.16) with (4.17) gives an evolution formula for W

$$W_w=\frac{C_w}{AB}\left(A_y+B_w\right)\ , \tag{4.18}$$

which can be combined with (4.10) to produce

$$W_w=-\frac{C_w\big(Bp_w+Ap_y\big)}{AB(\rho+p)}\ . \tag{4.19}$$

Multiplying the yy EFE (4.7) by $-B^2C^2C_w$ gives

$$\begin{aligned}&-\frac{2CC_w^2A_w}{A^3}+\frac{2CC_wC_{ww}}{A^2}-\frac{2CC_w}{AB}\Big[B_w+A_y\Big]\left[\frac{C_w}{A}+\frac{C_y}{B}\right]\\&-C_w\left[\frac{C_y^2}{B^2}+2\frac{C_wC_y}{AB}-1\right]=-\kappa pC^2C_w+C^2C_w\Lambda\ ,\end{aligned} \tag{4.20}$$

and recognising the W_w of (4.18) in the 3rd term of (4.20) and the W of (4.17) in the 3rd & 4th terms, we substitute and rearrange it to produce

$$\frac{C_w^3}{A^2}+\frac{2CC_wC_{ww}}{A^2}-\frac{2CC_w^2A_w}{A^3}-C_w(W^2-1)-2CWW_w-C^2C_w\Lambda=-\kappa pC^2C_w\ . \tag{4.21}$$

This expression can be rewritten as a w derivative,

$$\frac{\partial}{\partial w}\left(\frac{CC_w^2}{A^2}-C(W^2-1)-\frac{C^3\Lambda}{3}\right)=-\kappa pC^2C_w \tag{4.22}$$

$$\frac{CC_w^2}{A^2}-C(W^2-1)-\frac{C^3\Lambda}{3}=2M(w,y)\ , \tag{4.23}$$

where $M(w,y)$ is a second undetermined function, which describes the total gravitational mass within a comoving shell of radius C. With this, (4.22) defines the pressure as

$$\kappa p=-\frac{2M_w}{C^2C_w}\ . \tag{4.24}$$

The y derivatives of (4.17) and (4.23) are

$$W_y=\frac{C_{wy}}{A}+\frac{C_{yy}}{B}-\frac{C_wA_y}{A^2}-\frac{C_yB_y}{B^2} \tag{4.25}$$

$$2M_y = \frac{2CC_wC_{wy}}{A^2} - \frac{2CC_w^2A_y}{A^3} - 2CWW_y + \left(\frac{C_w^2}{A^2} - W^2 + 1 - C^2\Lambda\right)C_y \ . \tag{4.26}$$

Combining A^2BC^2W times (4.5) and $(-ABC^2C_y)$ times (4.6) we find

$$\begin{aligned}
\kappa(\rho+p)BC^2\left(\frac{C_w}{A}+\frac{C_y}{B}\right) - (\kappa p-\Lambda)C^2C_y &= A^2BC^2\left(\frac{C_w}{A}+\frac{C_y}{B}\right)G^{ww} - ABC^2C_yG^{wy} \\
&= -2C\left(\frac{C_{yy}}{B} - \frac{C_yA_y}{AB} - \frac{C_yB_y}{B^2}\right)\left(\frac{C_w}{A}+\frac{C_y}{B}\right) \\
&\quad - \left(\frac{2CC_{wy}}{AB} - 1 + \frac{2C_wC_y}{AB} + \frac{C_y^2}{B^2} + \frac{2CC_yA_y}{AB^2}\right)C_y \\
&= \frac{2CC_wC_{wy}}{A^2} - 2C\left(\frac{C_{wy}}{A} + \frac{C_{yy}}{B} - \frac{C_wA_y}{A^2} - \frac{C_yB_y}{B^2}\right)\left(\frac{C_w}{A}+\frac{C_y}{B}\right) \\
&\quad - \frac{2CC_w^2A_y}{A^3} + \left(\frac{C_w^2}{A^2} + 1 - \left(\frac{C_w}{A}+\frac{C_y}{B}\right)^2\right)C_y \\
&= \frac{2CC_wC_{wy}}{A^2} - 2CW_yW - \frac{2CC_w^2A_y}{A^3} + \left(\frac{C_w^2}{A^2} + 1 - W^2\right)C_y
\end{aligned} \tag{4.27}$$

where W_y and W from (4.25) and (4.17) were used in the last step. Comparing the above with (4.26) and utilising (4.17) and (4.24) in the following, we see that

$$\begin{aligned}
\kappa\rho BC^2\left(\frac{C_w}{A}+\frac{C_y}{B}\right) + \kappa p\frac{BC^2C_w}{A} + \Lambda C^2C_y &= 2M_y + \Lambda C^2C_y \\
\kappa\rho BC^2W &= 2M_y + \kappa pC^2\left(C_y - WB\right) \\
&= 2M_y - \kappa p\frac{BC^2C_w}{A} \\
\kappa\rho &= \frac{2M_y}{C^2BW} + \frac{2M_w}{C^2AW} \ .
\end{aligned} \tag{4.28}$$

From (4.23) the evolution equation of C is given by

$$\frac{C_w}{A} = \pm\sqrt{\frac{2M}{C} + f + \frac{\Lambda C^2}{3}} \ , \tag{4.29}$$

$$\text{where} \qquad f(w,y) = W^2 - 1 \qquad \leftrightarrow \qquad W = \sqrt{1+f} \ . \tag{4.30}$$

This shows how each spherical shell expands or contracts with time, but it cannot be solved by itself because it contains unknown functions of time such as A, f and M. From (4.17) we make C_y/B the subject and then substitute for C_w and f from (4.29) and (4.30) which gives

$$\frac{C_y}{B} = \sqrt{1+f} \mp \sqrt{\frac{2M}{C} + f + \frac{\Lambda C^2}{3}} \ . \tag{4.31}$$

From the conservation equations (4.9) times A^2 and (4.10) times AB, we substitute $p = p(\rho)$ in the terms that contain p_w and rearrange them as follows

$$\left(1 + \frac{\mathrm{d}p}{\mathrm{d}\rho}\right)\frac{\rho_w}{(\rho + p(\rho))} = -\frac{A}{B}\frac{p_y}{(\rho+p(\rho))} - \left(\frac{2C_w}{C} + \frac{2B_w}{B} + \frac{A_y}{B}\right) \ , \tag{4.32}$$

$$\left(\frac{\mathrm{d}p}{\mathrm{d}\rho}\right)\frac{\rho_w}{(\rho+p(\rho))} = -\frac{A}{B}\frac{p_y}{(\rho+p(\rho))} - \left(\frac{B_w+A_y}{B}\right) \ . \tag{4.33}$$

where $\mathrm{d}p/\mathrm{d}\rho$ is the derivative of the equation of state for the perfect fluid. To eliminate ρ_w, multiply (4.32) by $\mathrm{d}p/\mathrm{d}\rho$, (4.33) by $(1+\mathrm{d}p/\mathrm{d}\rho)$ and equate them, giving

$$0 = \left(1-\frac{\mathrm{d}p}{\mathrm{d}\rho}\right)\frac{B_w}{B} + \frac{A}{B}\frac{p_y}{(\rho+p(\rho))} + \frac{A_y}{B} - \left(\frac{\mathrm{d}p}{\mathrm{d}\rho}\right)\frac{2C_w}{C} \ . \tag{4.34}$$

Next substitute (4.29) into (4.34) for the value of C_w, and then rearrange the result as an evolution equation for B_w, which leads to

$$B_w = -\frac{A_y}{\left(1-\frac{\mathrm{d}p}{\mathrm{d}\rho}\right)} - \frac{A\,\mathrm{d}p/\mathrm{d}\rho}{\left(1-\frac{\mathrm{d}p}{\mathrm{d}\rho}\right)}\left[\frac{\rho_y}{(\rho+p(\rho))} \mp 2B\sqrt{\frac{2M}{C^3}+\frac{f}{C^2}+\frac{\Lambda}{3}}\right] \ . \tag{4.35}$$

Finding an expression for A_w is more tricky because substituting the w-derivative of (4.29) into (4.7) eliminates A_w. The $\theta\theta$, ww, and wy EFEs can be combined to produce

$$\begin{aligned} ABC^2G^{\theta\theta} + \frac{A^3B}{2}G^{ww} - A^2B^2G^{wy} = \frac{A_{wy}}{A} + \frac{B_{wy}}{B} - \frac{A_wA_y}{A^2} - \frac{B_wB_y}{B^2} \\ + \frac{A_{yy}}{B} - \frac{A_yB_y}{B^2} - \frac{2C_wC_y}{C} - \frac{AC_y^2}{BC^2} + \frac{AB}{C^2} - \frac{\kappa(p+\rho)}{2}AB = 0 \ . \end{aligned} \tag{4.36}$$

Rearranging (4.36) as a y derivative plus extra terms gives

$$\frac{\partial}{\partial y}\left[\frac{A_w}{A}+\frac{B_w+A_y}{B}\right] - \left[\frac{2C_wC_y}{C^2}+\frac{AC_y^2}{BC^2}-\frac{AB}{C^2}\right] - \frac{\kappa(p+\rho)}{2}AB = 0 \ , \tag{4.37}$$

and using (4.23) with (4.17), the second term of (4.37) can be replaced by the mass term, i.e.

$$\frac{\partial}{\partial y}\left[\frac{A_w}{A}+\frac{B_w+A_y}{B}\right] + AB\left[\frac{2M}{C^3}+\frac{\Lambda}{3}-\frac{\kappa(p+\rho)}{2}\right] = 0 \ , \tag{4.38}$$

which integrates to give

$$A_w = A\left\{\int_0^y\left[\frac{\kappa(p+\rho)}{2}-\frac{2M}{C^3}-\frac{\Lambda}{3}\right]AB\,dy - \left[\frac{B_w+A_y}{B}\right]+\Phi(w)\right\} \ , \tag{4.39}$$

where $\Phi(w)$ is an arbitrary function of integration. Finally we substitute (4.35) into (4.39) giving

$$A_w = A\left\{U + \frac{\mathrm{d}p/\mathrm{d}\rho}{\left(1-\frac{\mathrm{d}p}{\mathrm{d}\rho}\right)}\left[\frac{A_y}{B}+\frac{A}{B}\frac{\rho_y}{(p(\rho)+\rho)} \mp 2A\sqrt{\frac{2M}{C^3}+\frac{f}{C^2}+\frac{\Lambda}{3}}\right]+\Phi\right\} \ , \tag{4.40}$$

where
$$U = \int_0^y\left[\frac{\kappa(p(\rho)+\rho)}{2}-\frac{2M}{C^3}-\frac{\Lambda}{3}\right]AB\,dy \ . \tag{4.41}$$

The integration in U can be evaluated along each light cone of constant w, but at present it is just a formal expression, as $C(w,y)$, $M(w,y)$ and $\rho(w,y)$ are not yet known. As noted earlier, there is a freedom in the w coordinate which translates into a freedom in A. The observer's worldline at $y=0$ is the obvious place to fix it, e.g. $A(w,0)=1$ makes w the observer's proper time. More generally, if

$$A(w,0) = \tilde{A}(w) \ , \tag{4.42}$$

then

$$A_w(w,0) = \tilde{A}_w \ , \tag{4.43}$$

and this can be used to fix Φ from $\tilde{A}_w$ (or vice-versa).

Eqs (4.18), (4.24), (4.29), (4.35), and (4.40) are a set of differential equations (DEs) for W_w, M_w, C_w, B_w and A_w, that govern the dynamics of the model in observer coordinates, given a set of initial values. This sytem of DEs can be integrated directly with respect to w to give numerical values for $W(w,y)$, $M(w,y)$, $A(w,y)$, $B(w,y)$ and $C(w,y)$ once the arbitrary functions have been determined on the observer's PNC.

4.3 The Transformation from (w,y) to (t,r) Coordinates

This section makes the connection between the above metric quantities in observer coordinates (w,y,θ,ϕ) and the solution of the Lemaître model in standard (t,r,θ,ϕ) coordinates. This is a useful cross-check on the above equations, and it assists with comparing a numerical solution with an original model.

We define the time coordinate $t(w,y)$ along worldlines of constant y by

$$t - \hat{t} = \int_{w_0}^{w} A\, e^{-\sigma}\, dw \quad \leftrightarrow \quad A = t_w\, e^{\sigma} \quad \leftrightarrow \quad t_w = A\, e^{-\sigma} \ . \tag{4.44}$$

where σ is a kind of lapse function in the (t,r) coordinate system, which is related to the choice of time coordinate t, and $\hat{t}(y) = t(w_0,y)$ is its value on the PNC. Because t is defined in terms of σ, a newly introduced function of two coordinates, a gauge choice will be needed to fix $\hat{t}$ on $w=w_0$ (or some other initial value for t), and another to fix t along the central worldline (or some other one). Having defined t, we define $r(w,y)$ to equal y so that we have

$$r_w = 0 \ , \qquad\qquad r_y = 1 \ . \tag{4.45}$$

Applying an orthogonality condition between the t and r coordinates, produces

$$\begin{aligned} 0 = g^{ab}\,(\partial_a t)\,(\partial_b r) &= \frac{t_w\,r_y + t_y\,r_w}{AB} + \frac{t_y\,r_y}{B^2} \\ &= \frac{A\,e^{-\sigma}}{AB} + \frac{t_y}{B^2} \\ t_y = -B\,e^{-\sigma} \quad &\leftrightarrow \quad B = -t_y\,e^{\sigma}\ . \end{aligned} \tag{4.46}$$

Thus $Be^{-\sigma}$ is the negative of the rate of variation of the t coordinate with respect to y down the past null cone. We combine (4.44) and (4.46) into a consistency or integrability condition

$$\begin{aligned} t_{wy} = \frac{\partial}{\partial y}\left(A\,e^{-\sigma}\right) &= A_y\,e^{-\sigma} - A\,\sigma_y\,e^{-\sigma} \\ = \frac{\partial}{\partial w}\left(-B\,e^{-\sigma}\right) &= -B_w\,e^{-\sigma} + B\,\sigma_w\,e^{-\sigma} \qquad (4.47) \\ \rightarrow \qquad A_y + B_w &= A\,\sigma_y + B\,\sigma_w \qquad (4.48) \end{aligned}$$

According to (4.44), (4.45) and (4.46) we define the Jacobi matrix and its inverse by:

$$J = \frac{\partial(t,r)}{\partial(w,y)} = \begin{pmatrix} t_w & t_y \\ r_w & r_y \end{pmatrix} = \begin{pmatrix} Ae^{-\sigma} & -Be^{-\sigma} \\ 0 & 1 \end{pmatrix} \tag{4.49}$$

and

$$J^{-1} = \frac{\partial(w,y)}{\partial(t,r)} = \begin{pmatrix} w_t & w_r \\ y_t & y_r \end{pmatrix} = \begin{pmatrix} \frac{1}{t_w} & -\frac{t_y}{t_w} \\ 0 & 1 \end{pmatrix} = \begin{pmatrix} \frac{e^{\sigma}}{A} & \frac{B}{A} \\ 0 & 1 \end{pmatrix}\ , \tag{4.50}$$

where subscripts t and r mean $\partial/\partial t$ and $\partial/\partial r$. Further, we define $\lambda(w,y)$ by

$$e^{\lambda/2} = B\ . \tag{4.51}$$

Now we can recover some of the equations from section 2.2.

Firstly, writing $dw = w_t\,dt + w_r\,dr$ and $dy = y_t\,dt + y_r\,dr$, and using (4.50) and (4.51), we transform the metric (4.1) into (2.1).

Next the transformation between $C(w,y)$ and $C(t,r)$ allows us to write, using (4.50) to substitute for w_t and y_t,

$$C_t = C_w w_t + C_y y_t = C_w\left(\frac{e^{\sigma}}{A}\right)\ , \tag{4.52}$$

and we find, using (4.29), that

$$C_t = \pm e^{\sigma}\sqrt{\frac{2M}{C} + f + \frac{\Lambda C^2}{3}}\ , \tag{4.53}$$

which reproduces (2.15).

Using this and the definition of t, we obtain a formal integral from the bang to the PNC,

$$\int_0^{\hat{C}} \frac{dC}{\pm\sqrt{\frac{2M}{C}+f+\frac{\Lambda C^2}{3}}} = \tau = \int_{a(r)}^{\hat{t}} e^{\sigma} dt \ , \tag{4.54}$$

where τ is the proper time along the worldlines from bang to PNC, and it involves $a(r)$ which fixes the initial time $t = a$, when $C = 0$, at each $r = y$.[1] For all other times before and after $\hat{t}$ the integral is

$$\int_C^{\hat{C}} \frac{dC}{\pm\sqrt{\frac{2M}{C}+f+\frac{\Lambda C^2}{3}}} = \int_t^{\hat{t}} e^{\sigma} dt \ . \tag{4.55}$$

The '$\pm$' allows for the possibility that expansion may change to collapse along some worldlines. Though this equation seems to give $t(C, y)$ or $C(t, r)$, the left hand side depends on M and f which are not currently known, and the chosen value of Λ. In principle, the solution is identical to that of the L metric (2.22) in standard coordinates.[2] The main purpose of writing this and other formal integrals is to highlight the functions of integration that will arise.

Additionally we have

$$C_r = C_w w_r + C_y y_r = C_w(B/A) + C_y \ , \tag{4.56}$$

which (4.29) and (4.31) convert to

$$C_r = \pm B\sqrt{\frac{2M}{C}+f+\frac{\Lambda C^2}{3}} + B\sqrt{1+f} \ \mp B\sqrt{\frac{2M}{C}+f+\frac{\Lambda C^2}{3}} \ , \tag{4.57}$$

thus leading to

$$B = \frac{C_r}{\sqrt{1+f}} = \frac{C_r}{W} \ . \tag{4.58}$$

Hence, using (4.58) and (4.46) we obtain the following differential equation:

$$t_y = \frac{-C_r\, e^{-\sigma}}{\sqrt{1+f}} \ . \tag{4.59}$$

This equation measures how much t changes for a given value of y, when holding w constant, though it cannot be integrated as is, until we fix σ by choosing a suitable gauge on each worldline of constant w. Then its integration gives

$$t(w, y) = \int_0^y \frac{-C_r\, e^{-\sigma}}{\sqrt{1+f}}\, dy + \gamma(w) \ , \tag{4.60}$$

[1] In the general case it is not guaranteed C ever goes to zero, but in the context of cosmology we assume this.

[2] In the case of zero pressure and zero Λ, we have the simple inhomogeneous Lemaître-Tolman model, and this equation can be solved parametrically, $\{C(\eta, y), t(\eta, y)\}$, for each y, with the exact form determined by the sign of f. In this case however, M and f are also varying with time and therefore with C.

where

$$\gamma(w) = t(w, 0) \tag{4.61}$$

is an arbitrary function of integration which can be fixed on the central worldline.

Similarly, combining

$$C_w = C_t\, t_w + C_r\, r_w \ , \tag{4.62}$$

$$M_w = M_t\, t_w + M_r\, r_w \ , \tag{4.63}$$

$$M_y = M_t\, t_y + M_r\, r_y \ , \tag{4.64}$$

with (4.49) in (4.24) and (4.28) recovers (2.13) and (2.14):

$$\kappa p = \frac{-2(M_t\, A\, e^{-\sigma})}{C^2(C_t\, A\, e^{-\sigma})} = \frac{-2M_t}{C^2 C_t} \ , \tag{4.65}$$

$$\kappa\rho = \frac{2(-M_t\, B\, e^{-\sigma} + M_r)}{C^2 BW} + \frac{2(M_t\, A\, e^{-\sigma})}{C^2 AW} = \frac{2M_r}{C^2 BW} = \frac{2M_r}{C^2 C_r} \ , \tag{4.66}$$

where (4.58) was used in the last step.

Lastly the conservation equations are transformed as follows. Using (4.48), the conservation equation (4.10) becomes an exact copy of (2.8)

$$\frac{Bp_w}{A} + p_y + (\rho + p)\left(\sigma_y + \frac{B\sigma_w}{A}\right) = p_r + (\rho + p)\sigma_r = 0 \tag{4.67}$$

since

$$p_r = p_w\, w_r + p_y\, y_r = p_w\, \frac{B}{A} + p_y \ , \tag{4.68}$$

$$\sigma_r = \sigma_w\, w_r + \sigma_y\, y_r = \sigma_w\, \frac{B}{A} + \sigma_y \ . \tag{4.69}$$

It is clear that σ_r is connected to the pressure gradient. Also, from (4.68) and (4.12) we get that $p_r = 0$ ensures geodesic worldines, and if the pressure $p = 0$ then the model will reduce to the normal Lemaitre-Tolman (LT) model, which is pure dust.

Combining (4.14) with (4.51) we get

$$\frac{\lambda_w}{2} = -\frac{\rho_w}{(p + \rho)} + 2\frac{C_w}{C} \ , \tag{4.70}$$

and from the chain rules

$$\rho_w = \rho_t\, A\, e^{-\sigma} \ , \qquad \lambda_w = \lambda_t\, A\, e^{-\sigma} \ , \qquad C_w = C_t\, A\, e^{-\sigma} \ , \tag{4.71}$$

this becomes

$$\lambda_t = -\frac{2\rho_t}{(p + \rho)} + \frac{4C_t}{C} \ , \tag{4.72}$$

which is identically (2.7).

The solution process in (t, r) has shown that the familiar L metric equations can be recovered from the OC form of the metric. They involve the coordinates $t(w, y)$, $r = y$ and the characteristic functions $f(w, y)$ or $W(w, y)$, $M(w, y)$, $\sigma(w, y)$, $\lambda(w, y)$, including three arbitrary functions of integration $a(y)$, $\gamma(w)$, and $\lambda_0(y)$. The function $\gamma(w)$ allows the freedom to rescale the t relative to w.

To get an evolution equation for σ, we solve (4.48) for σ_w and substitute for B_w using (4.35), arriving at

$$\sigma_w = -\frac{A}{B}\left\{\sigma_y + \frac{\frac{\mathrm{d}p}{\mathrm{d}\rho}}{\left(1-\frac{\mathrm{d}p}{\mathrm{d}\rho}\right)}\left[\frac{A_y}{A} + \frac{\rho_y}{\rho + p(\rho)} \mp \frac{2B}{C}\sqrt{\frac{2M}{C} + f + \frac{\Lambda C^2}{3}}\,\right]\right\} . \tag{4.73}$$

In practice, to solve (4.73), we must determine σ_y along each worldline of constant w, as discussed below.

The above collection of loosely connected results will be merged into a solution algorithm in sections 4.5-4.7.

4.4 Observables

In this section we will summarise the observational relations of 3.4 and 2.4 as they apply to the metric form (4.1). The incoming light rays obey

$$w = \text{constant} , \qquad dw = 0 \tag{4.74}$$

with the $w = w_0$ being the PNC of present day observations.

Redshift The redshift of comoving sources is related to the metric function $\hat{A}_e = \hat{A}$ evaluated on the PNC via (3.26) with $\sqrt{|\alpha|} = A$,

$$\hat{A}_e = \frac{\hat{A}_o}{(1+z)} . \tag{4.75}$$

The Diameter & Luminosity Distances The treatment in sections 2.4.2, 2.4.3 and 3.4 holds here too, except that $\hat{R}$ is replaced by $\hat{C}$. In particular, we have

$$d_D(z) = \hat{C}(z) = \frac{D(z)}{\delta(z)} = \frac{d_L}{(1+z)^2} \tag{4.76}$$

$$d_L(z) = \sqrt{\frac{L(z)}{\ell(z)}}\, d_{10} . \tag{4.77}$$

Number Density From (3.37), using $\alpha = A^2$, $\beta = AB$ and $R = C$,

$$\mu n = \hat{\rho}\hat{B}\hat{C}^2\frac{\mathrm{d}y}{\mathrm{d}z} \ , \tag{4.78}$$

4.5 The Metric from Data

We have shown that the Lemaître model is fully characterized by a set of functions, these are $f = \sqrt{1+W}, M, \sigma, \lambda$ and $p(\rho)$. Respectivly these are the total energy per unit mass or the curvature function, the total gravitational mass, the two functions that reflect the coordinate freedom in each of t and r, and the equation of state. In order to obtain these functions from the cosmological data $\hat{A}(z)$, $\hat{C}(z)$ and $\mu n(z)$, we shall first derive DEs for their values on the observer's PNC, then DEs for their evolution to the future and past. This will define the process for extracting these metric functions from the data.

4.5.1 Gauge Choices

In order to obtain the metric functions from observational data, we have to make some gauge choices to fix the coordinate freedom. This can be tackled as follows.

- The freedom in the w coordinate is fixed by specifying $A(w,0) = \tilde{A}(w)$ on the observer's worldline. At the centre of the PNC, we fix the value of $\hat{A}_o$, giving

$$\hat{A}(0) = \hat{A}_o = \tilde{A}(w_0) = 1 \tag{4.79}$$

$$\rightarrow \qquad \hat{A} = \frac{1}{(1+z)} \ . \tag{4.80}$$

  To fix $\tilde{A}$ fully we either choose

$$\mathrm{P}: \qquad \Phi(w) = 0 \ , \qquad \text{and} \quad \tilde{A}(w_0) = 1 \tag{4.81}$$

$$\rightarrow \qquad \tilde{A}_w, \ \& \ \tilde{A} \text{ fixed by (4.40) and (4.43)} \tag{4.82}$$

  or we choose

$$\mathrm{A}: \qquad \tilde{A}(w) = 1 \tag{4.83}$$

$$\rightarrow \qquad \tilde{A}_w = 0 \ , \quad \Phi \text{ fixed by (4.40) and (4.43)} \ , \tag{4.84}$$

  where the options are labelled 'A' and 'P'.

- We need to specify $\hat{\sigma}$ on the past null cone, therefore one may choose[3]

$$\sigma(w_0, y) = \hat{\sigma} = 0 \quad \rightarrow \quad \hat{\sigma}_y = 0 \ . \tag{4.85}$$

[3] In these coordinates, $[\sigma_y]_\wedge = [\hat{\sigma}]_y = \hat{\sigma}_y$.

- The freedom in the t coordinate allows us to choose $w = t$ along the central world-line, thus fixing the value of $\sigma(w, 0)$. Using (4.61), (4.44) and (4.83),

$$\gamma_w = \tilde{A}\, e^{-\sigma(w,0)} \quad \text{and} \quad \gamma(w) = w \quad \rightarrow \tag{4.86}$$

$$1 = \tilde{A}\, e^{-\sigma(w,0)} \quad \leftrightarrow \quad \tilde{A} = e^{\sigma(w,0)} \quad \leftrightarrow \quad \sigma(w, 0) = \ln(\tilde{A}) \ , \tag{4.87}$$

  so on the PNC, by (4.79),

$$1 = e^{\hat{\sigma}_0} \quad \leftrightarrow \quad \hat{\sigma}_0 = \sigma(w_0, 0) = 0 \ . \tag{4.88}$$

- Similarly fixing the freedom in the y coordinate fixes the value of B. We consider two options here, the observer coordinate OC and Lemaître L options. In the 'L' option, with reference to (4.46), we choose

$$\text{L}: \qquad \hat{t}_y = -e^{-\hat{\sigma}_0} = -1 \quad \rightarrow \quad \hat{B} = 1 \ . \tag{4.89}$$

  In the 'OC' option we choose $A(w_0, y) = B(w_0, y)$ on our past null cone, as in the OC papers, and that implies

$$\text{OC}: \qquad \hat{B} = \hat{A} = \frac{1}{(1+z)} \quad \rightarrow \quad \hat{t}_y = -\frac{1}{(1+z)} \ . \tag{4.90}$$

  These expressions for $\hat{t}_y$ leave $\hat{t}(0)$ free. Since we won't know the bang time until the evolution is calculated, we set

$$\hat{t}(0) = 0 \ , \tag{4.91}$$

  and we can later add a constant to all times, $t \rightarrow t - a(0)$, $a \rightarrow a - a(0)$ (and $a(0)$ would of course be negative).

4.5.2 DE for $y(z)$

The first DE we must solve is the one that relates the coordinate y to the redshift z. All others depend on this one. To obtain a DE for $y(z)$, we define

$$\varphi = \left.\frac{\mathrm{d}y}{\mathrm{d}z}\right|_{\wedge} \ , \tag{4.92}$$

and because the coordinate y is not observable, we must rewrite the foregoing DEs in terms of z derivatives rather than y derivatives along the PNC, via the following relationship. For any quantity $Q(w, y)$, the chain rule gives

$$\frac{\mathrm{d}\hat{Q}}{\mathrm{d}y} = \frac{\hat{Q}_z}{\varphi} \qquad \text{and} \qquad \frac{\mathrm{d}^2\hat{Q}}{\mathrm{d}y^2} = \frac{\hat{Q}_{zz}}{\varphi^2} - \frac{\hat{Q}_z\varphi_z}{\varphi^3} \ , \tag{4.93}$$

where subscript z denotes a total derivative along the PNC $w = w_0$ with respect to redshift. We evaluate (4.5) on the PNC, using (4.93), which gives

$$\frac{\hat{A}_z\hat{C}_z}{\hat{A}\hat{C}} + \frac{\hat{B}_z\hat{C}_z}{\hat{B}\hat{C}} - \frac{\hat{C}_{zz}}{\hat{C}} + \frac{\hat{C}_z\varphi_z}{\hat{C}\varphi} - \frac{\kappa\hat{\rho}\hat{B}^2\varphi^2}{2} - \frac{\kappa p(\hat{\rho})\hat{B}^2\varphi^2}{2} = 0 \ , \tag{4.94}$$

then, using (4.80) to substitute for $\hat{A}_z/\hat{A}$, and (4.78) for $\hat{\rho}$, we rearrange the above equation as a DE for φ,

$$\varphi_z = \varphi\left(\frac{1}{(1+z)} - \frac{\hat{B}_z}{\hat{B}} + \frac{\hat{C}_{zz}}{\hat{C}_z} + \frac{\kappa\mu n\,\hat{B}\varphi}{2\hat{C}\hat{C}_z} + \frac{\kappa p\left(\frac{\mu n}{\hat{B}\hat{C}^2\varphi}\right)\hat{B}^2\hat{C}\varphi^2}{2\hat{C}_z}\right) \ . \tag{4.95}$$

Here $p(\rho)$ is the equation of state function, e.g. for a barotropic fluid, which must be chosen by the user. Applying the two alternative gauge choices for $\hat{B}$, we convert (4.95) to

$$\text{OC}: \quad \varphi_z = \varphi\left(\frac{2}{(1+z)} + \frac{\hat{C}_{zz}}{\hat{C}_z} + \frac{\kappa\mu n\varphi}{2\hat{C}\hat{C}_z(1+z)} + \frac{\kappa p\left(\frac{\mu n(1+z)}{\hat{C}^2\varphi}\right)\hat{C}\varphi^2}{2\hat{C}_z(1+z)^2}\right) \tag{4.96}$$

$$\text{L}: \quad \varphi_z = \varphi\left(\frac{1}{(1+z)} + \frac{\hat{C}_{zz}}{\hat{C}_z} + \frac{\kappa\mu n\varphi}{2\hat{C}\hat{C}_z} + \frac{\kappa p\left(\frac{\mu n}{\hat{C}^2\varphi}\right)\hat{C}\varphi^2}{2\hat{C}_z}\right) \ . \tag{4.97}$$

In each of these, the DE for $\varphi(z)$ depends on φ itself and known functions, specifically the equation of state $p(\rho)$, the observables $\kappa\mu n(z)$ and $\hat{C}(z)$, and their derivatives $\hat{C}_z$ and $\hat{C}_{zz}$. Integrating (4.96) or (4.97) followed by (4.92) yields $\varphi_(z)$ and then $y(z)$,

$$y(z) = \int_0^z \varphi(z)\,dz \ . \tag{4.98}$$

This allows us to transform between functions of z and functions of y on the PNC.

4.5.3 DE for $M(z)$ & $W(z)$

To obtain $\hat{M}_z$ we substitute (4.17) and (4.24) into (4.28) to eliminate M_w and then C_w/A, then evaluate on the PNC using (4.95) which gives

$$\hat{M}_z = \frac{\kappa\mu n\hat{W}}{2} + \kappa p\left(\frac{\mu n}{\hat{B}\hat{C}^2\varphi}\right)\frac{\hat{C}^2}{2}\left(\hat{W}\hat{B}\varphi - \hat{C}_z\right) \ , \tag{4.99}$$

where (4.78) has been used to substitute for ρ in $p(\rho)$. Now using the two gauge choices for $\hat{B}$, (4.99) gives the following alternative DEs for $\hat{M}_z$:

$$\text{OC}: \quad \hat{M}_z = \frac{\kappa\mu n\hat{W}}{2} + \kappa p\left(\frac{\mu n(1+z)}{\hat{C}^2\varphi}\right)\frac{\hat{C}^2}{2}\left(\frac{\hat{W}\varphi}{(1+z)} - \hat{C}_z\right) \ , \tag{4.100}$$

$$\mathrm{L}: \quad \hat{M}_z = \frac{\kappa\mu n\hat{W}}{2} + \kappa p\left(\frac{\mu n}{\hat{C}^2\varphi}\right)\frac{\hat{C}^2}{2}\left(\hat{W}\varphi - \hat{C}_z\right) \ . \tag{4.101}$$

On the other hand, squaring (4.31), solving for W, and specialising to the PNC yields

$$\hat{W} = \frac{\hat{B}}{2\hat{C}_y}\left(1 - \frac{2\hat{M}}{\hat{C}} - \frac{\Lambda\hat{C}^2}{3}\right) + \frac{\hat{C}_y}{2\hat{B}} \ , \tag{4.102}$$

then, converting to z derivatives with (4.93), the $\hat{W}$ equation becomes

$$\hat{W} = \frac{\hat{B}\varphi}{2\hat{C}_z}\left(1 - \frac{2\hat{M}}{\hat{C}} - \frac{\Lambda\hat{C}^2}{3}\right) + \frac{\hat{C}_z}{2\hat{B}\varphi} \ . \tag{4.103}$$

Again applying the gauge choices for $\hat{B}$ gives

$$\mathrm{OC}: \quad \hat{W} = \frac{\varphi}{2\hat{C}_z(1+z)}\left(1 - \frac{2\hat{M}}{\hat{C}} - \frac{\Lambda\hat{C}^2}{3}\right) + \frac{\hat{C}_z(1+z)}{2\varphi} \ , \tag{4.104}$$

$$\mathrm{L}: \quad \hat{W} = \frac{\varphi}{2\hat{C}_z}\left(1 - \frac{2\hat{M}}{\hat{C}} - \frac{\Lambda\hat{C}^2}{3}\right) + \frac{\hat{C}_z}{2\varphi} \ . \tag{4.105}$$

Once φ is known, $\hat{M}$ & $\hat{W}$ are solved together by combining (4.100) with (4.104) or (4.101) with (4.105).

4.5.4 Obtaining $\hat{t}(z)$

Converting (4.89) and (4.90) from y to z derivatives gives

$$\mathrm{OC}: \quad \hat{t}_z = -\frac{\varphi}{(1+z)} \tag{4.106}$$

$$\mathrm{L}: \quad \hat{t}_z = -\varphi \ , \tag{4.107}$$

and once $\varphi(z)$ is known, these integrate to

$$\mathrm{OC}: \quad \hat{t}(z) - \hat{t}(0) = \int_0^z \frac{\varphi}{(1+z)}\,dz \tag{4.108}$$

$$\mathrm{L}: \quad \hat{t}(z) - \hat{t}(0) = \int_0^z \varphi\,dz \ . \tag{4.109}$$

where $\hat{t}_0 = \hat{t}(0)$. Eq (4.108) or (4.109) gives $\hat{t}(z)$ or $\hat{t}(y)$, the time coordinate on the PNC.

4.6 Time Evolution DEs

The above PNC results provide initial conditions for the evolution equations contained in sections 4.2 & 4.3. We here collect the equations that will form a system of interlinked DEs for the evolution of the model.

Looking at (4.29) and (4.30) and defining

$$\Psi = \pm\sqrt{\frac{2M}{C^3} + \frac{f}{C^2} + \frac{\Lambda}{3}} \ , \qquad f = W^2 - 1 \ , \tag{4.110}$$

we have,

$$C_w = AC\Psi \ . \tag{4.111}$$

We substitute Eq (4.29) into (4.24) to produce

$$M_w = -\frac{\kappa p(\rho)}{2} C^3 A\Psi \ , \tag{4.112}$$

and from (4.35) we obtain

$$B_w = -\frac{A_y}{\left(1 - \frac{\mathrm{d}p}{\mathrm{d}\rho}\right)} - \frac{A\,\mathrm{d}p/\mathrm{d}\rho}{\left(1 - \frac{\mathrm{d}p}{\mathrm{d}\rho}\right)} \left[\frac{\rho_y}{(\rho + p(\rho))} - 2B\Psi\right] . \tag{4.113}$$

Substituting (4.111) and (4.113) into (4.18) gives the W_w DE

$$W_w = -\frac{C\Psi\left(\frac{\mathrm{d}p}{\mathrm{d}\rho}\right)}{\left(1 - \frac{\mathrm{d}p}{\mathrm{d}\rho}\right)} \left[\frac{A_y}{B} + \frac{A\rho_y}{B\,(\rho + p(\rho))} - 2A\Psi\right] \ , \tag{4.114}$$

and of course $f_w = 2WW_w$. From A^2 times (4.9) minus AB times (4.10), and using (4.29) and (4.35) to substitute for C_w and B_w, we obtain the density evolution equation as

$$\rho_w = \frac{(\rho + p(\rho))}{\left(1 - \frac{\mathrm{d}p}{\mathrm{d}\rho}\right)} \left[\frac{A_y}{B} + \frac{A\rho_y\left(\frac{\mathrm{d}p}{\mathrm{d}\rho}\right)}{B\,(\rho + p(\rho))} - 2A\Psi\right] \ . \tag{4.115}$$

Finally Equation (4.40) gives the A_w DE as follows,

$$A_w = A\left\{U + \frac{\left(\frac{\mathrm{d}p}{\mathrm{d}\rho}\right)}{\left(1 - \frac{\mathrm{d}p}{\mathrm{d}\rho}\right)} \left[\frac{A_y}{B} + \frac{A}{B}\frac{\rho_y}{(\rho + p(\rho))} - 2A\Psi\right] + \Phi\right\} \ , \tag{4.116}$$

where from (4.41), using $dy = \varphi\, dz$,

$$U = \int_0^z \left[\frac{\kappa(\rho + p(\rho))}{2} - \frac{2M}{C^3} - \frac{\Lambda}{3}\right] AB\varphi\, dz \ . \tag{4.117}$$

These DEs form a closed system, as the right hand sides of (4.111)-(4.116), depend only on A, B, C, M, W, ρ, and $p(\rho)$.

In addition to these equations, we also have the Lemaître quantities in standard (t, r) coordinates. The DE for σ_w is (4.73)

$$\sigma_w = -\frac{A}{B}\left\{\sigma_y + \frac{\left(\frac{\mathrm{d}p}{\mathrm{d}\rho}\right)}{\left(1 - \frac{\mathrm{d}p}{\mathrm{d}\rho}\right)} \left[\frac{A_y}{A} + \frac{\rho_y}{\rho + p(\rho)} - 2B\Psi\right]\right\} \ , \tag{4.118}$$

and by (4.51) λ is know as soon as B is known. Lastly, the coordinate time t is found from (4.44), which gives

$$t_w = Ae^{-\sigma} \ . \tag{4.119}$$

Assuming an expanding universe, $C_w > 0$, and a small value for Λ, there will be, on each worldline, a time in the past when $C = 0$. The t value at which this occurs is the "bang time", $t = a(y)$.

Having the above coupled system of DEs and their initial values on the PNC $w = w_0$, we can create a numerical procedure to integrate the DEs in parallel, thus giving $A(w, y)$, $B(w, y)$, $C(w, y)$, $M(w, y)$, $W(w, y)$, $\rho(w, y)$, and $p(w, y)$, as well as $\sigma(w, y)$, $\lambda(w, y)$ and $t(w, y)$ everywhere. Note that, after each step in w, we have new values for A, B, C, M, W, ρ and we must calculate A_y, ρ_y, p, σ_y, and $\mathrm{d}p/\mathrm{d}\rho$ as well as U to get the DEs for the next integration step.

4.7 Algorithm

The OC form of the Lemaître model is characterized by coordinate (w, y, θ, ϕ), the matter functions ρ and p, the equation of state $p(\rho)$, the cosmological constant Λ, the metric functions A, B and C, and the auxilliary functions M, $W = \sqrt{1 + f}$. The standard form involves coordinates (t, r, θ, ϕ) and metric functions σ, λ and R. In order to determine them, we present the following algorithm in two parts. Part I determines the metric quantities on the observer's PNC, providing initial conditions for part II, the calculation of the evolution.

I. OC Solution on the Observer's Past Null Cone

Our present-day observations come to us along the past null cone, and this is effectively a single null cone as the entirety of our observations are instantaneous compared with cosmological timescales.[4] This PNC is labelled w_0.

- Given a set of observations of sources on the PNC, we assume that smooth functions have been fitted to the data, and thus we assume that the following observational functions have been obtained.

  redshift z,
  apparent luminosity $\ell(z)$ and absolute luminosity $L(z)$,
  (and/or angular diameter $\delta(z)$ and true diameter $D(z)$),
  number density of sources in redshift space $n(z)$ and mass per source $\mu(z)$.

[4] Time variation of deep cosmological observations is not considered here, though it may be observed before long.

- From these the diameter distance $\hat{C} = d_D(z)$ is calculated using (4.76) or (4.77), and the redshift space mass density is just the product $\mu n(z)$.
- We specify the equation of state $p(\rho)$ and the cosmological constant Λ.
- We make gauge choices as in (4.79), (4.81) or (4.83), (4.85), (4.86), (4.89) or (4.90), and (4.91) to fix $\tilde{A}$, $\hat{A}$, γ, $\hat{\sigma}$, $\hat{B}$ and $\hat{t}$, as explained in §4.5.1.
- Integrate (4.96) or (4.97) down the PNC to calculate the function $\varphi(z)$, then integrate $\varphi(z)$ as in (4.98) to produce $y(z)$ and its inverse $z(y)$.
- Integrate (4.100) with (4.104) or (4.101) with (4.105) down the PNC to calculate $\hat{M}(z)$ and $\hat{W}(z)$, which transform to $\hat{M}(y)$ and $\hat{W}(y)$.
- From (4.78) we calculate $\hat{\rho}(z) = \rho(w_0, y) \to \hat{\rho}(y)$, thus ρ_y will be determined too.
- We integrate (4.108) or (4.109) to calculate the coordinate time on the PNC $\hat{t}(z) \to t(w_0, y)$.

II. Evolution away from the Past Null Cone

Once the functions $\hat{C}$, $\hat{A}$, $\hat{B}$, φ, y, $\hat{M}$ and $\hat{W}$ have been calculated on the observer's null cone, then the evolution of the model with respect to w can be determined from a system of interlinked DEs that must be integrated together. These DEs are tabulated below.

DE for	Equation	Output
C_w	(4.111)	$C(w, y)$
M_w	(4.112)	$M(w, y)$
B_w	(4.113)	$B(w, y)$
W_w	(4.114)	$W(w, y)$
ρ_w	(4.115)	$\rho(w, y)$
A_w	(4.116)	$A(w, y)$

It may be easily verified that this is a complete system in that there is a DE for each unknown function on the right of the equations. However, some of the DE's contain y derivatives, ρ_y and A_y, or integrals, U given in (4.41), of the functions being solved for, thus the integration procedure must evaluate these quantities prior to each iteration in w. In general, we have to integrate away from the PNC both backwards and forwards.

Having determined the OC metric functions in (w, y) coordinates, we proceed to calculate t and r, and the standard functions σ and λ, as follows. Again, σ_y needs to be calculated before each iteration of the w integration.

DE for	Equation	Output
σ_w	(4.118)	$\sigma(w, y)$
t_w	(4.119)	$t(w, y)$

Though these could be integrated one after the other, it makes sense to integrate them along with the above system of DEs. Then knowing $t(w, y)$ together with $r = y$ allows functions of (w, y) to be converted to functions of (t, r).

Chapter 5

Series Solutions Near The Origin and Near The Diameter Distance Maximum

Generally, integrating DEs analytically or numerically requires well behaved and continuous DE functions over the range of integration. But in the case where the DE functions contain singular points, standard numerical procedures may fail, even if there exist valid solutions. As long as these points are "regular" singular points, series solutions provide a good method for handling them. In the project of obtaining the Metric of the Cosmos from cosmological data [59, 63], they show that the procedure of doing numerical integration down the PNC requires special treatment in two regions: the origin and the maximum of the diameter distance, as we will see. Following their approach, in this chapter we will study the behavior of the DEs in the neighbourhood of the origin and the maximum, and present the series approximation to the solution of the DEs in these regions.

5.1 The PNC DEs

In chapter 4, we have shown that, in order to obtain the Lemaître model from cosmological data, we need to integrate a system of DEs on the PNC, which give the "initial conditions" for the evolution to the future and the past. In the OC gauge, these DEs are the comoving distance coordinate DE

$$y_z = \varphi(z) \ , \tag{5.1}$$

the redshift DE

$$\varphi_z = \varphi \left(\frac{2}{(1+z)} + \frac{1}{\hat{C}_z} \left\{ \hat{C}_{zz} + \frac{\kappa\mu n\varphi}{2\hat{C}(1+z)} + \frac{\kappa\hat{p}\hat{C}\varphi^2}{2(1+z)^2} \right\} \right) \ , \tag{5.2}$$

the mass DE

$$\hat{M}_z = \frac{\kappa\mu n W}{2} + \left\{ \frac{W\varphi}{(1+z)} - \hat{C}_z \right\} \frac{\kappa\hat{p}\hat{C}^2}{2} \ , \tag{5.3}$$

which must be combined with the expression for the total energy per unit mass or the curvature function

$$\sqrt{1+f} \ = W = \frac{\varphi}{2\hat{C}_z(1+z)} \left(1 - \frac{2\hat{M}}{\hat{C}} - \frac{\Lambda\hat{C}^2}{3} \right) + \frac{\hat{C}_z(1+z)}{2\varphi} \ , \tag{5.4}$$

and the numbercount-density relation (4.78)

$$\hat{\rho} = \frac{\hat{\mu} n (1+z)}{\hat{C}^2 \varphi} \ , \qquad \hat{p} = p(\hat{\rho}) \ . \tag{5.5}$$

Note that the factor $\hat{C}_z$ in the denominator of some terms in (5.2) and (5.4) could cause numerical problems if $\hat{C}_z = 0$, which does occur as we will see next. Similarly, $\hat{C}$ occurs in a couple of denominators, so $\hat{C} = 0$ is a problem point. We wish to integrate these DEs numerically down the PNC, including both problem points, to produce $\varphi(z)$, $y(z)$, $\hat{M}(z)$, $\hat{W}(z)$ and from them obtain $z(y)$, $\hat{M}(y)$ and $\hat{W}(y)$.

5.2 Origin Behaviour

The origin occurs at the center of the spherical coordinates, where $y = 0$, we have $C(w,0) = 0 \ \ \forall \ \ w$, and similarly, $C_w(w,0) = 0$ and $C_{ww}(w,0) = 0$ – for more details see [39, 68]. We already know from (4.80) that

$$\hat{A} \approx 1 - z + z^2 - z^3 \cdots \to 1 \ , \tag{5.6}$$

and our alternative gauge choices (4.89) and (4.90) both give

$$\hat{B} \to 1 \ . \tag{5.7}$$

Then (4.29) and (4.30) tell us that[1]

$$\frac{\hat{M}}{\hat{C}} \to 0 \ , \qquad \hat{M} \to 0 \ , \qquad \hat{f} \to 0 \ , \qquad \hat{W} \to 1 \ . \tag{5.8}$$

From (4.24), and assuming that the pressure p is finite and non-zero at the origin, we find

$$[M_w]_\wedge \sim -\frac{\kappa\hat{p}\hat{C}^2[C_w]_\wedge}{2} \tag{5.9}$$

[1]The origin limit of (4.29) must hold as $r \to 0$ on every time slice $t = t_s$, for which $C(t_s, r)$ is a different function of r.

and combining this with (4.28) and an assumption of finite density gives

$$\begin{aligned}\hat{M}_y &\sim \frac{\kappa\hat{\rho}\hat{C}^2\hat{B}\hat{W}}{2} + \frac{\kappa\hat{p}\hat{C}^2\hat{B}[C_w]_\wedge}{2\hat{A}} \\ &\sim \frac{\kappa\hat{\rho}\hat{C}^2}{2} \ . \end{aligned} \tag{5.10}$$

From (4.102) we get

$$\hat{W} \to \frac{\hat{B}}{2\hat{C}_y} + \frac{\hat{C}_y}{2\hat{B}} = 1 \ , \tag{5.11}$$

which implies

$$\hat{C}_y \to 1 \ , \tag{5.12}$$

so that

$$\hat{C} \sim y \ , \qquad \hat{M} \sim y^3 \ . \tag{5.13}$$

We can re-write (4.102) as

$$\hat{f} = \hat{W}^2 - 1 = \left(\frac{\hat{C}_y^2}{4\hat{B}^2} + \frac{\hat{B}^2}{4\hat{C}_y^2} - \frac{1}{2}\right) - \left(\frac{\hat{M}}{\hat{C}} + \frac{\Lambda\hat{C}^2}{6}\right)\left(1 + \frac{\hat{B}^2}{\hat{C}_y^2}\right) + \frac{\hat{B}^2}{\hat{C}_y^2}\left(\frac{\hat{M}}{\hat{C}} + \frac{\Lambda\hat{C}^2}{6}\right)^2 \tag{5.14}$$

and the above limiting behaviours show that

$$\hat{f} \sim y^2 \ , \tag{5.15}$$

since $\hat{M}/\hat{C}$ and $\Lambda C^2/3$ each $\sim y^2$, and even if $\hat{C}_y$ and $\hat{B}$ contain (non-leading) terms linear in y, the first bracket $\sim y^2$. By the Hubble law, $C \sim z$, and since $C \sim y$, we expect $\varphi = \frac{\mathrm{d}y}{\mathrm{d}z}$ to be finite and non-zero,

$$y \sim z \ , \tag{5.16}$$

and therefore (5.5) shows that

$$n \sim y^2 \sim z^2 \ . \tag{5.17}$$

These limits allow us to write appropriate near-origin series for the metric functions.

5.2.1 A Smooth Density at the Origin

Another consideration is the behaviour of the density near the origin. In many circumstances, we may expect or prefer the density function to go smoothly through the origin on a constant time slice, in other words,

$$\frac{\partial}{\partial r}\rho(t,r)\bigg|_{y=0} = 0 \qquad \to \qquad \rho_w|_{y=0} = \left[-\frac{A}{B}\rho_y\right]_{y=0} \ . \tag{5.18}$$

Combining this with (4.115), and re-solving for ρ_w, gives

$$\rho_w|_{y=0} = \left[(\rho+p)\left(\frac{A_y}{B} - 2A\Psi\right)\right]_{y=0} = \left[-\frac{A}{B}\rho_y\right]_{y=0} . \tag{5.19}$$

The right hand equality is a restriction which will be applied in the next section, after the general series results are obtained. Given that the observations will always have errors, it is unlikely that this condition would be exactly satisfied by the given data, even if it were true. Note that this condition is not needed to solve the evolution DEs, it is something we may want to impose; see (5.43)-(5.51).

5.3 The Origin Series Solution

From the analysis mentioned above it turns out that as $z \to 0$, several other quantities tend to 0 also, and we have 0/0 in the φ DE (5.2) which makes a direct numerical solution very difficult at the origin. For the PNC, $w = w_0$, it is useful to have more than just origin limits, as a cross-check. If for a range of small but non-zero z the series solution curve and the numerical solution curve overlap, we gain confidence in both.

5.3.1 Origin series on the PNC

In order to find the solution at the origin, we use a Taylor series approach, and we write the following series, in turn for the observational data, for the matter, for the known metric functions, and for the unknown metric functions;

$$\begin{aligned}
&\hat{C} = \sum_{i=1}^{\infty} C_i z^i , \qquad \kappa\mu n = \sum_{i=2}^{\infty} K_i z^i , \qquad \hat{\rho} = \sum_{i=0}^{\infty} \rho_i z^i , \qquad \hat{p} = \sum_{i=0}^{\infty} p_i z^i , \\
&\hat{A} = \sum_{i=0}^{\infty} (-1)^i z^i , \qquad \hat{B} = \hat{A} \ \text{ or } \ \hat{B} = 1 , \qquad \hat{\sigma} = 0 , \qquad \hat{\lambda} = 2\ln(B) , \\
&\hat{y} = \sum_{i=1}^{\infty} y_i z^i , \qquad M = \sum_{i=3}^{\infty} M_i z^i , \qquad f = \sum_{i=2}^{\infty} f_i z^i , \qquad \hat{t} = \sum_{i=0}^{\infty} t_i z^i .
\end{aligned} \tag{5.20}$$

In addition, $\hat{p}$ depends on $\hat{\rho}$ through the equation of state. If the central values at the observer are $\mathcal{P}_0 = p(w_0, 0)$ and $\rho_0 = \rho(w_0, 0)$, then we can write

$$\begin{aligned}
\hat{p} &= p_0 + \left.\frac{\mathrm{d}p}{\mathrm{d}\rho}\right|_0 (\hat{\rho} - \rho_0) + \left.\frac{\partial^2 p}{\partial \rho^2}\right|_0 \frac{(\hat{\rho} - \rho_0)^2}{2} + \cdots \\
&= \mathcal{P}_0 + \mathcal{P}_0^{(1)}(\hat{\rho} - \rho_0) + \mathcal{P}_0^{(2)} \frac{(\hat{\rho} - \rho_0)^2}{2} + \cdots ,
\end{aligned} \tag{5.21}$$

where the equation of state derivatives are

$$\mathcal{P}_0 = p(\rho)\Big|_{\rho=\rho_0} , \qquad \mathcal{P}_0^{(1)} = \left.\frac{\mathrm{d}p}{\mathrm{d}\rho}\right|_{\rho=\rho_0} , \qquad \mathcal{P}_0^{(2)} = \left.\frac{\mathrm{d}^2 p}{\mathrm{d}\rho^2}\right|_{\rho=\rho_0} , \qquad \text{etc} . \tag{5.22}$$

and they must be evaluated at $(w, y) = (w_0, 0)$. This gives the series coefficients for $\hat{p}(z)$ if those for $\hat{\rho}(z)$ are known.

Here we take the coeffificents C_i and K_i as known. In practice, they will be extracted from a polynomial fit to the observational data for $\hat{C}(z)$ and $\kappa\mu n(z)$ in the neighbourhood of $z = 0$. We substitute these series expressions into the above DEs, treat each power of z as a separate equation, and, working from the lowest order upwards, solve for the unknown coefficients in the series for y, $\varphi = y_z$, M, $W = \sqrt{1+f}$ and ρ. It is because of the EoS relationship (5.21) that the DEs depend on each other, even in series expansion. Thus, unlike the LT case, one has to solve the lowest powers in z in each of the above DEs before moving on to the next higher power; the sequence for the first 3 iterations is shown below.

Equation	Eq no	Power of z	What is solved for
f-W	(5.4)	0	y_1
$\kappa\hat{\rho}$	(5.5)	2	ρ_0
y	(5.1)	0	y_2
M	(5.3)	2	M_3
f-W	(5.4)	1	–
$\kappa\hat{\rho}$	(5.5)	3	ρ_1
y	(5.1)	1	y_3
M	(5.3)	3	M_4
f-W	(5.4)	2	f_2
$\kappa\hat{\rho}$	(5.5)	4	ρ_2
y	(5.1)	2	y_4
M	(5.3)	4	M_5

Notice that after 3 iterations we have 3 terms in the $\hat{M}$ and $\hat{\rho}$ series, 4 in the y series, and only 1 in the $\hat{f}$ series. The curvature is a higher order property of the metric. A Maple worksheet was written to carry out this calculation, and the results are as follows.

$$\hat{y} = C_1 z + (C_2 + C_1)\, z^2 + \left(C_3 + \frac{4C_2}{3} + \frac{C_1}{3} + \frac{\mathcal{P}_0 C_1^3}{12} + \frac{K_2}{12}\right) z^3 + \left(\mathcal{P}_0 \left\{\frac{5C_1^3}{24} + \frac{C_1^2 C_2}{4}\right\} + \mathcal{P}_0^{(1)} \left\{\frac{K_3}{24} - \frac{K_2}{24} - \frac{K_2 C_2}{6C_1}\right\} + C_4 + \frac{3C_3}{2} + \frac{C_2}{2} + \frac{K_2}{6} + \frac{K_3}{24} + \frac{K_2 C_2}{12C_1}\right) z^4 \cdots , \quad (5.23)$$

$$\frac{M}{z^3} = \frac{K_2}{6} + \left(\frac{K_3}{8} + \frac{\mathcal{P}_0 C_1^3}{8}\right) z + \left(\frac{K_4}{10} + \left\{1 - \frac{\Lambda C_1^2}{3}\right\} \frac{K_2}{20} - \frac{K_2^2}{60C_1} + \frac{C_1^5 \mathcal{P}_0^2}{40} + \mathcal{P}_0 \left(\left\{1 - \frac{\Lambda C_1^2}{3}\right\} \frac{C_1^3}{20} + \left\{2C_2 + \frac{K_2}{24}\right\} \frac{C_1^2}{5} \right) + \mathcal{P}_0^{(1)} \left\{ \frac{K_3}{10} - \frac{K_2}{10} - \frac{2K_2 C_2}{5C_1} \right\} \right) z^2 + \left(\left(\frac{K_5}{6} + \left\{1 - \frac{\Lambda C_1^2}{3}\right\} \frac{K_3}{12} - \left\{ \frac{1}{2} + \frac{\Lambda C_1^2}{6} + \frac{\Lambda C_1 C_2}{3} + \frac{7K_3}{12C_1} \right\} \frac{K_2}{6} + \left\{ \frac{1}{2} + \frac{C_2}{C_1} \right\} \frac{K_2^2}{18C_1} \right) + \mathcal{P}_0^2 \left(\frac{17C_1^5}{288} + \frac{C_2 C_1^4}{8} \right) + \mathcal{P}_0 \mathcal{P}_0^{(1)} \left(\frac{5K_3 C_1^2}{144} - \left\{ \frac{C_1^2}{18} + \frac{5C_1 C_2}{36} \right\} K_2 \right)$$

$$+\mathcal{P}_0\left(\left\{\frac{11C_1^2}{288}+\frac{C_1C_2}{36}\right\}K_2-\left\{C_2+\frac{C_1}{3}\right\}\frac{\Lambda C_1^4}{12}+\left\{\frac{C_2}{4}+\frac{5C_3}{4}+\frac{K_3}{96}\right\}\frac{C_1^2}{3}+\frac{5C_1C_2^2}{12}\right)$$
$$+\mathcal{P}_0^{(1)}\left(\left\{\frac{1}{8}+\frac{\Lambda C_1^2}{24}+\frac{\Lambda C_1C_2}{6}-\frac{C_2}{2C_1}-\frac{5C_3}{4C_1}-\frac{5C_2^2}{4C_1}+\frac{K_3}{48C_1}\right\}\frac{K_2}{3}\right.$$
$$\left.-\left(\frac{1}{2}+\frac{\Lambda C_1^2}{6}\right)\frac{K_3}{12}+\frac{K_4}{12}-\left\{1+\frac{C_2}{C_1}\right\}\frac{K_2^2}{36C_1}\right)$$
$$+\frac{\mathcal{P}_0^{(2)}}{\kappa}\left(\left\{\frac{1}{8}+\frac{C_2}{C_1}+\frac{2C_2^2}{C_1^2}\right\}\frac{K_2^2}{3C_1^3}-\left\{\frac{1}{12}+\frac{C_2}{3C_1}\right\}\frac{K_2K_3}{C_1^3}+\frac{K_3^2}{24C_1^3}\right)\Bigg)z^3\cdots\,, \tag{5.24}$$

$$\frac{f}{z^2}=\left(1-\frac{\Lambda C_1^2}{3}-\frac{2K_2}{3C_1}\right)-\left(1+\frac{\Lambda C_1^2}{3}+\frac{2\Lambda C_1C_2}{3}-\frac{K_2}{6C_1}+\frac{K_3}{4C_1}-\frac{K_2C_2}{3C_1^2}-\frac{\mathcal{P}_0C_1^2}{4}\right)z$$
$$+\left(\frac{5}{4}-\frac{\Lambda C_1^2}{6}-\frac{\Lambda C_2^2}{3}-\left\{2C_2+2C_3-\frac{K_2}{60}\right\}\frac{\Lambda C_1}{3}+\frac{\Lambda^2C_1^4}{36}+\frac{K_3}{12C_1}-\frac{11K_2}{60C_1}-\frac{K_4}{5C_1}\right.$$
$$+\frac{K_2C_3}{3C_1^2}+\frac{K_3C_2}{4C_1^2}-\frac{K_2C_2^2}{3C_1^3}+\frac{29K_2^2}{720C_1^2}+\frac{\mathcal{P}_0^2C_1^4}{80}+\mathcal{P}_0\left\{\frac{K_2C_1}{40}+\frac{C_1^2}{15}+\frac{9C_1C_2}{20}-\frac{\Lambda C_1^4}{20}\right\}$$
$$\left.-\mathcal{P}_0^{(1)}\left\{\frac{2K_2}{15C_1}+\frac{8K_2C_2}{15C_1^2}-\frac{2K_3}{15C_1}\right\}\right)z^2\cdots\,, \tag{5.25}$$

and the density series expansion gives

$$\rho_0=\frac{K_2}{C_1^3}\,, \tag{5.26}$$
$$\rho_1=-\left\{\frac{1}{C_1^3}+\frac{4C_2}{C_1^4}\right\}K_2+\frac{K_3}{C_1^3}\,, \tag{5.27}$$
$$\rho_2=-\left(\frac{\mathcal{P}_0K_2}{4C_1}+\frac{K_2^2}{4C_1^4}-\left\{\frac{1}{C_1^3}+\frac{4C_2-5C_3}{C_1^4}+\frac{11C_2^2}{C_1^5}\right\}K_2+\left\{\frac{1}{C_1^3}+\frac{4C_2}{C_1^4}\right\}K_3-\frac{K_4}{C_1^3}\right)\,. \tag{5.28}$$

5.3.2 The Origin Limits of the Time Evolution DEs

It is important to study the central behavior of the time evolution DEs, because some of the terms in (4.111)-(4.119) go to 0/0, but the central values are needed for themselves and for the y derivatives and integrals on each surface of constant w that are part of the w evolution algorithm.

The above z series are only valid at $w = w_0$, as some of the gauge choices are not applicable elsewhere. But for the evolution at the origin, the $z = 0$ limits of the above series provide the initial conditions. From (4.110)-(4.119), applying L'Hopital's rule, we find the following.

$$\Psi|_{z=0}=\sqrt{\frac{2M_3}{C_1^3}+\frac{f_2}{C_1^2}+\frac{\Lambda}{3}} \tag{5.29}$$
$$C_w|_{z=0}=0 \tag{5.30}$$

$$\left.\frac{C_w}{C}\right|_{z=0} = \frac{1}{C_1} \tag{5.31}$$

$$M_w|_{z=0} = 0 \tag{5.32}$$

$$\left.\frac{M_w}{C^3}\right|_{z=0} = \frac{-\kappa\mathcal{P}_0}{2C_1} \tag{5.33}$$

$$B_w|_{z=0} = \frac{1}{\left(1-\mathcal{P}_0^{(1)}\right)}\left\{\frac{1}{C_1} - \mathcal{P}_0^{(1)}\left\{\frac{\rho_1}{C_1\left(\rho_0+\kappa\mathcal{P}_0\right)} - \frac{2}{C_1}\right\}\right\} \tag{5.34}$$

$$W_w|_{z=0} = 0 \tag{5.35}$$

$$\left.\frac{W_w}{C}\right|_{z=0} = -\frac{1}{\left(1-\mathcal{P}_0^{(1)}\right)C_1}\left\{-\frac{3}{C_1} + \frac{\rho_1}{\left(\rho_0+\kappa\mathcal{P}_0\right)C_1}\right\} \tag{5.36}$$

$$\rho_w|_{z=0} = \frac{\kappa\mathcal{P}_0+\rho_0}{\left(1-\mathcal{P}_0^{(1)}\right)}\left\{-\frac{3}{C_1} + \frac{\mathcal{P}_0^{(1)}\rho_1}{\left(\rho_0+\kappa\mathcal{P}_0\right)C_1}\right\} \tag{5.37}$$

$$\begin{aligned} A_w|_{z=0} = &\left\{\frac{\rho_0+\kappa\mathcal{P}_0}{2} - \frac{K_2}{3C_1^3} - \frac{\Lambda}{3}\right\}C_1 \\ &- \frac{\mathcal{P}_0^{(1)}}{\left(1-\mathcal{P}_0^{(1)}\right)}\left\{-\frac{3}{C_1} + \frac{\rho_1}{\left(\rho_0+\kappa\mathcal{P}_0\right)C_1}\right\} + \Phi \end{aligned} \tag{5.38}$$

$$\sigma_w|_{z=0} = -\frac{\mathcal{P}_0^{(1)}}{\left(1-\mathcal{P}_0^{(1)}\right)}\left\{-\frac{3}{C_1} + \frac{\rho_1}{\left(\rho_0+\kappa\mathcal{P}_0\right)C_1}\right\} \tag{5.39}$$

$$\lambda_w|_{z=0} = \frac{2}{\left(1-\mathcal{P}_0^{(1)}\right)}\left\{\frac{1}{C_1} - \mathcal{P}_0^{(1)}\left\{\frac{\rho_1}{\left(\rho_0+\kappa\mathcal{P}_0\right)C_1} - \frac{2}{C_1}\right\}\right\} \tag{5.40}$$

$$t_w|_{z=0} = 1 \tag{5.41}$$

Using the z series in (4.117), we also find

$$\begin{aligned} U = \int_0^z \Bigg\{ &\left(\frac{K2}{6C_1^2} - \frac{\Lambda C_1}{3} + \frac{\mathcal{P}_0}{2}C_1\right) + \left(\mathcal{P}_0\left\{C_2 - \frac{C_1}{4}\right\} + \mathcal{P}_1\left\{\frac{K_3}{2C_1^2} - \left(\frac{2C_2}{C_1^3} + \frac{1}{2C_1^2}\right)\right\}K_2\right. \\ &- \left\{\frac{2C_2}{3C_1^3} + \frac{1}{2C_1^2}\right\}K_2 + \frac{K_3}{4C_1^2} - \frac{2\Lambda}{3}C_2\Bigg)\bar{z} + \Bigg(\frac{\mathcal{P}_0^{(2)}}{\kappa}\Bigg\{\left(\frac{2C_2}{C_1^6} + \frac{1}{4C_1^5} + \frac{4C_2^2}{C_1^7}\right)K_2^2 \\ &- \left(\frac{K_3}{2C_1^5} + \frac{2K_3C_2}{C_1^6}\right)K_2 + \frac{K_3^2}{4C_1^5}\Bigg\} - \left(C_3 + \frac{K_2}{20} + \frac{\mathcal{P}_0C_1^3}{20}\right)\Lambda - \left(\frac{1}{20C_1^3} + \frac{\mathcal{P}_0^{(1)}}{8C_1^3}\right)K_2^2 \\ &+ \left(\mathcal{P}_0\left(\frac{1}{40} - \frac{\mathcal{P}_0^{(1)}}{8}\right) + \mathcal{P}_0^{(1)}\left(\frac{3C_2^2}{2C_1^4} + \frac{9C_2}{5C_1^3} - \frac{5C_3}{2C_1^3} + \frac{7}{10C_1^2}\right) + \frac{C_2}{C_1^3} + \frac{3C_2^2}{2C_1^4}\right. \\ &+ \frac{2}{5C_1^2} - \frac{C_3}{C_1^3}\Bigg)K_2 + \frac{3\mathcal{P}_0^2C_1^3}{40} + \mathcal{P}_0\left(\frac{3C_3}{2} - \frac{11C_2}{20} - \frac{C_1}{10}\right) - \frac{3K_3C_2}{4C_1^3} \\ &+ \frac{\mathcal{P}_0^{(1)}}{C_1^2}\left(\frac{K_4}{2} - \frac{K_3C_2}{C_1} - \frac{7K_3}{10} + \frac{3K_4}{10C_1^2} - \frac{K3}{2C_1^2}\right)\Bigg)\bar{z}^2 + \cdots\Bigg\}d\bar{z} \end{aligned}$$

$$= \left(\frac{K2}{6C_1^2} - \frac{\Lambda C_1}{3} + \frac{\mathcal{P}_0}{2}C_1\right)z + \left(\mathcal{P}_0\left\{C_2 - \frac{C_1}{4}\right\} + \mathcal{P}_1\left\{\frac{K3}{2C_1^2} - \left\{\frac{2C_2}{C_1^3} + \frac{1}{2C_1^2}\right\}K_2\right\}\right.$$
$$- \left\{\frac{2C_2}{3C_1^3} + \frac{1}{2C_1^2}\right\}K_2 + \frac{K_3}{4C_1^2} - \frac{2\Lambda}{3}C_2\Bigg)\frac{z^2}{2} + \left(\frac{\mathcal{P}_0^{(2)}}{\kappa}\left\{\left(\frac{2C_2}{C_1^6} + \frac{1}{4C_1^5} + \frac{4C_2^2}{C_1^7}\right)K_2^2\right.\right.$$
$$\left.\left. - \left(\frac{K_3}{2C_1^5} + \frac{2K_3C_2}{C_1^6}\right)K_2 + \frac{K_3^2}{4C_1^5}\right\} - \left(C_3 + \frac{K_2}{20} + \frac{\mathcal{P}_0C_1^3}{20}\right)\Lambda - \left(\frac{1}{20C_1^3} + \frac{\mathcal{P}_0^{(1)}}{8C_1^3}\right)K_2^2\right.$$
$$+ \left(\mathcal{P}_0\left(\frac{1}{40} - \frac{\mathcal{P}_0^{(1)}}{8}\right) + \mathcal{P}_0^{(1)}\left(\frac{3C_2^2}{2C_1^4} + \frac{9C_2}{5C_1^3} - \frac{5C_3}{2C_1^3} + \frac{7}{10C_1^2}\right) + \frac{C_2}{C_1^3} + \frac{3C_2^2}{2C_1^4}\right.$$
$$\left. + \frac{2}{5C_1^2} - \frac{C_3}{C_1^3}\right)K_2 + \frac{3\mathcal{P}_0^2C_1^3}{40} + \mathcal{P}_0\left(\frac{3C_3}{2} - \frac{11C_2}{20} - \frac{C_1}{10}\right) - \frac{3K_3C_2}{4C_1^3}$$
$$\left. + \frac{\mathcal{P}_0^{(1)}}{C_1^2}\left(\frac{K_4}{2} - \frac{K_3C_2}{C_1} - \frac{7K_3}{10} + \frac{3K_4}{10C_1^2} - \frac{K3}{2C_1^2}\right)\right)\frac{z^3}{3} + \cdots$$

$$U|_{z=0} = 0 \tag{5.42}$$

The smooth central density condition, (5.19), combined with the above series, leads to

$$K_3 = 3\kappa\mathcal{P}_0C_1^3 + 4K_2\left(1 + \frac{C_2}{C_1}\right) \tag{5.43}$$

This is a correction to the K_3 from the data, and it should be made before the above are calculated. If this condition is applied, several of the above central limits simplify,

$$B_w|_{z=0} = \frac{1}{C_1} \tag{5.44}$$

$$\left.\frac{W_w}{C}\right|_{z=0} = 0 \tag{5.45}$$

$$\left.\frac{W_w}{C^2}\right|_{z=0} = \frac{1/C_1^3}{\left(1 - \mathcal{P}_0^{(1)}\right)(\kappa\mathcal{P}_0 + \rho_0)}\left\{-\frac{C_1^2\mathcal{P}_0^2}{2} + \left(-9\mathcal{P}_0^{(1)} - \frac{7K_2}{6C_1} - \frac{26C_2}{C_1} + \frac{\Lambda C_1^2}{3} - 15\right)\mathcal{P}_0\right.$$
$$\left. - \frac{9K_2\mathcal{P}_0^{(1)}}{C_1^3} + \frac{2K_4}{C_1^3} - \frac{2K_2^2}{3C_1^4} + \left(-\frac{10C_2^2}{C_1^5} - \frac{34C_2}{C_1^4} - \frac{10C_3}{C_1^4} + \frac{(\Lambda C_1^2 - 45}{C_1^3}\right)K_2\right\} \tag{5.46}$$

$$\rho_w|_{z=0} = -\frac{3(\kappa\mathcal{P}_0 + \rho_0)}{C_1} \tag{5.47}$$

$$A_w|_{z=0} = \Phi \tag{5.48}$$

$$\sigma_w|_{z=0} = 0 \tag{5.49}$$

$$\left.\frac{\sigma_w}{C}\right|_{z=0} = -\frac{\mathcal{P}_0^{(1)}}{C_1^3} \tag{5.50}$$

$$\lambda_w|_{z=0} = \frac{2}{C_1}\ , \tag{5.51}$$

and in particular, the W_w DE ensures that f and W don't develop a term linear in y or

z. Note that, on the PNC, the gauge choices P and A of (4.81) and (4.83) become the same.

Obviously C, M, f and U will remain zero at $y = 0$. In order to continue the evolution of quantities at the origin, we need to use a set of non-zero functions. We define

$$\mathcal{M} = \frac{M}{C^3} , \qquad \mathcal{F} = \frac{f}{C^2} \tag{5.52}$$

and, using the DEs (4.111) to (4.119) as well as the smooth central density condition (5.19), we obtain

$$\Psi|_{y=0} = \left[\sqrt{2\mathcal{M} + \mathcal{F} + \frac{\Lambda}{3}}\right]_{y=0} \tag{5.53}$$

$$\mathcal{M}_w|_{y=0} = \left[-A\Psi\left(\frac{\kappa p}{2} + 3\mathcal{M}\right)\right]_{y=0} \tag{5.54}$$

$$\mathcal{F}_w|_{y=0} = \left[-2\mathcal{F}A\Psi\right]_{y=0} \tag{5.55}$$

$$B_w|_{y=0} = \left[-A_y\right]_{y=0} \tag{5.56}$$

$$\rho_w|_{y=0} = \left[(\rho + p)\left(\frac{A_y}{B} - 2A\Psi\right)\right]_{y=0} \tag{5.57}$$

$$A_w|_{y=0} = \left[A\Phi\right]_{y=0} \tag{5.58}$$

$$\sigma_w|_{y=0} = \left[-\frac{A\sigma_y}{B}\right]_{y=0} \tag{5.59}$$

$$\lambda_w|_{y=0} = \left[-\frac{2A_y}{B}\right]_{y=0} \tag{5.60}$$

$$t_w|_{y=0} = \left[Ae^{-\sigma}\right]_{y=0} . \tag{5.61}$$

The initial values are given by the PNC results, (5.44)-(5.51) or (5.29)-(5.41), plus

$$\mathcal{M}|_{z=0} = \left.\frac{M}{C^3}\right|_{z=0} = \frac{M_3}{C_1^3} \tag{5.62}$$

$$\mathcal{F}|_{z=0} = \left.\frac{f}{C^2}\right|_{z=0} = \frac{f_2}{C_1^2} . \tag{5.63}$$

We see from (5.58) that gauge choices P and A are equivalent at all times, provided (5.19) holds. The evolution DEs for B, ρ, σ and λ depend on A_y and σ_y, and the latter quantities have to be obtained from y derivatives at the origin.

5.4 The Apparent Horizon

The apparent horizon is the locus where diameter distance $\hat{C}$ reaches its maximum value, labeled $\hat{C} = C_m$, $z = z_m$, where we have $\hat{C}_z = 0$. It has been shown that the relationship between C_m and the total gravitational mass inside the shell of radius C_m is independent

of any inhomogeneity and does not change even in when non-zero pressure is introduced (for more details about this see [2, 59, 63]). That relationship is given by

$$\frac{2M_m}{C_m} = 1 - \frac{\Lambda C_m^2}{3} \ , \tag{5.64}$$

and its significance is discussed in [35]. At the maximum, $\hat{C}_z = 0$ and (5.64) produce a $0/0$ singularity in the expression for W, (5.4). Furthermore, when rearranging (4.96), we obtain

$$\hat{C}_{zz} + \frac{\kappa\mu n\varphi}{2\hat{C}(1+z)} + \frac{\kappa\hat{p}\hat{C}\varphi^2}{2(1+z)^2} = \hat{C}_z\left(\frac{\varphi_z}{\varphi} - \frac{2}{(1+z)}\right) \ . \tag{5.65}$$

which shows that at $\hat{C}_z = 0$ we have

$$\hat{C}_{zz} = -\frac{\kappa\mu n\varphi}{2\hat{C}(1+z)} - \frac{\kappa p\left(\frac{\mu n}{\hat{C}^2\varphi}\right)\hat{C}\varphi^2}{2(1+z)^2} \ , \tag{5.66}$$

Similarly, this equation contributes a $0/0$ term in the DE for φ (5.2), which makes direct numerical integration impossible. The presence of $0/0$ instead of just 0^{-1} suggests that there may be regular limiting values at z_m, as is the case in FLRW models. Hence, series solutions are needed to solve this problem.

5.5 The Near-Maximum Series Solution

In order to pass the numerical integration of the DEs through the singular point at $\hat{C}_z = 0$, we do Taylor expansions around the point $z = z_m$. Hence, we write all the dependent variables as

$$\begin{aligned} &\hat{C} = C_m + \sum_{i=2}^{\infty} C_i \Delta z^i \ , \qquad \kappa\mu n = K_m + \sum_{i=1}^{\infty} K_i \Delta z^i \ , \qquad \hat{y} = y_m + \sum_{i=1}^{\infty} y_i \Delta z^i \ , \\ &M = M_m + \sum_{i=1}^{\infty} M_i \Delta z^i \ , \qquad \sqrt{1+f} \ = W = W_m + \sum_{i=1}^{\infty} W_i \Delta z^i \ , \qquad \Delta z = z - z_m \ , \end{aligned} \tag{5.67}$$

and substitute these expressions back into (5.1)-(5.5), and, with the help of a maple worksheet, we calculate the coefficients. We find

$$y_m = \text{ undetermined} \ , \tag{5.68}$$

$$\varphi_m = y_1 = \left\{-\frac{K_m}{2} \pm \frac{\sqrt{K_m^2 - 16\,C_m^3\,C_2\mathcal{P}_m}}{2}\right\}\frac{(1+z_m)}{C_m^2\mathcal{P}_m} \ , \tag{5.69}$$

$$\varphi_1 = y_2 = \mathcal{P}_m\left\{\frac{1}{(1+z_m)} + \frac{3C_3}{4C_2}\right\}\frac{C_m^2\,y_1^2}{X_m}$$

$$
\begin{aligned}
&- \mathcal{P}_m^{(1)} \left\{ \frac{K_m}{2} + \frac{(1+z_m)\ K_1}{2} \right\} \frac{y_1}{X_m} \\
&+ \left\{ \frac{1}{2} - \frac{(1+z_m)\ K_1}{2\,K_m} + \frac{3\ (1+z_m)\ C_3}{4\,C_2} \right\} \frac{K_m\, y_1}{X_m} \\
&- \left\{ \frac{4\ (1+z_m)\ C_2\, C_m}{X_m} + \frac{3\ (1+z_m)^2\ C_3\, C_m}{X_m} \right\} \ , \qquad (5.70)
\end{aligned}
$$

$$
\begin{aligned}
\varphi_2 = y_3 = \mathcal{P}_m &\left\{ \frac{1}{(1+z_m)^2} + \frac{C_3}{(1+z_m)\ C_2} - \frac{2\,C_4}{3\,C_2} + \frac{3\,C_3^2}{4\,C_2^2} \right. \\
&+ \frac{C_2}{3\,C_m} - \left\{ \frac{4}{(1+z_m)} + \frac{3\,C_3}{C_2} \right\} \frac{y_2}{y_1} + \left. \frac{4\,y_2^2}{y_1^2} \right\} \frac{C_m^2\, y_1^3}{Y_m} \\
&- \mathcal{P}_m^{(1)} \left\{ \frac{2}{3\ (1+z_m)} + \frac{C_3}{2\,C_2} + \frac{2\ (1+z_m)\ C_2}{3\,C_m} + \left\{ \frac{1}{3} + \frac{(1+z_m)\ C_3}{2\,C_2} \right\} \frac{K_1}{K_m} \right. \\
&+ \frac{(1+z_m)\ K_2}{3\,K_m} - \left\{ \frac{8}{3} + \frac{(1+z_m)\ C_3}{C_2} + \frac{4\,(1+z_m)\,K_1}{3K_m} \right\} \frac{y_2}{y_1} \\
&+ \left. \frac{8\,(1+z_m)\,y_2^2}{3\,y_1^2} \right\} \frac{K_m\, y_1^2}{Y_m} + \frac{\mathcal{P}_m^{(2)}}{\kappa} \left\{ \left\{ \frac{1}{6} + \frac{(1+z_m)\ K_1}{3\,K_m} + \frac{(1+z_m)^2\ K_1^2}{6\,K_m^2} \right\} y_1 \right. \\
&- \left. \left\{ \frac{2\ (1+z_m)}{3} + \frac{2\ (1+z_m)^2\ K_1}{3\,K_m} \right\} y_2 + \frac{2\ (1+z_m)^2\ y_2^2}{3\,y_1} \right\} \frac{K_m^2}{C_m^2\, Y_m} \\
&+ \left\{ \frac{1}{3\,(1+z_m)} + \frac{C_3}{2C_2} - \frac{2\,(1+z_m)\,C_4}{3C_2} + \frac{3\,(1+z_m)\,C_3^2}{4C_2^2} \right. \\
&- \frac{(1+z_m)\,C_2}{3C_m} - \left\{ \frac{1}{3} + \frac{(1+z_m)\,C_3}{2C_2} \right\} \frac{K_1}{K_m} + \left. \frac{(1+z_m)\,K_2}{3K_m} \right\} \frac{K_m y_1^2}{Y_m} \\
&- \left\{ \frac{4}{3} + \frac{2\,(1+z_m)\,C_3}{C_2} + \frac{4\,(1+z_m)\,K_1}{3K_m} \right\} \frac{K_m y_1 y_2}{Y_m} \\
&- \left\{ \frac{8\,C_2}{3} - \frac{16\ (1+z_m)^2\ C_4}{3} + \frac{3\,(1+z_m)^2\,C_3^2}{C_2} \right\} \frac{C_m y_1}{Y_m} \\
&+ \frac{4\,(1+z_m)\,K_m y_2^2}{3Y_m} + \left\{ \frac{16\,(1+z_m)\,C_2}{3} + 4\,(1+z_m)^2\,C_3 \right\} \frac{C_m y_2}{Y_m} \ . \qquad (5.71)
\end{aligned}
$$

For the sake of compactness, we do not substitute (5.69) for y_1 in the following

$$
M_m = \left\{ 1 - \frac{\Lambda C_m^2}{3} \right\} \frac{C_m}{2} \ , \qquad (5.72)
$$

$$
M_1 = M_1 \ , \qquad \text{i.e. undetermined} \qquad (5.73)
$$

$$
\begin{aligned}
M_2 = &- \mathcal{P}_m^2 \left\{ \frac{4}{(1+z_m)\ X_m} + \frac{3C_3}{C_2\, X_m} \right\} \frac{C_m^4\, y_1^3\, M_1}{H_m} \\
&+ \mathcal{P}_m \mathcal{P}_m^{(1)} \left\{ \frac{2K_m}{X_m} + \frac{2\,(1+z_m)\,K_1}{X_m} \right\} \frac{C_m^2\, y_1^2\, M_1}{H_m} \\
&+ \mathcal{P}_m \left\{ \left\{ \left\{ \left(-\frac{4}{X_m} - \frac{9\,(1+z_m)\,C_3}{2X_m\, C_2} \right) K_m + \frac{2\,(1+z_m)\,K_1}{X_m} \right. \right. \right.
\end{aligned}
$$

$$
\begin{aligned}
&+\frac{2}{(1+z_m)}+\frac{3C_3}{2C_2}\Bigg\}\frac{C_m^2y_1^2}{H_m}+\left(\frac{16\,(1+z_m)\,C_2}{X_m}+\frac{12\,(1+z_m)^2\,C_3}{X_m}\right)C_m^3y_1\Bigg\}\frac{M_1}{H_m}\\
&+\frac{\lambda_m\,C_2\,C_m^2\,y_1^2}{2H_m}-\frac{2\,(1+z_m)^2\,C_2^2\,C_m^3}{H_m}\Bigg\}\\
&+\mathcal{P}_m^{(1)}\Bigg\{\left(\frac{K_m}{X_m}-\frac{1}{(1+z_m)}+\frac{(1+z_m)\,K_1}{X_m}-\frac{K_1}{K_m}\right)y_1+2\,y_2\Bigg\}\frac{(1+z_m)\,K_m\,M_1}{H_m}\\
&+\Bigg\{\Bigg(\left\{-\frac{1}{(1+z_m)\,X_m}-\frac{3C_3}{2X_m\,C_2}\right\}K_m^2+\left\{\frac{K_1}{X_m}+\frac{1}{(1+z_m)^2}+\frac{3C_3}{2C_2\,(1+z_m)}\right\}K_m\\
&-\frac{K_1}{(1+z_m)}\Bigg)\frac{(1+z_m)^2\,y_1}{H_m}+\left\{\frac{8\,(1+z_m)^2\,C_2}{X_m}+\frac{6\,(1+z_m)^3\,C_3}{X_m}\right\}\frac{K_m\,C_m}{H_m}\Bigg\}M_1\\
&+\frac{\lambda_m\,(1+z_m)\,C_2\,K_m\,y_1}{2}+\frac{2\,(1+z_m)^3\;C_2^2\,C_m\,K_m}{y_1}\,, \qquad (5.74)
\end{aligned}
$$

$$
\begin{aligned}
M_3=\mathcal{P}_m&\Bigg\{\Bigg(\left\{-\frac{C_2}{C_m}-\frac{3}{(1+z_m)^2}-\frac{3C_3}{(1+z_m)\,C_2}+\frac{2C_4}{C_2}-\frac{9C_3^2}{4C_2^2}\right\}y_1^2\\
&+\left\{\left(\frac{8}{(1+z_m)}+\frac{6C_3}{C_2}\right)y_2-6y_3\right\}y_1-4y_2^2\Bigg)M_1+\Bigg\{\left(\frac{2}{(1+z_m)}+\frac{3C_3}{2C_2}\right)y_1^2\\
&-4y_1y_2\Bigg\}M_2-\left\{\left(\frac{C_2}{(1+z_m)}+\frac{C_3}{4}\right)y_1^2-2C_2y_1y_2\right\}\lambda_m-3C_mC_2C_3(1+z_m)^2\Bigg\}\frac{C_m^2}{D_m}\\
&+\mathcal{P}_m^{(1)}\Bigg\{\Bigg(\Bigg\{\left\{\frac{1}{(1+z_m)\,K_m}+\frac{3C_3}{2K_m\,C_2}\right\}K_1-\frac{K_2}{K_m}+\frac{2C_2}{C_m}+\frac{2}{(1+z_m)^2}\\
&+\frac{3C_3}{2\,(1+z_m)\,C_2}\Bigg\}M_1+\left\{-\frac{K_1}{K_m}-\frac{1}{(1+z_m)}\right\}M_2+\left\{\frac{K_1}{K_m}+\frac{1}{1+z_m}\right\}\lambda_mC_2\Bigg)y_1\\
&+\left(\left\{-\frac{2K_1}{K_m}-\frac{6}{(1+z_m)}-\frac{3C_3}{C_2}\right\}M_1+2\,M_2-\lambda_mC_2\right)y_2+3\,M_1\,y_3\\
&+\left\{4\,M_1\,y_2^2-\frac{2C_m\;(1+z_m)^2\,C_2^2K_1}{K_m}-2\,C_m\;(1+z_m)\,C_2^2\right\}\frac{1}{y_1}\\
&+\frac{4C_m\;(1+z_m)^2\,C_2^2y_2}{y_1^2}\Bigg\}\frac{(1+z_m)K_m}{D_m}\\
&-\frac{\mathcal{P}_m^{(2)}}{\kappa}\Bigg\{\frac{1}{2\,(1+z_m)^2}+\frac{K_1}{(1+z_m)\,K_m}+\frac{K_1^2}{2K_m^2}-\left(\frac{2}{(1+z_m)}+\frac{2K_1}{K_m}\right)\frac{y_2}{y_1}\\
&+\frac{2y_2^2}{y_1^2}\Bigg\}\frac{(1+z_m)^2\,K_m^2M_1}{C_m^2D_m}+\Bigg\{\Bigg\{\left(\frac{1}{(1+z_m)\,K_m}+\frac{3C_3}{2K_m\,C_2}\right)K_1-\frac{K_2}{K_m}+\frac{C_2}{C_m}\\
&-\frac{1}{(1+z_m)^2}-\frac{3C_3}{2(1+z_m)C_2}+\frac{2\,C_4}{C_2}-\frac{9C_3^2}{4C_2^2}\Bigg\}M_1+\left(-\frac{K_1}{K_m}+\frac{1}{(1+z_m)}+\frac{3C_3}{2C_2}\right)M_2\\
&+\left\{\frac{C_2\,K_1}{2K_m}-\frac{C_2}{2(1+z_m)}-\frac{C_3}{4}\right\}\lambda_m\Bigg\}\frac{y_1(1+z_m)K_m}{D_m}
\end{aligned}
$$

$$+\left\{\left\{\left(-\frac{2K_1}{K_m\left(1+z_m\right)^2}+\frac{2}{\left(1+z_m\right)^3}+\frac{3C_3}{\left(1+z_m\right)^2 C_2}\right)M_1\right.\right.$$
$$\left.-\frac{2M_2}{\left(1+z_m\right)^2}+\frac{\lambda_m C_2}{\left(1+z_m\right)^2}\right\}y_2-\frac{3M_1\,y_3}{\left(1+z_m\right)^2}$$
$$+\left\{\frac{2K_1}{K_m}+\frac{2}{1+z_m}+\frac{3\,C_3}{C_2}-\frac{4y_2}{y_1}\right\}\frac{C_m\,C_2^2}{y_1}\Bigg\}\frac{(1+z_m)^3\,K_m}{D_m}\ , \tag{5.75}$$

$$W_m=-\frac{M_1 y_1}{2\left(1+z_m\right)C_m C_2}\ , \tag{5.76}$$

$$W_1=\left\{-\frac{y_2}{\left(1+z_m\right)C_2\,C_m}+\left(\frac{1}{2C_2\,\left(1+z_m\right)^2 C_m}+\frac{3C_3}{4C_m\,\left(1+z_m\right)C_2^2}\right)y_1\right\}M_1$$
$$+\left\{\frac{\lambda_m}{4(1+z_m)}-\frac{M_2}{2\left(1+z_m\right)C_2}\right\}\frac{y_1}{C_m}+\frac{(1+z_m)\,C_2}{y_1}\ , \tag{5.77}$$

$$W_2=\Bigg\{\left\{\frac{1}{2C_m}-\frac{1}{2\left(1+z_m\right)^2 C_2}-\frac{3C_3}{4\left(1+z_m\right)C_2^2}+\frac{C_4}{C_2^2}-\frac{9C_3^2}{8C_2^3}\right\}y_1$$
$$+\left\{\frac{1}{\left(1+z_m\right)C_2}+\frac{3C_3}{2C_2^2}\right\}y_2-\frac{3y_3}{2C_2}\Bigg\}\frac{M_1}{\left(1+z_m\right)C_m}$$
$$+\left\{\left\{\frac{1}{2\left(1+z_m\right)C_2}+\frac{3C_3}{4C_2^2}\right\}y_1-\frac{y_2}{C_2}\right\}\frac{M_2}{\left(1+z_m\right)C_m}-\frac{M_3 y_1}{2\left(1+z_m\right)C_m C_2}$$
$$-\left\{\left\{\frac{1}{4\left(1+z_m\right)}+\frac{C_3}{8C_2}\right\}y_1-\frac{y_2}{2}\right\}\frac{\lambda_m}{\left(1+z_m\right)C_m}$$
$$+\frac{C_2}{y_1}+\frac{3\left(1+z_m\right)\,C_3}{2y_1}-\frac{2\left(1+z_m\right)\,C_2\,y_2}{y_1^2}\ , \tag{5.78}$$

and

$$\rho_{0m}=\frac{\left(1+z_m\right)\,K_m}{C_m^2\,y_1}\ , \tag{5.79}$$

$$\rho_{1m}=\frac{\left(1+z_m\right)\,K_1}{y_1\,C_m^2}+\frac{K_m}{y_1\,C_m^2}-\frac{2\left(1+z_m\right)\,K_m\,y_2}{y_1^2\,C_m^2}\ , \tag{5.80}$$

$$\rho_{2m}=\frac{K_1}{C_m^2\,y_1}+\frac{\left(1+z_m\right)\,K_2}{C_m^2\,y_1}-\frac{2(1+z_m)\,K_m\,C_2}{C_m^3\,y_1}$$
$$-\left\{\frac{2\left(1+z_m\right)\,K_1}{C_m^2}+\frac{2K_m}{C_m^2}\right\}\frac{y_2}{y_1^2}-\frac{3\left(1+z_m\right)\,K_m\,y_3}{C_m^2\,y_1^2}+\frac{4\left(1+z_m\right)\,K_m\,y_2^2}{C_m^2 y_1^3}\ , \tag{5.81}$$

where

$$\lambda_m=1-\Lambda C_m^2\ , \tag{5.82}$$

and

$$\mathcal{P}_m=p(\hat{\rho})\Big|_{\hat{\rho}=\hat{\rho}_m}\ ,\qquad \mathcal{P}_m^{(1)}=\frac{\mathrm{d}p}{\mathrm{d}\rho}\Big|_{\hat{\rho}=\hat{\rho}_m}\ ,\qquad \mathcal{P}_m^{(2)}=\frac{\mathrm{d}^2p}{\mathrm{d}\rho^2}\Big|_{\hat{\rho}=\hat{\rho}_m}\ , \tag{5.83}$$

and the constants X_m, Y_m, H_m and D_m have the following formulas

$$\begin{aligned} X_m &= 3\,C_m^2\,\mathcal{P}_m\,y_1 + K_m\,(1+z_m)\,(2-\mathcal{P}_m^{(1)})\ , \\ Y_m &= -X_m y_1 + 4C_2C_m\,(1+z_m)^2\ , \\ H_m &= C_m^2\,\mathcal{P}_m\,y_1^2 + K_m\,y_1\,(1+z_m) + 8\,(1+z_m)^2\,C_2\,C_m\ , \\ D_m &= C_m^2\,\mathcal{P}_m\,y_1^2 + K_m\,y_1\,(1+z_m) + 12\,(1+z_m)^2\,C_2\,C_m\ . \end{aligned} \tag{5.84}$$

It is clear that all the series coefficients are function of z_m, C_m, C_i, K_m and K_i, and in order to determine all of them, we must first estimate the latter from the given data near $z = z_m$. This will be done by performing a least squares fit to the cosmological data $\hat{C}(z)$, and $\hat{K}(z)$ near $z = z_m$.

We can see that the series expansion of $\hat{M}(z)$ and $y(z)$ are not complete, because M_1 and y_m are undetermined.[2] We also note all the M_i and W_i coefficients in (5.73)-(5.78) are linearly dependent on the unknown value of M_1, or equivalently W_m. In [58, 59, 63], Hellaby, Lu and McClure show that it is possible to obtain the values of y_m and M_1, by applying the idea of connecting or matching the series solution for $y(z)$ and $M(z)$ to their calculated numerical values y_a and M_a at $z_a < z_m$, as visualised in figure 5.1. In fact, matching $M(z)$ is not the only way to solve for M_1. Since all the coefficients of W are linear functions of M_1, this means that we can alternatively solve for M_1 (and W_m) by joining the numerical and the series solutions for $W(z)$ at z_a. Below we will see that, owing to data errors and the properties of C_m, this matching will need to be an iterative process.

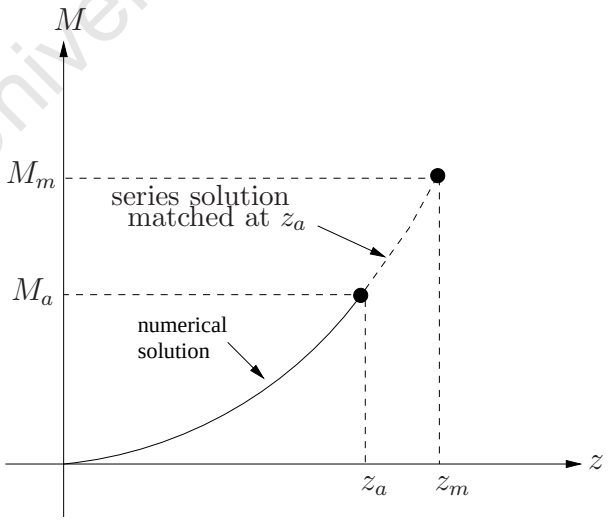

Figure 5.1: Shows how do we solve for M_1 by matching between the series and the numeric at some point z_a before the maximum z_m.

[2]Though we can't prove there are no further undetermined coefficients at higher order in the series solution, execution of the iteration process does seem to indicate this.

5.6 Data Correction at the Apparent Horizon

As it was pointed out by Hellaby [35], the maximum in $\hat{C}$ provides a cross-check on the cosmological observations. The basic idea is that, once $\hat{M}(z)$ is calculated by integrating down the PNC (including near origin series, numerical integration and near-maximum series), then it must agree with the result of M_m at z_m obtained from (5.64). If there is a discrepancy, this indicates either systematic errors in the observational data, for example our galaxy number counts don't include dark matter, or incorrect assumptions about the value of Λ or the equation of state $p(\rho)$.

When implementing this relationship with real data, we also have to take into account the effect of statistical errors — see McClure & Hellaby [63]. Statistical errors would cause discrepancies in (5.64), even if the matter description was correct and there were no systematic errors in the data.

In order to obtain a self-consistent solution, one with no singularity at $z = z_m$, it is necessary to make corrections to the observational data. Since we can only detect errors at one z value, the correction needs to be fairly simple. For example, if it is assumed that the mass per galaxy μ is too low, owing to the presence of dark matter, then the $\kappa\mu n$ data could be multiplied by a constant factor. At a more complicated level, owing to the difficulty of detecting faint sources, the number-counts are likely to be more underestimated as z increases. The number-counts should already be corrected according to some standard luminosity function, and the parameters of this function could in principle be adjusted. However, it is difficult to justify a complicated correction function, based on a discrepancy at one z value.

In practice, these discrepancies show up when trying to determine y_m and M_1 by joining numerical and series estimates at z_a. Clearly the correction process must be iterative — calculate the discrepancies, estimate corrections, re-do the entire integration, calculate new discrepancies, etc.

Chapter 6

Data Smoothing

The integration algorithm stated broadly in §4.7 requires as input a complete set of data of $\hat{C}(z)$, $\hat{C}_z(z)$, $\hat{C}_{zz}(z)$, and $\kappa\mu n(z)$ for a range of z values on the PNC. Observational data consists of many discrete measurements of individual galaxies that necessarily have both statistical and systematic errors. In addition, the z distribution of these points is quite irregular, owing to real clustering of galaxies. The theory, however, assumes the metric and the observational quantities are continuous functions. In contrast the numerical integration down the PNC constitutes discrete approximations to those continuous functions, requiring regularly spaced data values, and it also depends on the first and the second derivative $\hat{C}_z$, and $\hat{C}_{zz}$ of the given data $\hat{C}$, which should also be discrete approximations to smooth functions. The question that arises here is, how should we smooth the $\hat{C}$ data in order to obtain sensible values of $\hat{C}_z$, and $\hat{C}_{zz}$ from it, and which smoothing method is the most effective without causing unnecessary distortion of the data?

In practice, if the data were ideal, then it would be very easy to obtain smooth higher derivatives, and that could be done by applying any numerical derivative method, such as the three point or five point formulas. Since the main goal of this thesis is to create a generalised algorithm, and to implement a numerical program that can handle any realistic inhomogeneous data, therefore we consider other methods of smoothing, such as the moving average, or a smoothed polynomial spline.

In [59], smoothing was not a significant problem because the test data was ideal, and the only errors were the numerical errors in generating it. In [63], statistical errors in the data were introduced, and this test data was smoothed by means of a moving average. Given a set of noisy data values, the function (and its derivatives) at each point were obtained by fitting a low order polynomial to the data points within a small range on either side. Thus the range of data used in the fit was always centered on the point of interest, and moved with it. Obviously at the two ends, the fitted range was truncted by the lack of data. Here we will investigate smoothing by means of polynomial splines with

constraints.

6.1 The Spline Method

A spline $S(z)$ is a piecewise function, with each piece or segment a polynomial of a given order O, and continuity conditions are imposed at the "knots" or "breaks" where two pieces meet, so that the resulting curve looks smooth. The knots plus the left and right ends are "nodes", which are the endpoints of the segments. When used for interpolation, the spline must pass through every data point, and derivatives 1 to $O-1$ are required to be continuous at each knot (see figure 6.1a). If there are N data points (z_n, d_n), $n = 1 \cdots N$, then passing through them creates $2(N-1)$ conditions, at the left and right ends of the $N-1$ segments. Matching derivatives 1 to $O-1$ at each of the $N-2$ knots gives another $(N-2)(O-1)$ conditions. Since the $N-1$ segments have $(N-1)(O+1)$ polynomial coefficients, $O-1$ more conditions are required to complete the specification. For cubic splines, a pair of end conditions is usual.

When there is "noise" or random scatter in the data, it is not appropriate for the curve to pass through each data point, so a least-squares fit is done instead. The spline method of smoothing noisy data is widely used in many fields. In this case there are many data points M and only a few knots, the curve does not have to pass through any of the data points. The least squares process minimises the total squared error between each data point and the spline curve. The degree of smoothing is controlled by the order of the polynomials and the number of knots (see figure 6.1b). If there are N nodes, and the polynomial order is O, then the only constraints are the matching of the function values $S(z)$ and their $O-1$ derivatives at the $N-2$ knots, giving $(N-2)O$ conditions. Therefore there are $N+O-1$ parameters that can be used for the fitting.

On the one hand, real cosmological data are very noisy and full of statistical fluctuations which we want to smooth out, and on the other, we want to pick up any fluctuations that are really present. Therefore the aim is to find the right balance between smoothing and fitting. Any choice of fitting function must restrict or prejudice the result to some degree, but polynomial splines are about as flexible as one can get.

One may add a variety of constraints. For example, a "smoothing spline" attempts to reduce the second derivative of the fitted curve. Suppose there are M data points (z_m, d_m), $m = 1 \cdots M$, then the quantity to minimise is

$$\Delta = \sum_{m=1}^{M} \left[w_m \Big(d_m - S(z_m) \Big)^2 + v_m \Big(S^{(p)}(z_m) \Big)^2 \right] . \tag{6.1}$$

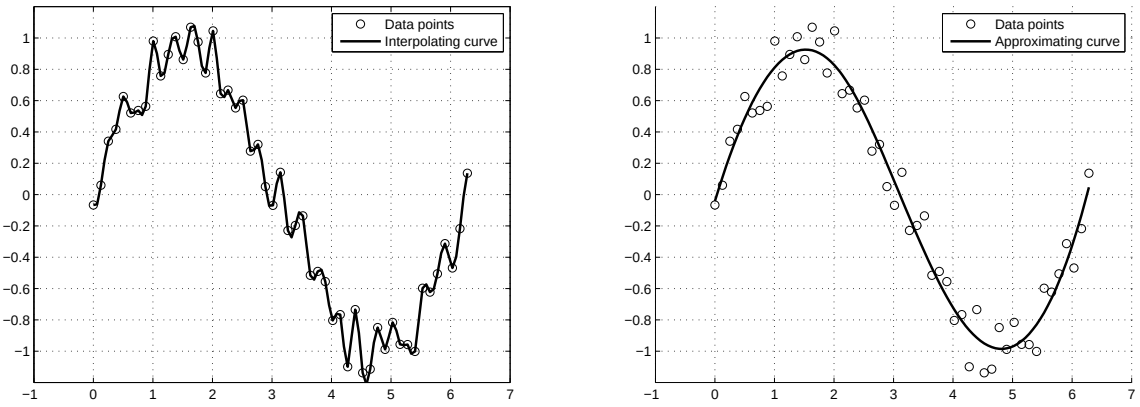

(a) Interpolating spline **(b)** Least squares spline

Figure 6.1: Illustration of fitting a spline to data (a) exactly, and (b) in a least squares sense.

Here $\big(d_m - S(z_m)\big)$ are the data errors, w_m are optional weights, $S^{(p)}$ is the pth derivative of the spline $S(z)$, and v_m are optional weights for smoothing. Usually $p = 2$. If all the v_m are zero, we have a standard least squares spline fit.

We found that a "smoothing spline" in which the second derivative is restricted everywhere, is not a good idea for the current problem. The $\hat{C}(z)$ curve rises steeply at small z, reaches a maximum, and then decreases asymptotically towards zero. Thus there are regions of high second derivative which we don't want to remove, and it won't be zero in general.

It is well known that polynomial fits to data are not good at the two ends, where the curves tend to bend strongly to one side. This is what we call a "moving tail", or Runge's phenomenon, and it is a problem in spline fitting too. To control this problem, we want to set the second and higher derivatives at the right end to zero.

In our case, we have certain expectations of our data. That is, the functions we fit to the data must have certain properties. For example, we expect $\hat{C}(z)$ to go through the origin, $\hat{C}(0) = 0$. Similarly, we expect $\kappa\mu n(z)$ and its first derivative to be zero at $z = 0$. Thus the ability to specify that the spline pass through certain points is required.

The above two requirements are exact constraints that need to be applied only at certain points. They cannot be included in the function to be minimised, so they are handled by means of Lagrange multipliers.

By far the most common order of spline is the cubic spline, $O = 3$. However, this is not suitable for fitting the $\hat{C}(z)$ data, because our equations involve the first and second derivatives, $\hat{C}_z$ and $\hat{C}_{zz}$, which must also be smooth. Cubic splines do have continuous 2nd derivatives, but the plot of such a $\hat{C}_{zz}$ is very angular. Therefore, we need an $O \geq 4$ spline.

The Matlab toolbox has many cubic spline functions with lots of constraint options. It also has some higher order spline functions, but these have very few options.

Therefore we use a least-squares spline fitting function written by C. Hellaby that includes the required options. The calculation uses B-splines (basis splines), which won't be discussed here. This function is a generalised smoothing spline of any order, that also has the flexibility of entering any end conditions that you choose. It is more general because it can produce splines of any desired order, and because it can limit any spline derivative or combination of derivatives, with different weightings v_{pm} at each data point. The generalised minimisation function is

$$\Delta = \sum_{m=1}^{M} \left[w_m \Big(d_m - S(z_m) \Big)^2 + \sum_{p=1}^{O} v_{pm} \Big(S^{(p)}(z_m) \Big)^2 \right] , \tag{6.2}$$

In addition, at the first and last nodes, the value of S and any of its derivatives up to O can be separately specified or left free. It is called with

```
[S, b, P, QR, x, xL, xR, bL, bR, ppc, ppC] =
                                    SmoothingBSpline(z, d, xx, H, w, v, cl, cv)
```

It accepts as input arguments, the data in two vectors `z` and `d`, the vector of nodes `xx` (these are z values), the polynomial "order" `H` (which is $O+1$), the vector of data weights `w`, the matrix of derivative-limiting weights `v`, and two vectors of end conditions `cl` and `cv`. `cv` fixes the values and derivatives at the end nodes, and `cl` is a 0-1 vector that turns on or off any given end condition. The outputs of interest are as follows. `P` is a vector giving the B-spline coefficients, `b` defines the basis splines (B-splines) themselves, and `ppC` is a matrix giving the polynomial coefficients in each segment. To plot the fitted spline, we use the call

```
[S, b, x, xL, xR, bL, bR, ppc, ppC] = CalcBSpline(xx, H, P, z)
```

where `S` is the vector of spline values at the points in the `z` vector.

6.2 Testing the Spline Fitting

Now that we have explained how splines work, we want to test the new Matlab spline fitting function with noisy data, and experiment with the smoothing constraints.

Firstly we took idea artificial data for $\hat{C}$ and $\kappa\mu n$, based on known metric functions in an inhomogeneous model, that was generated by a Matlab program by C. Hellaby. This idealised data was made more 'realistic' by adding statistical errors — random gaussian noise. In other words, we multiplied the ideal data by $1 + \epsilon$ where ϵ is a Matlab generated random data function with normal distribution and specified mean and standard deviation. This simulated data is used as input to the the fitting function.

Once the data are given, we fit a spline to the data, choosing order $O = 5$, and the number of knots $N - 2 = 4$. This provides $N + O - 1 = 10$ free polynomial coefficients. As noted above, there are 3 constraints that fix $\hat{C}(0) = 0$, $\kappa\mu n(0) = 0$ and $\kappa\mu n_z(0) = 0$, leaving 7 parameters that are set by least-squares fitting.

The fitted curves of $\hat{C}$ and $\kappa\mu n(z)$ plus the derivatives $\hat{C}_z$ and $\hat{C}_{zz}$ are shown in figures 6.2a and 6.2b. In this case, no derivative smoothing or end constraints were used, and the "moving tail" appears at the right end of Figures 6.3a & 6.3b. We will show in chapter 8 this effect will lead to unrealistic numerical results near the high-z end of the data.

Experiments with derivative smoothing showed that non-zero v_{pm}, even in limited regions, tended to make the fit worse, and not control the moving tail sufficiently. In order to have a reasonable fit, we add extra conditions to enforce zero higher derivatives at the high z end of the data. If we set the second and all higher spline derivatives to zero at the right end, this adds $O - 1 = 4$ constraints, leaving just 2 to fit the data. Now the function fitted the data produced good fits to the diameter distance and the redshift-space which were also smooth, as it is shown in figures 6.5–6.7. As we can clearly see at the right end of the $\hat{C}_z$ and $\hat{C}_{zz}$ in figure 6.6a & figure 6.6b, this method also shows a good reduction in the moving tail, compared to the previous one. We note that the fitting discrepancy in fig 6.2 is almost as good as in figure 6.5, despite the extra constraints and the reduced number of fittin parameters. After experimenting with this function, we find that it can produce reasonable fits, even with fairly large statistical error, up to a standard deviation of 30% times the original data.

(a) Ideal, simulated and fitted curves for $\hat{C}(z)$.

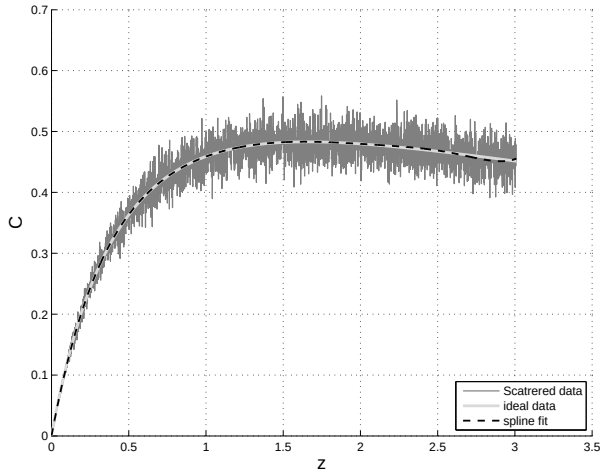

(b) Fitted $\hat{C}$ curve discrepancy.

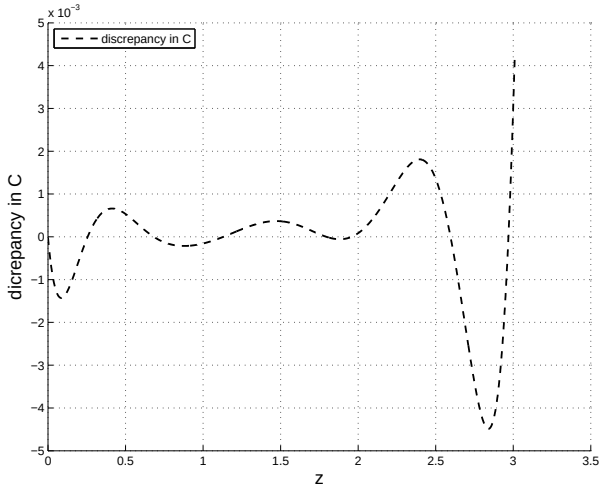

Figure 6.2: **(a)** shows the ideal data curve for the diameter distance $\hat{C}(z)$ in a strongly inhomogeneous model (light gray), the simulated noisy data with 5% standard deviation added (dark gray), and the spline fit (dashed-black). **(b)** shows the discrepancy $\hat{C}_{\text{spline}} - \hat{C}_{\text{ideal}}$.

(a) $\hat{C}_z$ from the spline fit.

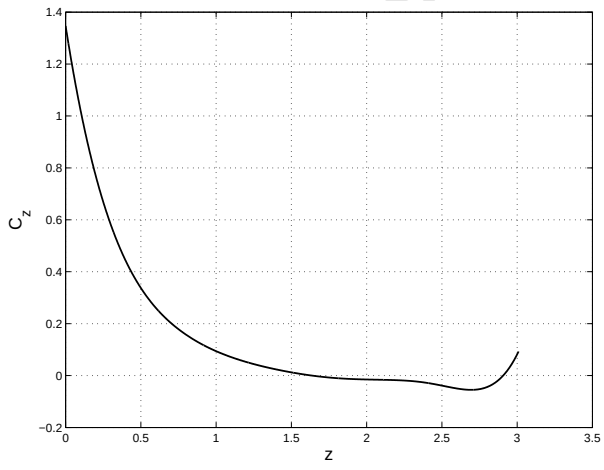

(b) $\hat{C}_{zz}$ from the spline fit.

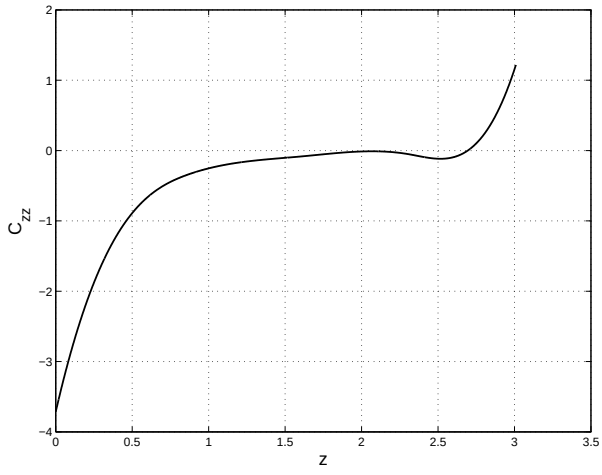

Figure 6.3: The "moving tail effect" or "Runge phenomenon", is apparent at the right ends of the graphs of the first and second derivatives of the spline fitted $\hat{C}(z)$ of figure 6.2. This shows why end conditions are needed.

(a) Ideal, simulated and fitted curves for $\kappa\mu n$.

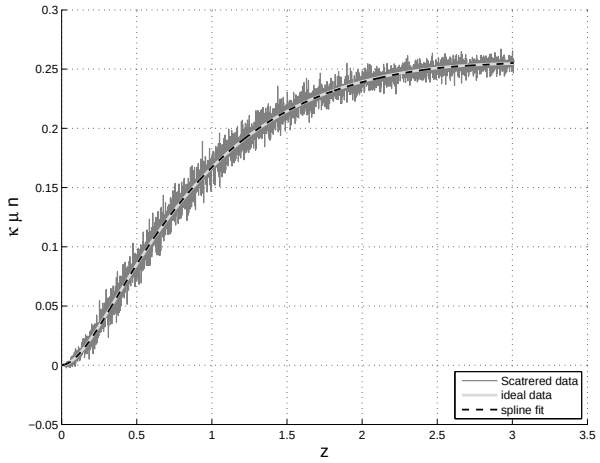

(b) Fitted $\kappa\mu n$ curve discrepancy.

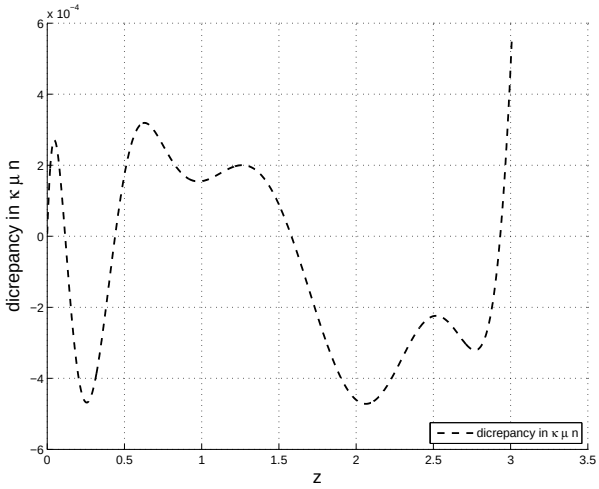

Figure 6.4: **(a)** Comparison between the ideal redshift-space density $\kappa\mu n$ (light gray), the simulated noisy data (dark gray) and the smoothed curve obtained from a least squares spline fit (dashed-black). **(b)** plots the discrepancy $\kappa\mu n_{\text{spline}} - \kappa\mu n_{\text{ideal}}$. The ideal model is the same as for figure 6.2, the added noise has standard deviation 5%.

(a) Ideal, simulated and fitted curves for $\hat{C}(z)$.

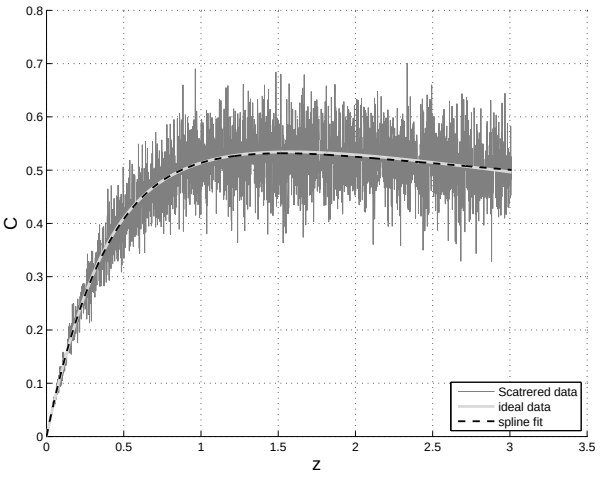

(b) Fitted $\hat{C}$ curve discrepancy.

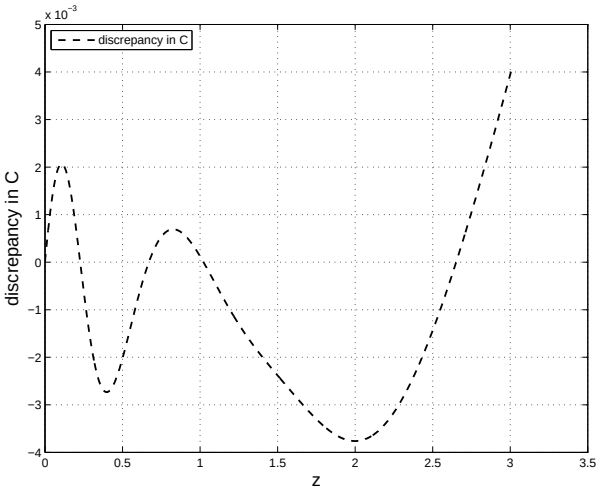

Figure 6.5: Spline fitting with end conditions. In this case the second and higher derivatives at the right end were set to zero. **(a)** shows the ideal data curve for $\hat{C}(z)$ in the same strongly inhomogeneous model (light gray), the noisy data with 10% standard deviation (dark gray), and the spline fit (dashed-black). **(b)** shows the discrepancy $\hat{C}_{\text{spline}} - \hat{C}_{\text{ideal}}$.

(a) $\hat{C}_z$ from the spline fit.

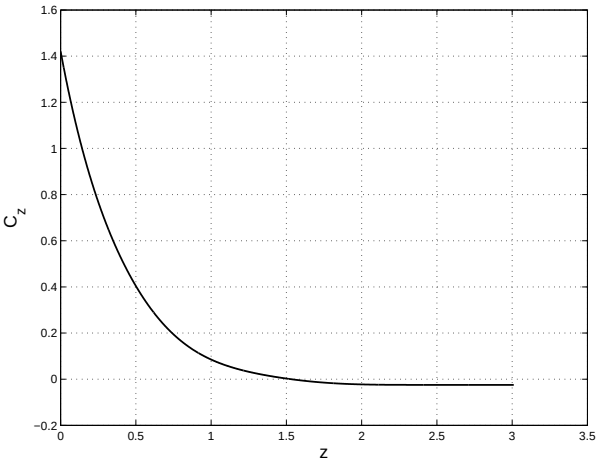

(b) $\hat{C}_{zz}$ from the spline fit.

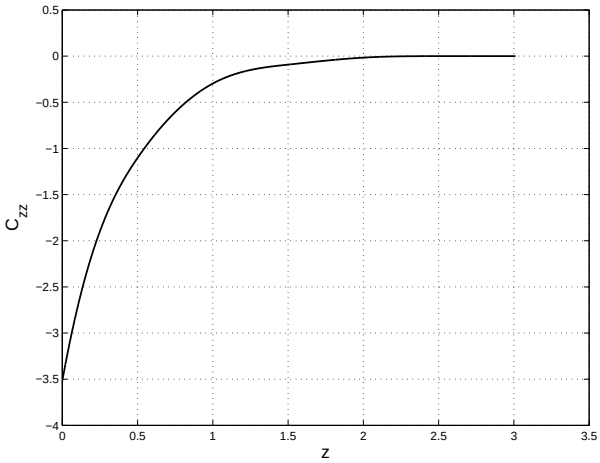

Figure 6.6: Spline fitting with end conditions. The plots of $\hat{C}_z(z)$ and $\hat{C}_{zz}(z)$, for the fit shown in figure 6.5, display much better behaviour, without any deflection, when end conditions are applied.

(a) Ideal, simulated and fitted curves for $\kappa\mu n$.

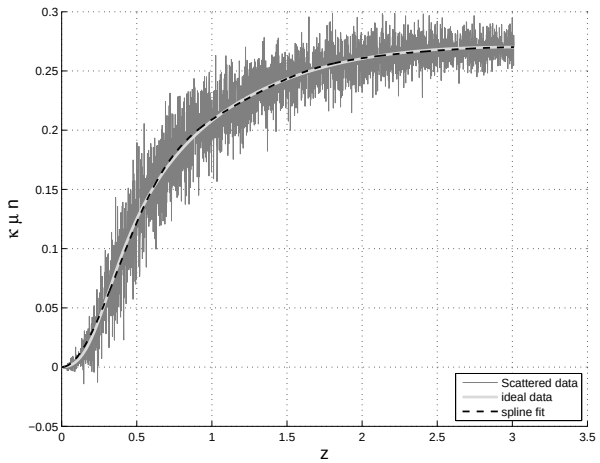

(b) Fitted $\kappa\mu n$ curve discrepancy.

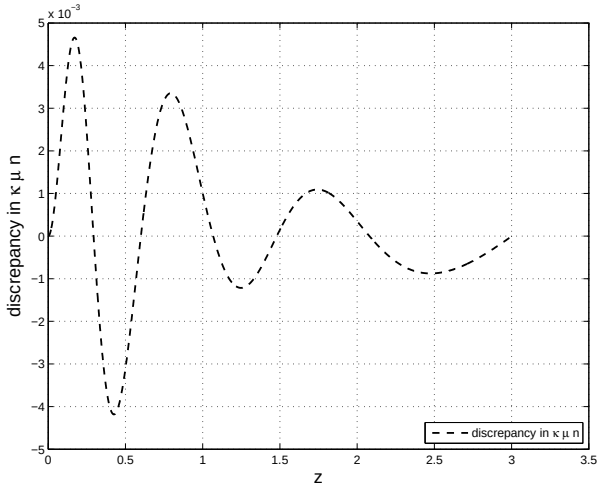

Figure 6.7: **(a)** Comparison of the ideal (light gray), noisy (dark gray), and fitted (dashed-black) curves for the redshift-space density $\kappa\mu n$. The ideal model and fitting constraints are the same as for figure 6.5, and the added noise has standard deviation 10%. **(b)** Plot of the discrepancy $\kappa\mu n_{\text{spline}} - \kappa\mu n_{\text{ideal}}$.

Chapter 7

Numerical Implementation

In this chapter, we describe the numerical implementation of the theoretical algorithms mentioned in chapters 4-5. Then we test the ability of the numerical codes to extract a Lemaître model from artificial but realistic, inhomogeneous data on the PNC, and calculate its evolution. The various stages of the overall algorithm can be summarised as follows.

I. Data Conversion

   (a) Convert the raw data for $\ell(z)$, $L(z)$, $\delta(z)$, $D(z)$, $n(z)$, $\mu(z)$ to the input functions $\hat{C}(z)$, $\kappa\mu n(z)$

   (b) Use least squares spline fitting to turn the discrete data for $\hat{C}(z)$, $\kappa\mu n(z)$ into smooth functions.

II. Assumptions

   (a) Choose the equations of state $p(\rho)$

   (b) Choose the value of Λ

   (c) Make the gauge choices that fix the coordinates

III. PNC Integration

   (a) Use the near-origin series to begin the solution near $z = 0$

   (b) Do a numerical integration of the DEs up to near the maximum C_m in the diameter distance

   (c) Use the near-maximum series, and join it to the end of the numerical integration

   (d) There is likely to be a discrepancy, owing to statistical and systematic errors in the data, so estimate a correction to the data from the apparent horizon relation

(e) Iterate the above 4 steps until a good match is obtained

(f) Continue the numerical solution beyond C_m as far as the data allows.

IV. Evolution

(a) integrate the evolution equations backwards and forwards from the PNC, $w = w_0$

Matlab programs were written to carry out these steps, and the details of the coding and testing will be discussed later, especially points of difficulty.

7.1 Data and Assumptions

The collection and reduction of observational data, and the discussion of the many observational issues, such as luminosity functions, are outside the scope of this work. The smoothing by means of spline fitting was adequately discussed in chapter 6. The main issue for any given data set, is whether it merits more or less parameters, that is, how many nodes to use in the spline. This depends on how much noise or scatter there is, and how much meaningful detail can be extracted.

The equation of state and the Λ value to assume are a matter of theoretical judgment, and some simple options will be considered below. It may be that different choices allow more or less satisfactory fits to the data, but this has yet to be determined.

The gauge choices were listed in section 4.5.1. In our numerical implementation, the 'OC' gauge was assumed.

7.2 PNC Integration

The range of available data determines the maximum z value, z_e, and here we assume $z_e \approx 3$. The range $[0, z_e]$ is divided into 3000 integration intervals.

There are four regions involved in the numerical integration down the PNC, see figure 7.1 below, and each requires a different treatment.

(1) The origin: The initial conditions for integrating the PNC DEs of section 4.5 are set at the origin $z = 0$, but obviously, galaxy redshift surveys have no sources exactly at the origin, even if a few blueshifts are measured. Therefore we use the near-origin Taylor series solution, as mentioned in section 5.3. The polynomial coefficients for the input data, C_i and K_i, come from the segment of the spline fit to the observations that includes the origin.

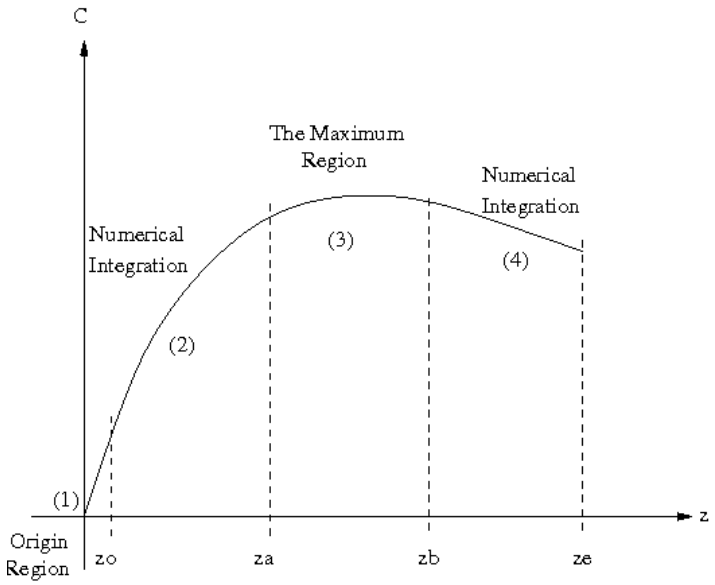

Figure 7.1: Schematic illustration of the different numerical regions, as shown on the $\hat{C}(z)$ curve.

(2) The first numerical integration region: This is the region that is bounded by $z_o \leq z \leq z_a$, and it requires a normal numerical integration method, such as the fourth order Runge-Kutta method. As explained in chapter 5, the DEs are singular at the origin $\hat{C} = 0$. Therefore the initial conditions for the numerical integration are obtained from the near-origin series solution values of φ, y, M, W, etc at some $z = z_o > 0$. Figures 7.2 and 7.3 show the comparison between the near-origin series solution and the numerical integration solution for $\varphi(z)$, and they verify that there is a range of good agreement of about 0.2%.

We see that z values in the range $0.025 < z_o < 0.07$ give good agreement. In our programme we have used $z_o = 0.047$, which is approximately 50 points away from the orgin of z data.

(3) The maximum region: We have shown that our DEs have an inevitable singularity at the maximum in $\hat{C}(z)$ where $z = z_m$. Thus we have to stop the numerical integration before this becomes a problem, and use the near-maximum Taylor series solution of section 5.5 to pass the integration through this region. The polynomial coefficients for the input data are again obtained from the spline segment that includes the maximum. Thus z_m and C_m are determined, and M_m is obtained from C_m. But this series solution is incomplete. It requires data from the end of the numerical integration to determine M_1 or equivalently W_m, which requires regions (2) and (3) to be joined. However, as explained in section 5.6, the apparent horizon condition (5.64) must hold at $\hat{C} = C_m$. There will certainly be statistical

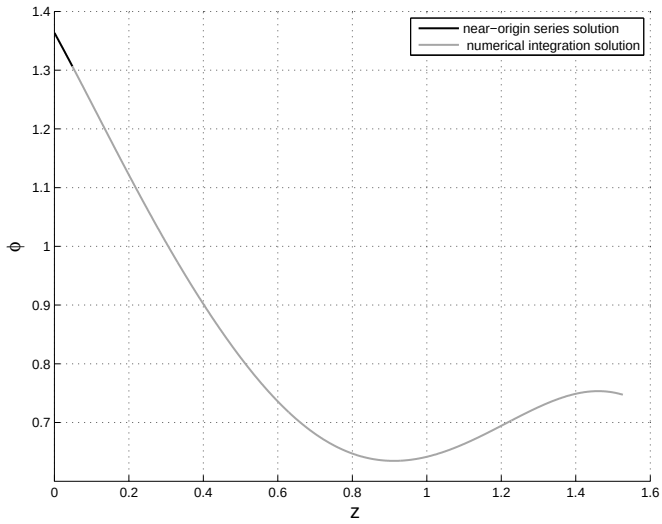

Figure 7.2: Comparison of near-origin and numerical solutions on the PNC. The dark curve shows the near-origin series for $\varphi(z)$, the light curves show numerical integration solutions starting from different z values, with initial conditions given by points in the series solution (for φ, y, M, W).

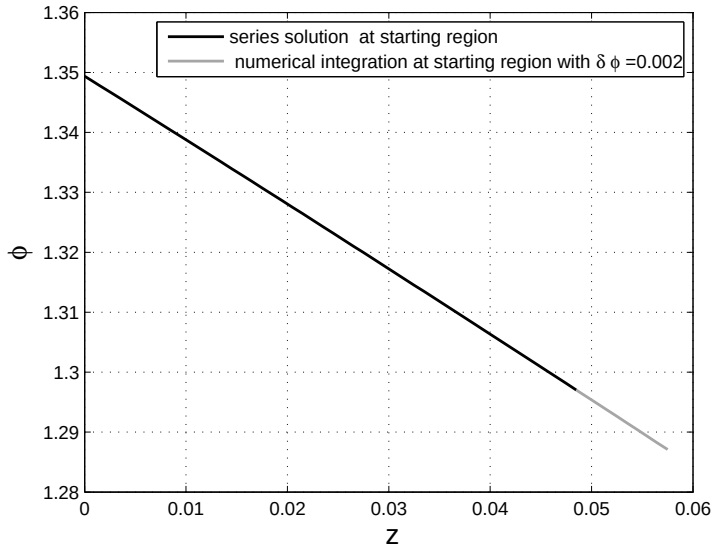

Figure 7.3: Magnified comparison of near-origin and numerical solutions of figure 7.2 in the range of good agreement. The two curves have a discrepancy of $\delta\varphi_{\text{series - integration}} = 0.0022$.

and systematic errors in the observational data, therefore the condition will not be exactly satisfied, and a good junction between the solution curves on the two sides will not be possible. In order to obtain a self-consistent solution, a correction must be applied to data.

We see that the junction of regions (2) and (3) is tricky because data at z_m provides information that feeds back to $z < z_m$ region. In other words, the failure to match the φ, M and W curves properly shows the data needs correction, but correction of the data means that the $\hat{C}(z)$ and $\kappa\mu n(z)$ functions all change, and the value and location of the maximum (z_m, C_m) also change. Therefore the fitting and integration needs to be re-done all the way from $z = 0$. Thus we require an iterative correction process. This is discussed in more detail in §7.3.

(4) The region after maximum: This is the final part of our numerical integration along the PNC, and it is bounded between $z_b \leq z \leq z_e$. It also uses the fourth order Runge-Kutta method, and the end of the maximum series, $z = z_b$, provides the initial values for this final part.

7.3 Matching Point and Iterative Correction

The procedure for finding a good matching point between the numerical and series the solutions before the maximum in $\hat{C}$ is slightly different from those mentioned in [58, 59, 63], but it still shares the same mathematical concept. We use $\varphi(z)$ rather than $y(z)$, $M(z)$ or $W(z)$ to determine the matching point, and decide where to stop the numerical integration, because φ is the only near-maximum series that has all its coefficients fully determined by the input data, and the others do not. In fact, finding the best point z_a to switch between the first numerical integration and the near-maximum series is not a trivial problem. We extend the Runge-Kutta solution of (5.2) as close to z_m as possible, and we calculate the near-maximum series solution using (5.69)-(5.71) so that there's plenty of overlap. If the input data were exact, then it should be easy to find a z value where the numerical and series calculations of φ agree. However, at the start we have erroneous data, so the two curves may cross at an angle, cross more than once, or even not cross at all. Thus the program compares the two curves over a range of z values, $\Delta z_{\text{join}} = 0.02$, calculating the net squared discrepancy for $\delta\varphi = \sum(\varphi_{j\ \text{numerical}} - \varphi_{j\ \text{series}})^2$ where the sum is over all the calculated z values within $z_{\text{join}}/2$ of some point z_*. By moving z_*, it looks for a region where the total squared discrepancy $\delta\varphi$ is smallest. The middle of this range z_* is used for the junction point z_a, and the discrepancy $\delta\varphi$ is recorded.

To obtain a self-consistent solution, a correction of the input data is needed. Since we only have one point where discrepancies can be detected, we keep the correction function simple. We assume the $\kappa\mu n(z)$ data are more affected by systematic errors than $\hat{C}(z)$, so we multiply all the $\kappa\mu n$ data by a constant factor, ε. The initial ε value is a guess, e.g. 1.1. We then begin the calculation process again; data fitting, origin series, numerical integration, maximum series, new matching point, new discrepancy $\delta\varphi$, new ε. We keep iterating this procedure, using a bisection method, until $\delta\varphi < 10^{-8}$, and the φ curves are sufficiently close to each other. For the bisection method to work, the first two $\delta\varphi$ values must have opposite signs. Therefore, before the main iteration, a range of ε values is scanned, following a pattern such as 1, 1.1, 0.9, 1.2, 0.8, $\cdots$, until one is found with a flipped $\delta\varphi$ sign. A similar approach was mentioned in [63], but the correction procedure was not automated.

Plotting the numerical and series curves over the same range of z values, as shown in figures 7.5 and 7.6, we can see that the numerical solution diverges as the singularity at z_m is approached, while the series solution is good near $z = z_m$ but not accurate away from z_m.

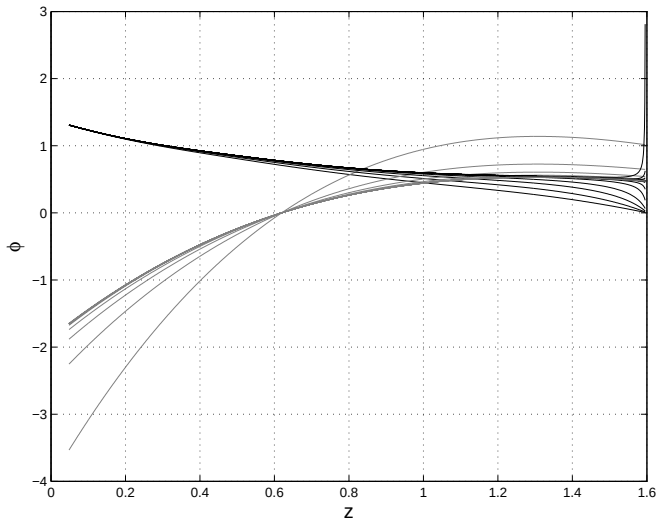

Figure 7.4: The iteration process for finding the matching point z_a. The gray curves represent the series solution for $\varphi(z)$, and the black curves represents the $\varphi(z)$ obtained from numerical integration. The improvment in the iteration process in the series and the numerics solution occurs from bottom to top.

Now, once we have determined the matching point z_a, we let the computer calculate M_a, W_a, and y_a from the numerical integration results. We can then find the value of M_1 from the numerical values of M_a and other quantities at z_a, by inverting the near-

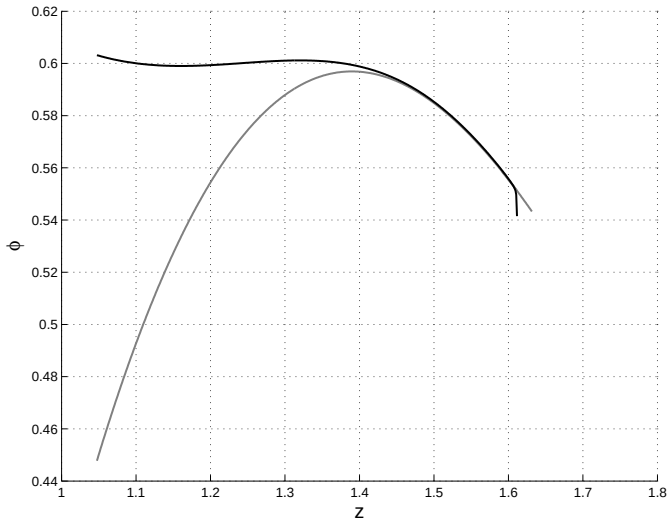

Figure 7.5: Finding the matching point z_a. The gray curve represents the series solution for $\varphi(z)$, and the black curve represents the $\varphi(z)$ obtained from numerical integration. The maximum in the diameter distance $\hat{C}_m$ is at $z_m = 1.615$. As expected, the series solution is only good near z_m, while the numerical solution diverges close to z_m. In this case there is a region of good agreement around $z = 1.55$.

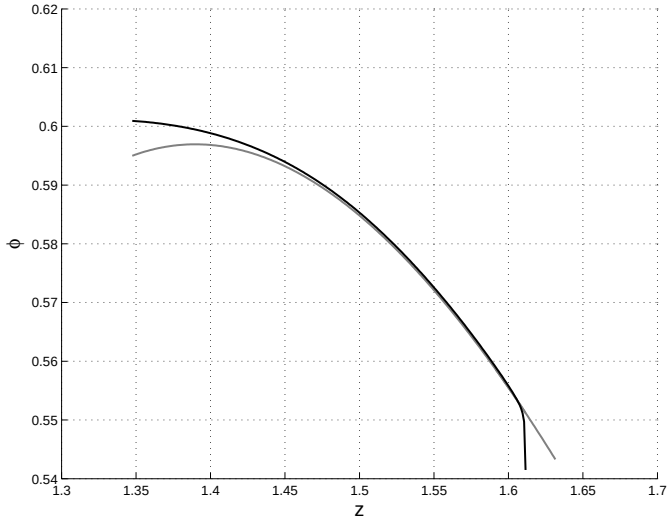

Figure 7.6: Magnification of the overlap between the series and numerical integration curves for $\varphi(z)$ just before z_m, showing a good matching occurs near $z = 1.553$.

maximum series solution in chapter 5. Thus, from (5.67)

$$M_a = M_m + M_1(z_a - z_m) + M_2(z_a - z_m)^2 + M_3(z_a - z_m)^3 \ , \tag{7.1}$$

$$W_a = W_m + W_1(z_a - z_m) + W_2(z_a - z_m)^2 + W_3(z_a - z_m)^3 \ . \tag{7.2}$$

where the coefficients M_2, M_3, W_m, W_1 and W_2 are given in §5.5. Since these coefficients are linear function of M_1, thus (7.1) and (7.2) can be simplified to

$$M_a = M_m + M_1(z_a - z_m) + (\mathcal{A}_2 M_1 + \mathcal{C}_2)(z_a - z_m)^2 + (\mathcal{A}_3 M_1 + \mathcal{C}_3)(z_a - z_m)^3 \ , \tag{7.3}$$

$$W_a = \mathcal{E}_m M_1 + (\mathcal{E}_1 M_1 + \mathcal{D}_1)(z_a - z_m) + (\mathcal{E}_2 M_1 + \mathcal{D}_2)(z_a - z_m)^2 + (\mathcal{E}_3 M_1 + \mathcal{D}_3)(z_a - z_m)^3 \ . \tag{7.4}$$

It is clear that there are two ways to find the numerical value of M_1. Firstly, if we use $M(z)$ for matching, then we find

$$M_1 = \frac{(M_a - M_m)/(z_a - z_m) - \mathcal{C}_2(z_a - z_m) - \mathcal{C}_3(z_a - z_m)^2}{1 + \mathcal{A}_2(z_a - z_m) + \mathcal{A}_3(z_a - z_m)^2} \ , \tag{7.5}$$

Secondly, if we use $W(z)$ for matching, then the value of M_1, would be

$$M_1 = \frac{W_a - \mathcal{D}_1(z_a - z_m) - \mathcal{D}_2(z_a - z_m)^2 - \mathcal{D}_3(z_a - z_m)^3}{\mathcal{E}_m + \mathcal{E}_1(z_a - z_m) + \mathcal{E}_2(z_a - z_m)^2 + \mathcal{E}_3(z_a - z_m)^3} \ . \tag{7.6}$$

Here $\mathcal{A}_i$, and $\mathcal{E}_i$ are the coefficients of M_1 in equations (5.73)-(5.75) and (5.76)-(5.78) while $\mathcal{C}_i$ and $\mathcal{D}_i$ are the free coefficients of M_1 in the same set of equations–for more details again see §5.5.

Having M_1 from (7.5) or (7.6), we evaluate the series solution for, $M(z)$, and $W(z)$ in the near-maximum z range. However, it turns out that we can't exactly match both the $M(z)$ and $W(z)$ curves at z_a. This is because the data is imperfect, whereas the AH equation (5.64) relates the true values of C_m and M_m. The above focuses on achieving a good matching at the first connection point, z_a. At the second connection point, z_b, the near-maximum series values provide the initial conditions for re-starting the numerical integration. As we will see, and as noted in [63], it is difficult to get a really good matching of both M and W at this point.

Up to this stage, our numerical code is working well and producing good matching results from the origin up to the maximum zone. The re-join between the the near-maximum series and the second numerical integration is set at the second connection point z_b, such that $z_m - z_a = z_b - z_m$. As with the end of the near-origin series, the initial values for the numerical integration are read off from the series values of $y(z_b)$, $\varphi(z_b)$, $M(z_b)$, and $W(z_b)$.

7.4 Evolution

With regards to the model evolution from initial surface of constant $w = w_0$, forward in time, we do the following: The numerical procedure down the PNC provides a full set of data for $A(w_0, y)$, $B(w_0, y)$, $C(w_0, y)$, $M(w_0, y)$, $W(w_0, y)$, and $\rho(w_0, y)$, $p(w_0, y)$, $\sigma(w_0, y)$, $\lambda(w_0, y)$, and $t(w_0, y)$. These data can be considered as initial conditions for the numerical integration of the time evolutions DEs. As stated earlier in §4.7, the time evolution DEs involved $\Phi, \Lambda, \sigma_y, A_y, \rho_y, U,$ and $dp/d\rho$, so that we cannot evolve the model until we calculate them. In our program we fix the value of Φ using the gauge choice mentioned before, and we set Λ to zero for simplicity. The remaining A, σ, ρ derivatives with respect to y are calculated using the numerical derivative method "the five point formula", U is calculated using numerical integration method along y, and $dp/d\rho$ is calculated from the equation of state as well.

Having the initial data and all the extra input data ready, we wrote a set of MATLAB functions that uses the Euler's method to propagate the entire PNC by integrating the coupled system of time DEs backwards or forwards in time from each y point on the PNC. Note that the integration procedure at each step in w, requires A_y, ρ_y, σ_y and U, and these must calculated before we update the initial conditions for the next iteration in time. The last thing that must be carefully done is the boundary conditions at central worldline. To provide boundary conditions for the DEs at the central point of each w surface, we wrote another program that uses the result of in §5.3.2 to evolve the origin along the central worldline. Hence, at each step in w we fit a low order polynomial to extract all the coefficients that is need to update the initial conditions for the next integration step. Once the integration is made, the origin evolution will be added to the model evolution along each surface of constant w. This simple integration procedure allows us to trace the historical evolution of the cosmology, to the past and future of it's presently observed state, using just the data on the PNC and an assumption about the EoS.

Chapter 8

Models and Results

In chapter 6 we presented our method for obtaining a smoothed data curve and its higher derivatives from realistic, noisy, discrete data, and in chapter 7 we discussed the numerical methods used to implement the theory of chapters 4 & 5. In this chapter, our main objective is to test a working numerical code, that allows us to deduce and evolve an inhomogeneous Lemaître model from observational data. To this end, we will use a set of artificial ideal and realistic (i.e. noisy) data, generated from mildly and strongly inhomogeneous models.[1] Testing is important to validate the numerical code, and also to demonstrate that the method works. Naturally, tests involve artificial data, as one doesn't know the correct output for real data.[2] The 'realistic' or 'noisy' data used here were generated by adding some statistical errors or Gaussian noise to the ideal data; this is similar to the procedure of McClure & Hellaby [63]. We added gaussian noise by multiplying the ideal data by $(1+\epsilon)$, where ϵ is a set of random values (one for each data point), generated by the Matlab function `randn`, having mean 0 and varying values for the standard deviation.

8.1 Ideal Data

In this section we will test our numerical implementation scheme using an ideal data-set where there is no statistical error added to it. The data are generated from a homogeneous model labelled `AAA1`. See appendix C for descriptions of the models used. We use the standard Matlab spline function SPAP2 to fit the data.

[1] The data we are using here was originally generated by C.Hellaby for the purpose of another project. The terminology 'ideal' data refers to data with no statistical fluctuations, i.e, accurate and smooth.

[2] The generation of artificial data for the Lemaitre model is an ongoing project, so the testing reported here is unfortunately incomplete.

8.1.1 Run 1

In this run we have tested the code using ideal data that are generated from a homogeneous model, `AAA1`. No noise was added, and Matlab's SPAP2 was used to fit the data. Figures 8.1-8.4 show the numerical result for y vs z, φ vs z, M vs z, and W vs z, when the DEs are integrated for a barotropic equation of state ($p = \chi\rho$, with $\chi = 0.008$)[3] down the PNC. In figure 8.4 we can see that there is a small jump in W at the second connection point, z_b, while y, φ, and M are smooth. As noted above, the curvature is a higher-order feature of a metric, and so it is more sensitive to small errors.

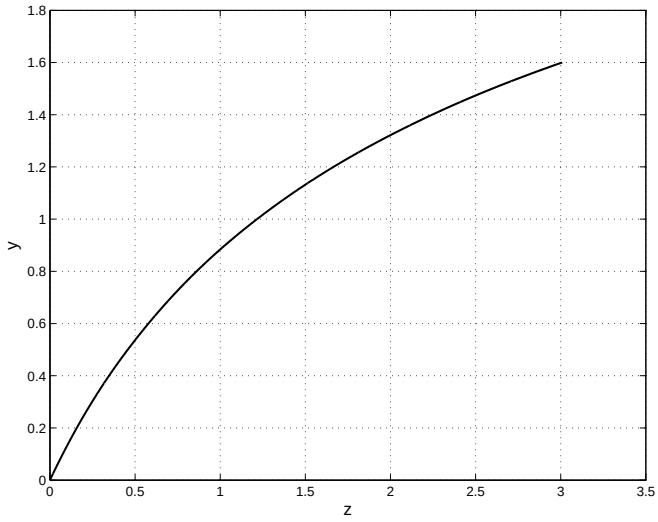

Figure 8.1: This figure shows the numerical results for y vs z **Run 1**.

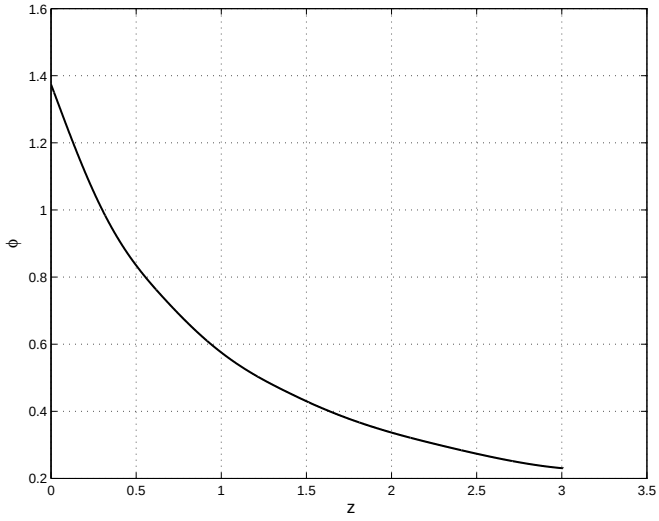

Figure 8.2: This figure shows the numerical results for φ vs z **Run 1**.

[3] A small non-zero χ was used to avoid numerical difficulties with exactly 0, but keep the pressure effectively zero.

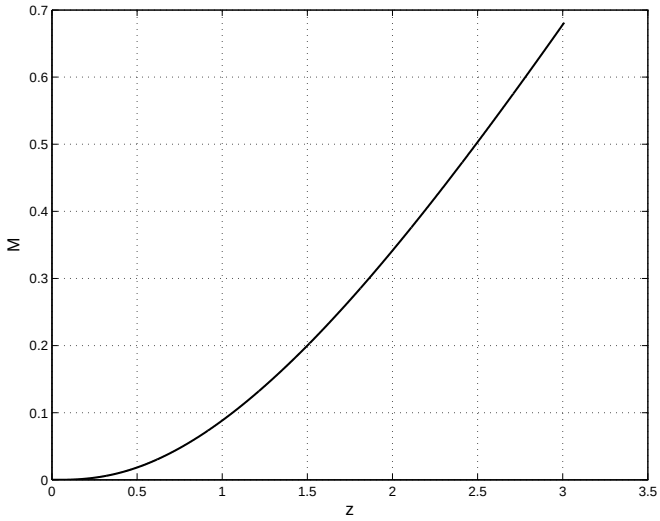

Figure 8.3: This figure shows the numerical results for M vs z **Run 1**.

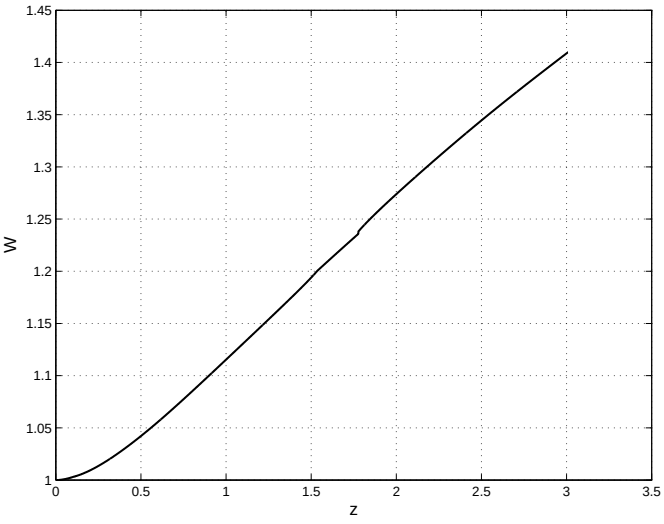

Figure 8.4: This figure shows the numerical results for W vs z from **Run 1**.

8.2 Statistical Errors and Smoothing

The next two runs add statistical fluctuations to ideal data. Either SPAP2 or `SmoothingBSpline` was used to smooth the realistic (noisy) data. Below we will use the same set of data used in §8.1.1 above, but the code will respond differently according to the smoothing method.

8.2.1 Run 2

In this run we use the data in model `AAA1`, then the PNC DEs are integrated for a barotropic equation of state $\chi = 0.008$ and simulated realistic data that has standard deviation 10% added to the ideal data. Then, we used standard Matlab spline function SPAP2 to smooth the data. Finally, the numerical results for y vs z, φ vs z, M vs z, and W vs z on the PNC are shown in figures 8.5-8.8. Here, the problem of the end conditions, the 'moving tail', still affects our numerical integration result, and leads to uncontrolled behavior at the end of the numerical integration. This is clearly shown at the right end of figures 8.6 and 8.8. We also note that the W curve still suffers a small jump at the second connection point z_b.

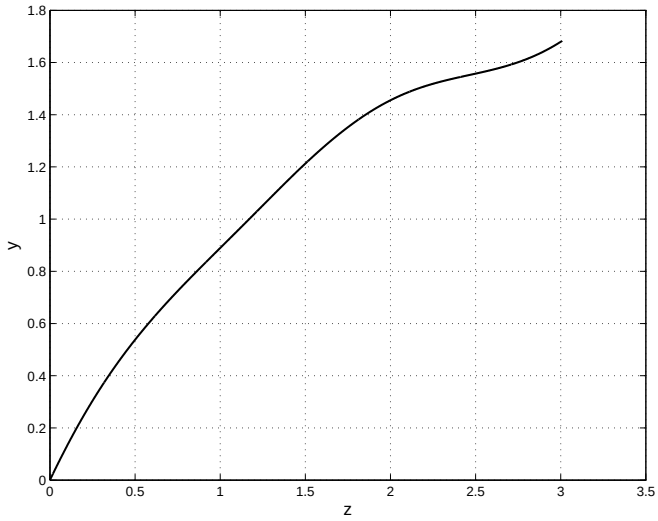

Figure 8.5: This figure shows the numerical results for y vs z from **Run 2**.

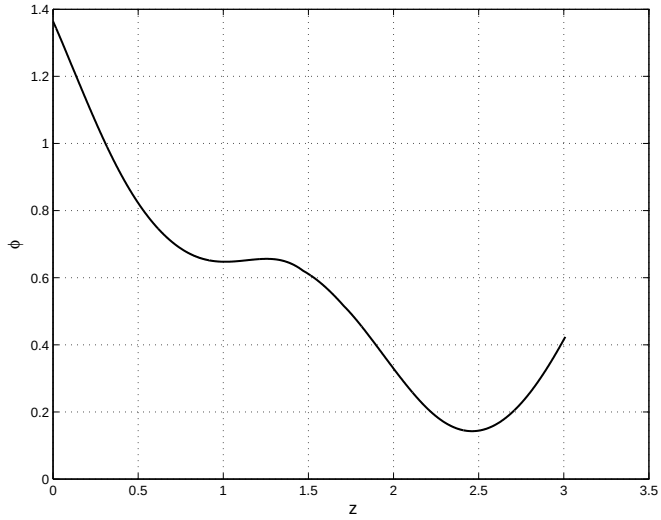

Figure 8.6: This figure shows the numerical results for φ vs z from **Run 2**.

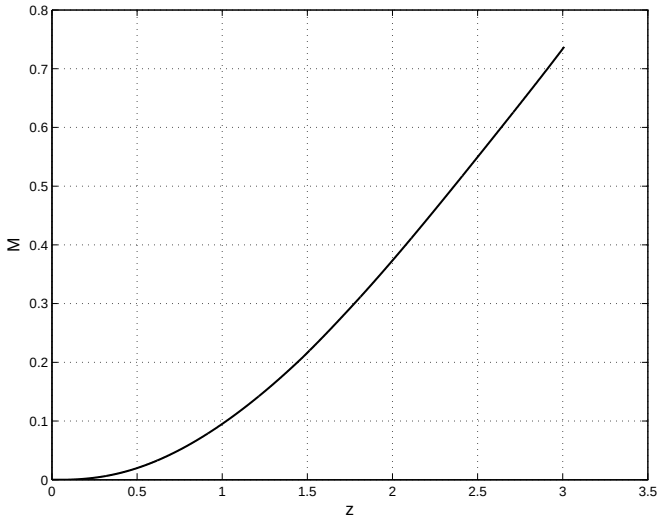

Figure 8.7: This figure shows the numerical results for M vs z from **Run 2**.

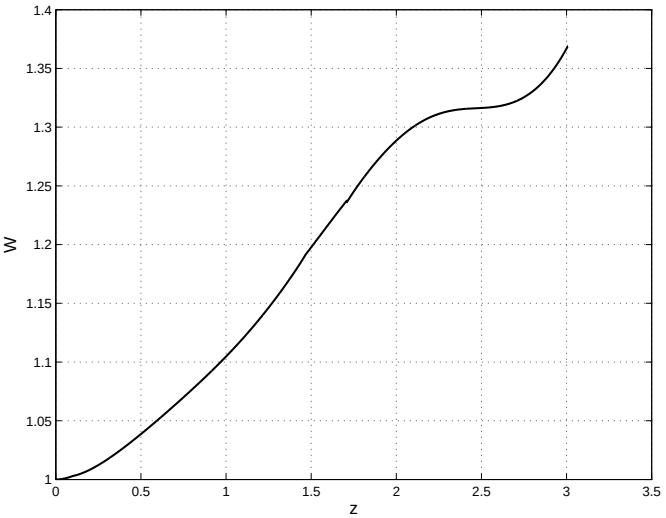

Figure 8.8: This figure shows the numerical results for W vs z from **Run 2**.

8.2.2 Run 3

As explained, the real data $\hat{C}$ and $\kappa\mu n$ are likely to suffer from systematic errors. Because of the AH condition (5.64), this means that a correction must be applied to the $\kappa\mu n$ data — see section 5.6. Systematic errors may take many forms, such as number-counts that are too low, or luminosity distances that are too high. Assumptions about the value of Λ or the equation of state would also cause systematic errors. Here we assume a non-zero pressure, when the ideal data were generated from a zero-pressure model.

In this run we test our code using realistic data that are generated from the `AAA1` model. The realistic data are generated by adding gaussian random noise with standard deviation 10%. Then the PNC DEs are integrated, with choice of equation of state $\chi = 0.1$. Lastly, figures 8.9 to 8.12 which represent the numerical integration y vs z, φ vs z, M vs z, and W vs z are the best result we obtained, when we used the generalised spline fitting function with polynomial order $O = 5$ and number of knots 6 to smooth the data. This method improves the accuracy in W, and reduces the jump at z_b to the minimum possible value.

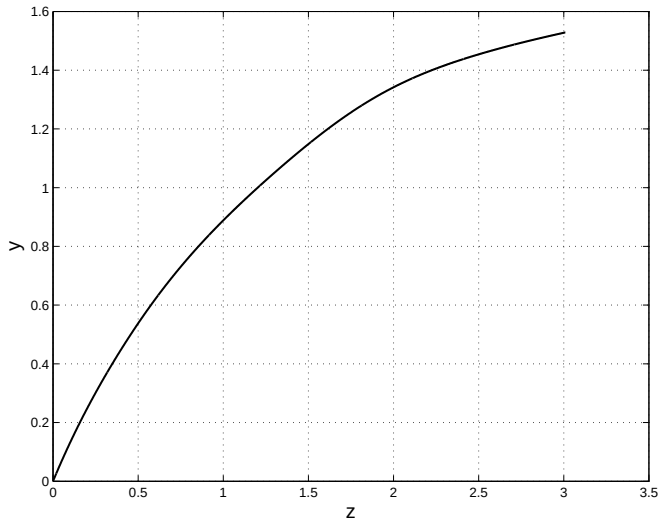

Figure 8.9: This figure shows the numerical results for y vs z **Run 3**.

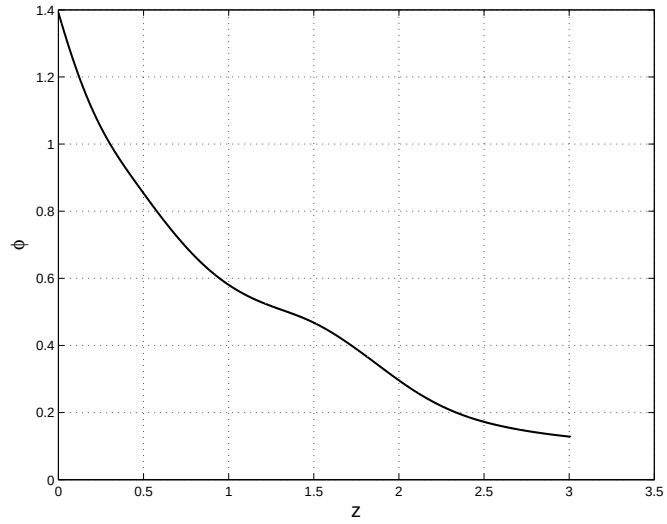

Figure 8.10: This figure shows the numerical results for φ vs z **Run 3**.

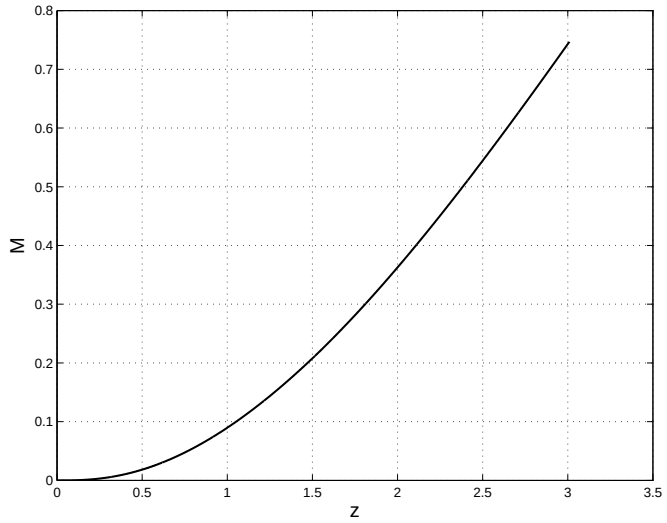

Figure 8.11: This figure shows the numerical results for M vs z **Run 3**.

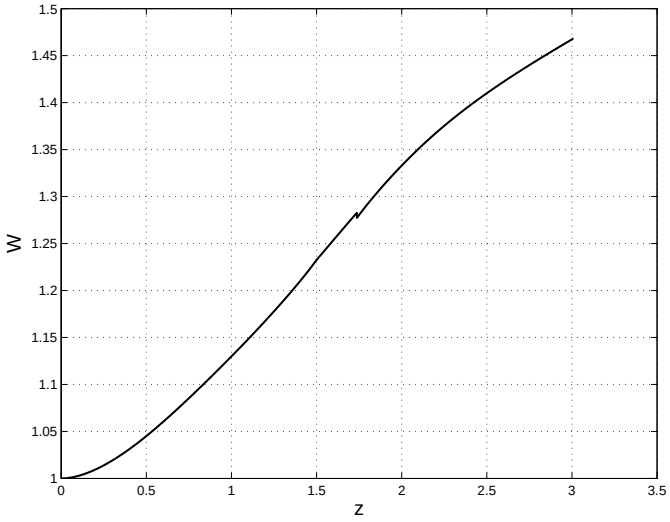

Figure 8.12: This figure shows the numerical results for W vs z **Run 3**.

8.3 Tests with Different Inhomogeneous Models

For diversity of testing, we will next test the numerical integration procedure down the PNC for different inhomogeneous models, including nonzero Λ and nonzero pressure.

8.3.1 Run 4

We used the `AAA8` data-set, and simulated realistic data by adding 20% statistical errors to this ideal data. The generalised spline function `SmoothingBSpline` was used to smooth the data, with polynomial order $O = 5$ and number of knots 8. Figures 8.13-8.16 are the numerical results of y vs z, φ vs z, M vs z, and W vs z of the integration procedure down the PNC when the equation of state $\chi = 0.008$ was used.

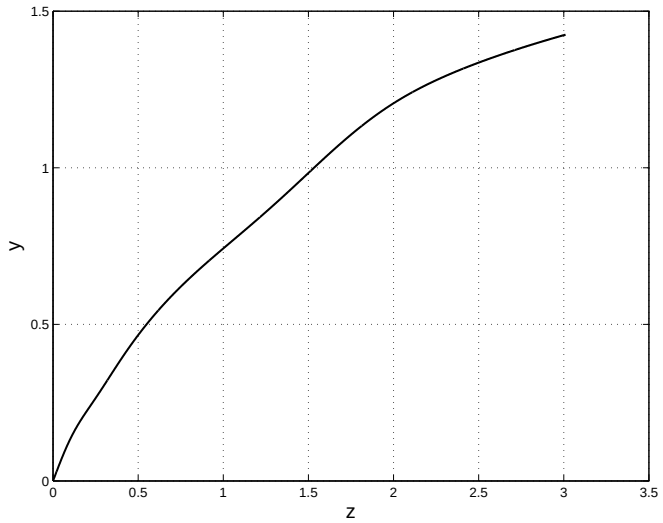

Figure 8.13: The numerical result for y vs z from **Run 4**.

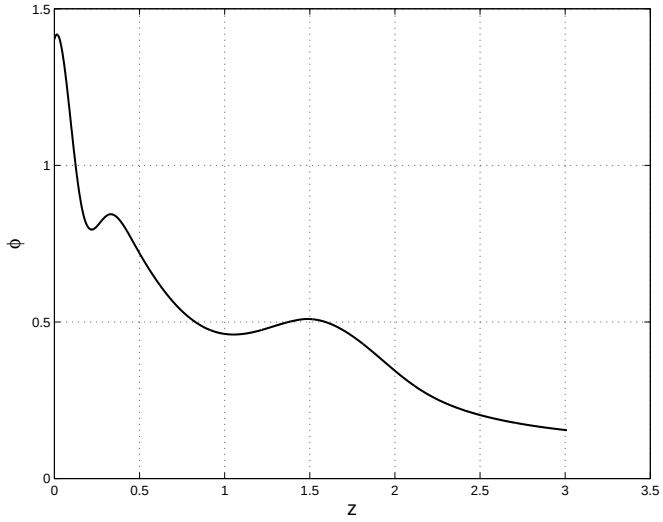

Figure 8.14: The numerical result for φ vs z from **Run 4**.

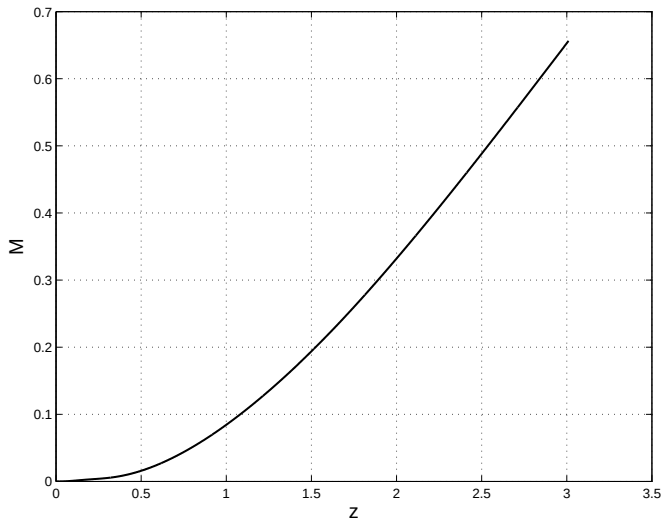

Figure 8.15: The numerical result for M vs z from **Run 4**

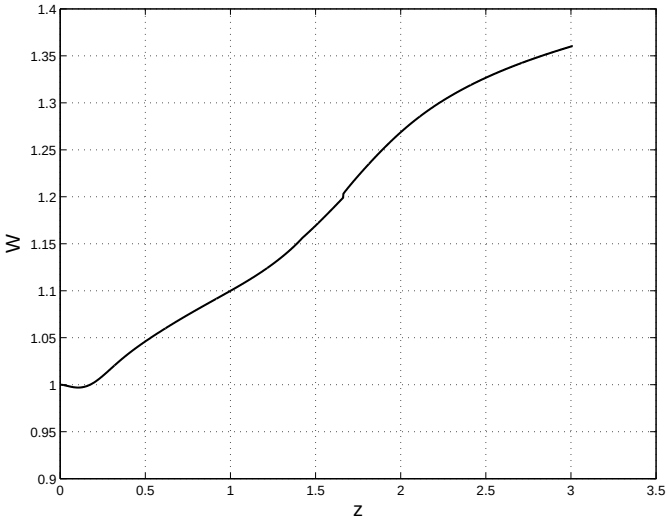

Figure 8.16: The numerical result for W vs z from **Run 4**.

8.3.2 Run 5

We used the `ACA1` data-set, and 20% statistical error was added to make it realistic. The generalised spline function `SmoothingBSpline` was used to smooth the data, with polynomial order $O = 5$ and 6 knots. The results are shown in figures 8.17-8.20, showing the numerical results for y vs z, φ vs z, M vs z, and W vs z when the DEs are integrated down the PNC when the equation of state $\chi = 0.008$ was considered in the integration procedure.

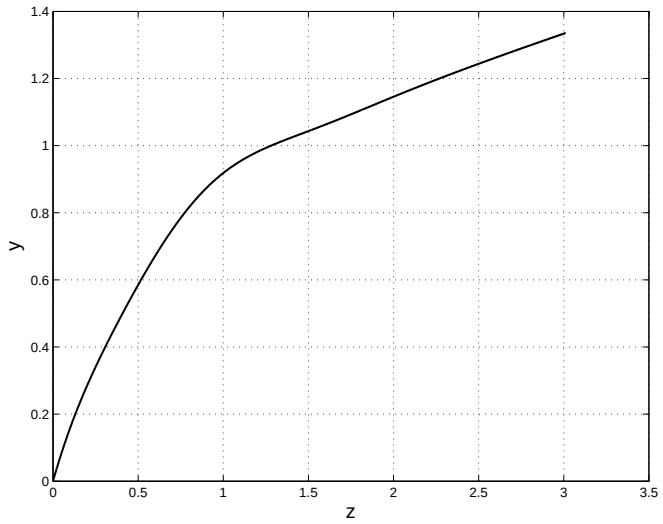

Figure 8.17: The numerical result for y vs z, from **Run 5**.

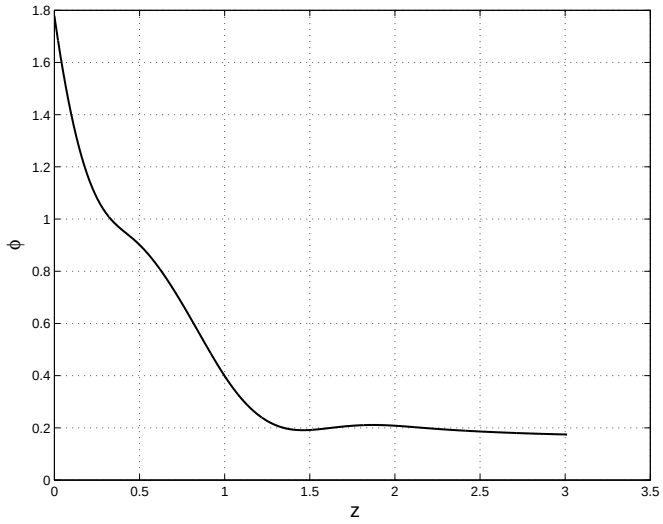

Figure 8.18: The numerical result for φ vs z from **Run 5**.

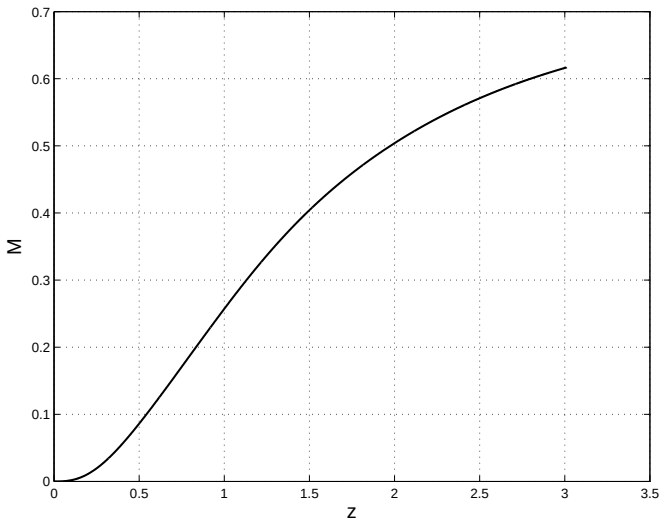

Figure 8.19: The numerical result for M vs z from **Run 5**.

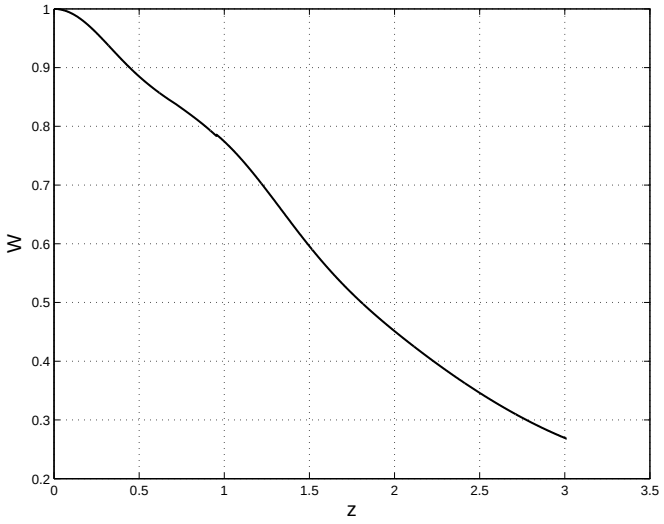

Figure 8.20: The numerical result for W vs z from **Run 5**.

8.4 Evolution

To illustrate the model evolution away from the PNC, we have used the data from §?? with the assumption of a barotropic equation of state, $\chi = 0.008$. The evolution DEs are integrated from the initial surface of constant $w = w_0$, "the PNC", and then evaluated forward in time using an Euler integration method. The results in figures 8.21-8.28 are the surface plots of $A(w, y)$, $B(w, y)$, $C(w, y)$, $M(w, y)$, $W(w, y)$, $\rho(w, y)$, $\lambda(w, y)$ and $\sigma(w, y)$, and they represent the cosmological evolution of the Lemaître model, that is generated from the initial data on the observer's PNC. The result here illustrates the output of the numerical evolution component of the Matlab code, derived from the 'initial conditions' produced by the PNC solution. It was found the slight W jumps remains with time.

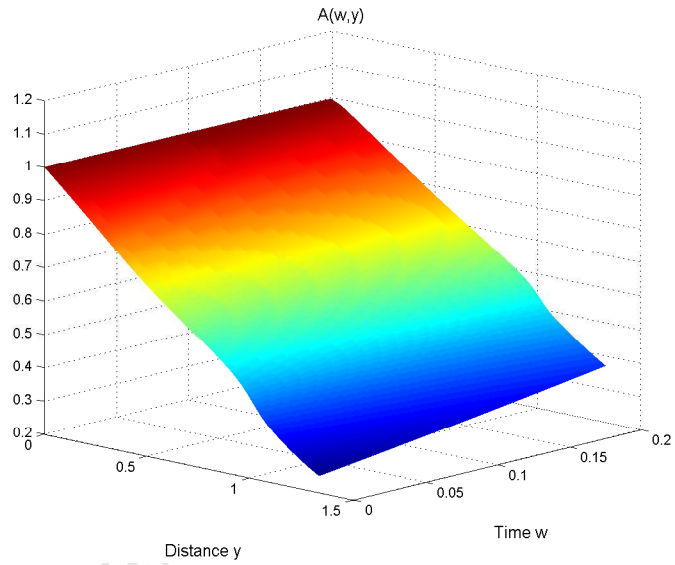

Figure 8.21: Numerical results for the evolution of Lemaître model in the "OC" gauge. The numerical solution gives the value of $A(w, y)$ every where.

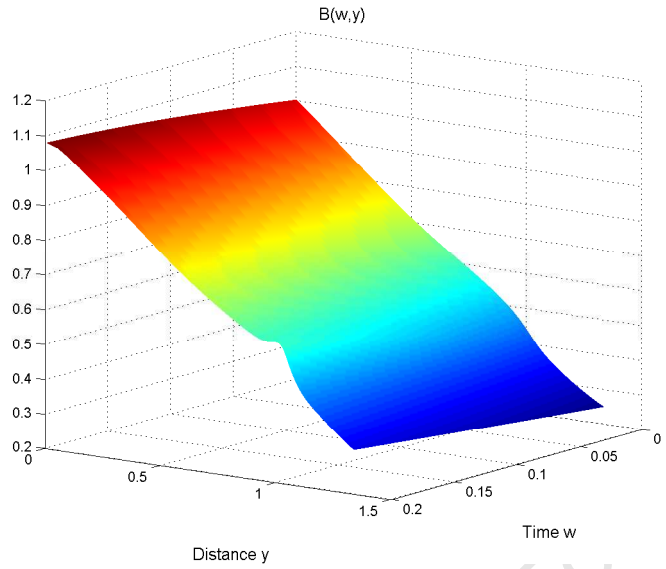

Figure 8.22: Numerical results for the evolution of Lemaître model in the "OC" gauge. The numerical solution gives the value of $B(w, y)$ every where.

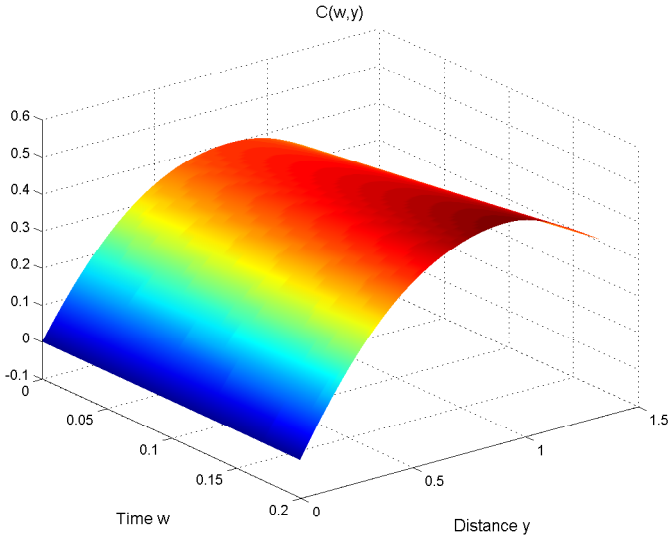

Figure 8.23: Numerical results for the evolution of Lemaître model in the "OC" gauge. The numerical solution gives the value of $C(w, y)$ every where.

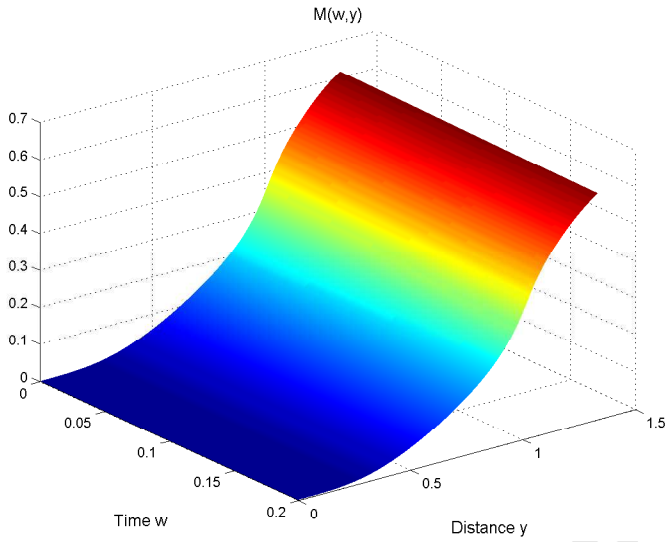

Figure 8.24: Numerical results for the evolution of Lemaître model in the "OC" gauge. The numerical solution gives the value of $M(w, y)$ every where.

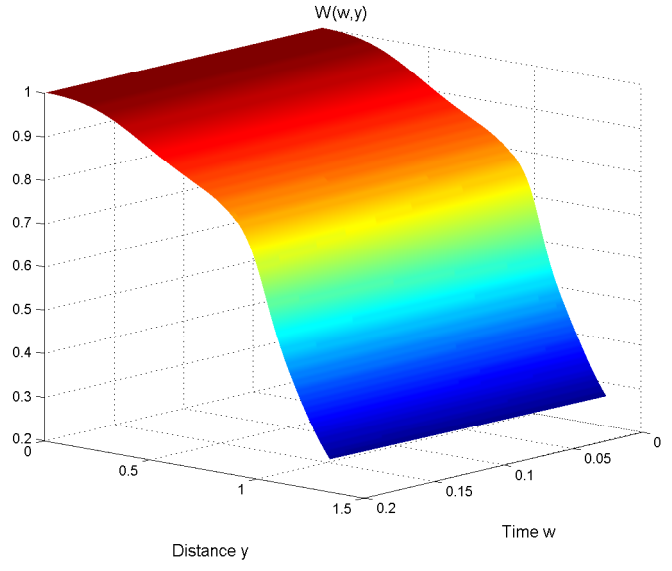

Figure 8.25: Numerical results for the evolution of Lemaître model in the "OC" gauge. The numerical solution gives the value of $W(w, y)$ every where.

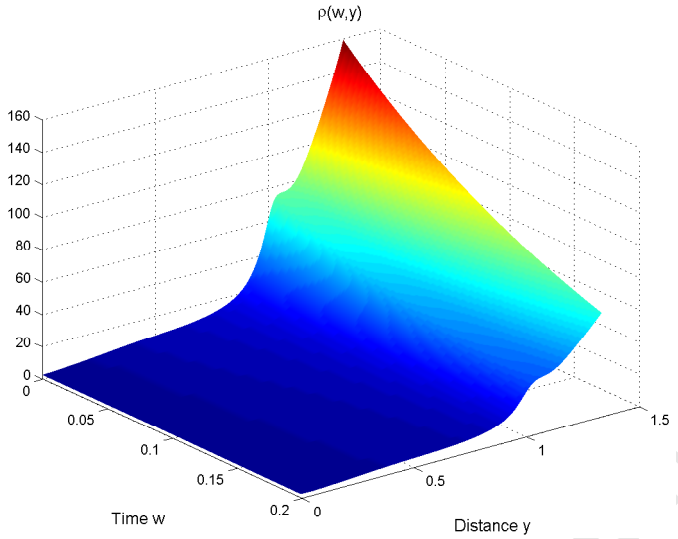

Figure 8.26: Numerical results for the evolution of Lemaître model in the "OC" gauge. The numerical solution gives the value of $\rho(w, y)$ every where.

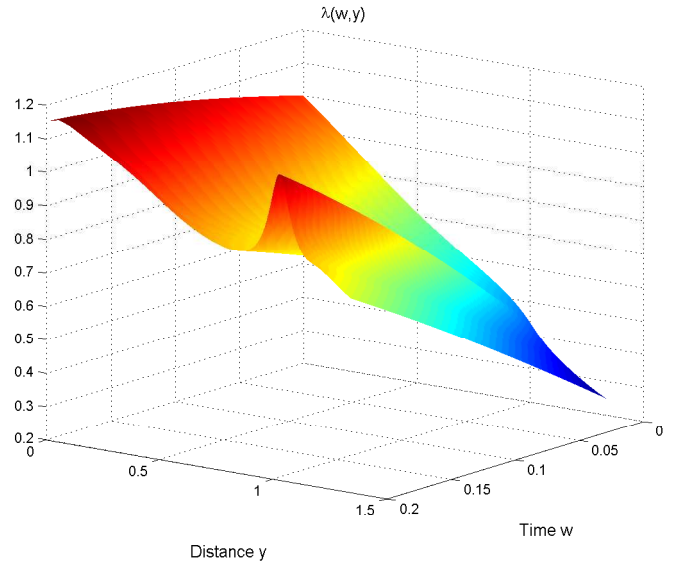

Figure 8.27: Numerical results for the evolution of Lemaître model in the "OC" gauge. The numerical solution gives the value of $\lambda(w, y)$ every where.

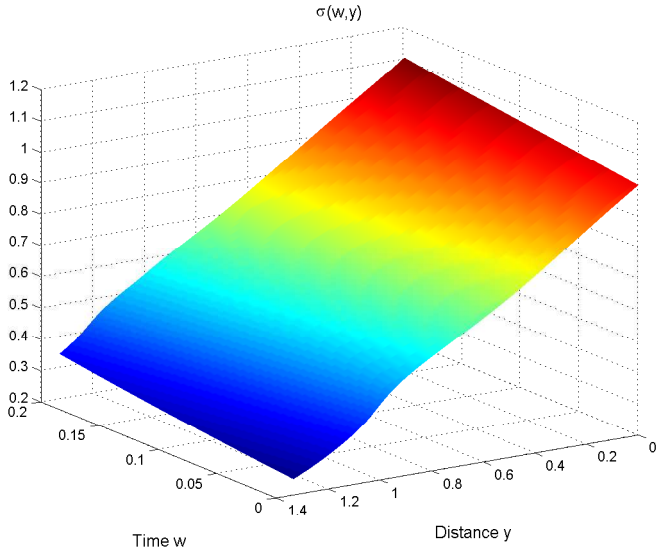

Figure 8.28: Numerical results for the evolution of Lemaître model in the "OC" gauge. The numerical solution gives the value of $\sigma(w, y)$ every where.

8.5 Discussion

These runs provide a demonstration that the methods of the previous chapter can be implemented and give reasonable results. Sections 8.1.1-8.3.2 and figures 8.1-8.20 show the metric on the PNC can be derived from observations, and section 8.4 with figures 8.21-8.28 shows the PNC initial data can be evolved to generate 4-d spacetime. Certainly, further testing is desirable, and further experimentation with the various parameters, such as the degree of the spline polynomial, or the number of nodes in the spline fit, could improve results, but these runs are a good start.

The issue of finding the best matching point in the numerical procedure down the PNC that is mentioned in section 7.3 is applied in all runs **Run 1-5** here. The calculation of M_1 at the matching point was automatically generated by the program itself. In all figures 8.4, 8.8, 8.12, 8.16 & 8.20 the programme used W curves to calculate the value of M_1 at the matching point z_a, therefore we observe that the jump in M is completely absent, and the result from the numerical integration is in good agreement, "connecting" with the series solution before and after the maximum $\hat{C}_m$. In other words, when connecting M to M, and W to W at the ends of the series bridge, the curve of M does not suffer any discrepancy at all, and the jump in W is minimal. In practice, this can be considered as a satisfactory result.

In the case of data with systematic errors, the correction procedure improves the data to generate a self-consistent Lemaitre model. This is certainly better than the output using the uncorrected data. However, the apparent horizon equation only holds at a single

distance, whereas systematic errors occur over a range of distances, so the correction derived from the AH must be relatively simple, and we can't be sure the correction is entirely accurate away from the AH.

Chapter 9

Conclusion

The main objective of this thesis was to work out the 'Metric of the Cosmos' (MoC) solution algorithm assuming a Lemaître metric, for the cosmological model, including both the past null cone solution and the model evolution as well. In other words, this is a generalization of the Lemaître-Tolman (LT) cosmology assumed in previous work, that includes both non-zero pressure p, and cosmological constant Λ.

This is a part of the long term MoC project began by Mustapha, Lu, McClure and Hellaby. As with the earlier papers [35, 59, 63, 69], the purpose is to develop an algorithm that will take as input, observational data from galaxy surveys, and output the metric of the spacetime we live in. The galaxy data considered here consists of the redshift, the luminosity and/or diameter distance, and number count density in redshift space, combined with the corresponding evolution functions, the true diameter, the absolute luminosity and the mass per source.

This project is important firstly because it is interesting in its own right — it is a primary application of Einstein's field equations (EFEs), and secondly because the assumption of homogeneity is built in to most of the cosmological data reduction that is done, and if we don't rigorously test for inhomogeneity, there is a danger of a circular argument. As cosmological data becomes more complete and more accurate, the assumptions of our cosmological models should be thoroughly tested.

With regard to the theoretical part, the spherically symmetric, inhomogeneous Lemaître model, and its solution from the EFEs were reviewed clearly in Chapter 2. Then the observational functions — the theoretical relations between the source quantities, the redshift z, the luminosity distance d_L, the angular diameter distance d_D, and the redshift-space density $\kappa\mu n$, were derived. The PNC part of the MoC solution was successfully generalised. This was not taken further, however, because the main effort was to complete the 'OC' form of the algorithm.

The observer coordinates (OC) approach [25, 61, 82–85] given in chapter 3 was used

as an alternative formalism to find a solution algorithm for the Metric of the Cosmos problem, for the case of the Lemaître metric. We used two approaches; (i) work from the OC form of the metric, and derive the solution process, and (ii) start from the known solution in normal time-space coordinates, and transform this to the OC form. In the first approach, the EFEs were solved and reduced to a system of differential equations (DEs) plus arbitrary functions of integration. This approach developed a method for integrating the model evolution with respect to the OC coordinates (w, y), instead of the space time coordinates (t, r), something that had not been found in LT case [37].

The non-zero pressure of the Lemaître model, and the associated EoS function $p(\rho)$, introduced new functions and made several functions depend on time that did not found in LT metric, i.e. M, f, W, A. Thus generalising the algorithm required significant modifications and new ideas. A time definition was introduced, as it helped to clarify the evolution.

In §4.5, the DEs for calculating the OC form of the Lemaître metric functions from observations were obtained, and some useful gauge choices were presented. In §4.7 we have clearly presented a step-by-step an algorithmic solution, as the basis for a numerical implementation.

Similarly to the Lemaître-Tolman case, there are four regions to PNC integration that need different treatments; the origin, the first numerical region, the maximum region and the last numerical integration region. The reason for this is that the DEs we derived are not defined at the origin, and also at the maximum in the diameter distance, where terms approach 0/0. The problem is overcome in chapter 5 by doing series expansions in the regions near these two singular points, and then connecting them with the numerical integration regions. The origin series is also needed because there is no actual data at the origin, so a fit to low-z data is needed to start the integration. The maximum in the diameter distance, where $\frac{\mathrm{d}\hat{C}}{\mathrm{d}z} = 0$, is also the apparent horizon (AH), and a unique relationship holds there, which connects the values of $\hat{C}$, $\hat{M}$ and Λ. This relationship is independent of any inhomogeneity, and so it provides a very useful cross-check on the results, and allows the correction of systematic errors.

As we have mentioned, real data has random statistical errors, but the DE integration procedure requires the data functions to be $\hat{C}$, $\hat{C}_z$, $\hat{C}_{zz}$, and $\kappa\mu n$ to be sufficiently smooth. Chapter 6 considered how best to smooth the data, and found that a specially written Matlab program that does a higher order polynomial spline fit was very effective. The program allows a wide range of end conditions that enabled the moving tail effect to be eliminated. Matlab's own spline functions were found to be either of too low order, or

lacking the necessary end conditions. The smoothing method was tested on simulated real data that was generated by adding random Gaussian fluctuations to the ideal data of a known model.

The last part of this thesis was to implement the theoretical algorithm numerically, and get a working computer code that can produce an Lemaître model and its evolution from the data. In chapter 7 we wrote a set of Matlab codes that can perform the algorithm components of the previous chapters. Firstly the data was smoothed with a least squares polynomial spline fit. The low z part of the spline provided the coefficients for the origin series, and the initial conditions for the first numerical integration. Then a Runge-Kutta forth order method was used to integrate the DEs along the PNC up to some point just before the maximum in $\hat{C}$. The near-maximum series used the spline coefficients in that z region, and used them to evaluate the series solution around the maximum zone. The first matching point between the numerical integration and the series solution was automatically found by the program, as the middle of the region where the total squared discrepancy between numerical and series data for φ was smallest. The φ DE was used for finding the matching point, since that is the only DE for which all the near-maximum-series coefficients are fixed by the data. This clearly shown in Figure 7.5 or 7.6. The rejoin point was calculated as same z distance beyond the maximum, and then the second numerical integration was calculated using the initial conditions at this rejoin point. However, the AH condition, which holds at the maximum in $\hat{C}$, allows us to check the results of the numerical integration up to that point. Correction of the data is inevitably required, due to data errors, and this means the whole numerical process has to be redone up to the maximum region. This correction process was made iterative. Once completed, discrepancies are small, and a self-consistent solution is generated.

The PNC solution was used as the initial conditions, for the time evolution, and a Euler method was used to integrate the time DEs, with derivatives of several functions calculated at each step. Thus the Lemaître model evolution was successfully generated.

A series of runs was done in chapter 8, and the numerical results for the PNC solution and the time evolution were plotted. The 'observational' data used for these runs was generated numerically from some homogeneous and inhomogeneous models. The data was made more realistic by adding varying amounts of statistical and systematic error. It was found that the program works well. Although complete testing was not possible because of other unfinished work, several tests were passed successfully. The smooth join between the origin series and the first numerical integration indicates that both are correct. The convergence of the iterative data-correction procedure also indicates this is

a valid process. The smooth overlap between the near-maximum series and the numerical regions, after the data-correction is completed is a further confirmation of the algorithm.

For the future work, further testing is essential. In the longer term, the goal is to test this program with real data. Galaxy surveys such as the SDSS or 2dF survey or 2MASS are still too limited in z and completeness, but this situation is likely to change in a few years. As SNIa surveys get bigger, this will greatly improve the accuracy of distance measures. The inclusion of alternative data sources, such as the galaxy age data used in [15], should also be pursued. Once we have datasets of high completeness out to $z > 2.5$, we will be in a position to test the assumption of homogeneity. Testing the output for homogeneity is a goal of the Metric of the Cosmos project; thus it is important to add a numerical facility to check for homogeneity.

Bibliography

[1] A.H.A. Alfedeel. *Observations in Inhomogeneous Cosmology and the Cosmic Mass.* Msc thesis, University of Cape Town, 2009.

[2] A.H.A. Alfedeel and C. Hellaby. The lemaître model and the generalisation of the cosmic mass. *General Relativity and Gravitation*, 42(8):1935–1952, 2010.

[3] M.E. Araújo, R.C. Arcuri, M.L. Bedran, L.R. de Freitas, and W.R. Stoeger. Integrating einstein field equations in observational coordinates with cosmological data functions: Nonflat friedmann-lemaître-robertson-walker cases. *The Astrophysical Journal*, 549:716–20, 2001.

[4] M.E. Araújo, S.R.M.M. Roveda, and W.R. Stoeger. Perturbed Spherically Symmetric Dust Solution of the Field Equations in Observational Coordinates with Cosmological Data Functions. *The Astrophysical Journal*, 560:7–14, 2001.

[5] M.E. Araújo and W.R. Stoeger. Erratum: Exact spherically symmetric dust solution of the field equations in observational coordinates with cosmological data functions [Physical Review D 60, 104020 (1999)]. *Physical Review D*, 64(4):049902, 2001.

[6] M.E. Araújo and W.R. Stoeger. Obtaining the Time Evolution for Spherically Symmetric Lemaître-Tolman-Bondi Models Given Data on Our Past Light Cone. *Physical Review D*, 80:123517, 2009.

[7] M.E. Araújo and W.R. Stoeger. The Angular-Diameter-Distance-Maximum and Its Redshift as Constraints on $\Lambda \neq 0$ FLRW Models. *Monthly Notices of the Royal Astronomical Society*, 394(1):438–442, 2009.

[8] M.E. Araújo and W.R. Stoeger. Finding a Spherically Symmetric Cosmology from Observations in Observational Coordinates – Advantages and Challenges. *Journal of Cosmology and Astroparticle Physics*, 1107:029, 2011.

[9] M.E. Araújo and W.S. Stoeger. Using time drift of cosmological redshifts to find the mass-energy density of the universe. *Physical Review D*, 82:123513, 2010.

[10] M.E. Araújo, W.S. Stoeger, R.C. Arcuri, and M.L. Bedran. Solving Einstein Field Equations in Observational Coordinates with Cosmological Data Functions: Spherically Symmetric Universes with Cosmological Constant. *Physical Review D*, 78(6), 2008.

[11] N. Bishop and P. Haines. Observational Cosmology and Numerical Relativity. *Quaestiones Mathematicae*, 19:259, 1996.

[12] A. Biswas and K.R.S. Mani. Relativistic perihelion precession of orbits of Venus and the Earth. *Central European Journal of Physics*, 6(3):754–758, 2008.

[13] K. Bolejko. Structure formation in the quasispherical Szekeres model. *Physical Review D*, 73:123508, 2006.

[14] K. Bolejko. Evolution of cosmic structures in different environments in the quasispherical Szekeres model. *Physical Review D*, 75:043508, 2007.

[15] K. Bolejko, C. Hellaby, and A.H.A. Alfedeel. The metric of the cosmos from luminosity and age data. *Journal of Cosmology and Astroparticle Physics*, 2011(09):011+, 2011.

[16] K. Bolejko, A. Krasiński, C. Hellaby, and M.-N. Célérier. *Structures in the Universe by Exact Methods: Formation, Evolution, Interactions*. Cambridge Monographs on Mathematical Physics. Cambridge University Press, 2009.

[17] H. Bondi. Spherically symmetrical models in general relativity. *Mon. Not. R. Astron. Soc*, 107:410, 1947. Reprinted, with historical comments, in *General Relativity and Gravitation*. 31:1777, 1999.

[18] M.E. Cahill and G.C. McVittie. Spherical Symmetry and Mass-Energy in General Relativity. I. General Theory. *Journal of Mathematical Physics*, 11:1382–91, 1970.

[19] M.-N. Célérier. Do we really see a cosmological constant in the supernovae data? *Astronomy and Astrophysics*, 353:63–71, 2000.

[20] D.J.H. Chung and A.E. Romano. Mapping Luminosity-Redshift Relationship to LTB Cosmology. *Physical Review D*, 74:103507, 2006.

[21] C.A. Clarkson, A.A. Coley, R. Maartens, and C.G. Tsagas. CMB limits on large-scale magnetic fields in an inhomogeneous universe. *Classical and Quantum Gravity*, 20:1519–1528, 2003.

[22] M.P. Dabrowski, T. Denkiewicz, and M.A. Hendry. How far is it to a sudden future singularity of pressure? *Physical Review D*, 75, 2007.

[23] M.P. Dabrowski and M.A. Hendry. The Hubble Diagram of Type Ia Supernovae in Non-Uniform Pressure Universes. *The Astrophysical Journal*, 498(1):67, 1998.

[24] G.F.R. Ellis. General relativity and cosmology. *Proc. Int. School of Physics Enrico Fermi (Varenna)*, Course XLVII:104–79, 1971.

[25] G.F.R. Ellis, S.D. Nel, R. Maartens, W.R. Stoeger, and A.P. Whitman. Ideal observational cosmology. *Physics Reports*, 124(56):315 – 417, 1985.

[26] G.F.R. Ellis and G. Tivon. Observational Relationships in Inflationary Universes and Other Cosmologies. *The Observatory*, 105:189, 1985.

[27] I.M.H. Etherington. On the definition of distance in general relativity. *Phil. Mag. VII*, 15:761–73, 1933. Reprinted, with historical comments, in *General Relativity and Gravitation.* 39, 1055–67, 2007.

[28] M. Fermi. Sopra i fenomeni che avvengono in vicinonza di una linear oraria (About phenomenons near a world line). *Atti R. Accad Lincei Rend., Cl. Sci. Fis. Mat. Nat.*, 31(1):21–23, 51–52, 1922.

[29] A. Friedmann. Uber die Krümmung des Raumes. *Zeitschrift für Physik*, 10:377, 1922. Reprinted, with historical comments, in *General Relativity and Gravitation.* 31:1991, 1999.

[30] A. Friedmann. Uber die Möglichkeit einer Welt mit konstanter negativer Krümmung des Raumes. *Zeitschrift für Physik*, 21:326, 1924. Reprinted, with historical comments, in *General Relativity and Gravitation.* 31:2001, 1999.

[31] W. Godłowski, J. Stelmach, and M. Szydłowski. Can the Stephani model be an alternative to FRW accelerating models? *Classical and Quantum Gravity*, 21(16):3953, 2004.

[32] A.H. Guth. The Inflationary Universe: A Possible Solution to the Horizon and Flatness Problems. *Physical Review D*, 23:347–356, 1981.

[33] S.A. Hayward. Gravitational energy in spherical symmetry. *Physical Review D*, 53:1938–1949, 1996.

[34] C. Hellaby. Multicolour observations, inhomogeneity and evolution. *Astronomy and Astrophysics*, 372(2):357–363, 2001.

[35] C. Hellaby. The mass of the cosmos. *Monthly Notices of the Royal Astronomical Society*, 370(1):239–244, 2006.

[36] C. Hellaby. Modelling Inhomogeneity in the Universe. *PoS*, ISFTG:005, 2009.

[37] C. Hellaby and A.H.A. Alfedeel. Solving the Observer Metric. *Physical Review D*, 79(4), 2009.

[38] C. Hellaby and A. Krasinski. You can't get through Szekeres wormholes: Or, regularity, topology and causality in quasispherical Szekeres models. *Physical Review D*, 66:084011, 2002.

[39] C. Hellaby and K. Lake. Shell crossings and the Tolman model. *Astrophysical Journal*, 290:381–387, 1985; plus errata in: (1985) Astrophysical Journal 300, 461.

[40] P. Hobson, G.P. Efstathiou, and A.N. Lasenby. *General Relativity: An Introduction for Physicists*. Cambridge University Press, 2006.

[41] B. Hoffmann, V. Hlavatỳ, Czechoslovak Society of Arts, and Sciences in America. *Perspectives in geometry and relativity: essays in honor of Václav Hlavatỳ*. Indiana University Press, 1966.

[42] E. Hubble. A relation between distance and radial velocity among extra-galactic nebulae. *Proceedings of the National Academy of Sciences*, 15(3):168–173, 1929.

[43] H. Iguchi, T. Nakamura, and K.-I. Nakao. Is dark energy the only solution to the apparent acceleration of the present universe? *Prog.Theor. Phys*, 108:809–818, 2002.

[44] M. Ishak. On Perfect Fluid Models in Non-Comoving Observational Spherical Coordinates. *Physical Review D*, 65:124027, 2004.

[45] C. Clarkson J.-P. Uzan and G.F.R. Ellis. Time drift of cosmological redshifts as a test of the Copernican principle. *Physical Review Letters*, 100:191303, 2008.

[46] N. Jarosik, C.L. Bennett, J. Dunkley, B. Gold, M.R. Greason, M. Halpern, R.S. Hill, G. Hinshaw, A. Kogut, E. Komatsu, D. Larson, M. Limon, S.S. Meyer, M.R. Nolta, N. Odegard, L. Page, K.M. Smith, D.N. Spergel, G.S. Tucker, J.L. Weiland, E. Wollack, and E.L. Wright. Seven-year Wilkinson Microwave Anisotropy Probe (WMAP)

Observations: Sky Maps, Systematic Errors, and Basic Results. *The Astrophysical Journal Supplement Series*, 192(2):14+, 2011.

[47] E. Komatsu, K.M. Smith, J. Dunkley, C.L. Bennett, B. Gold, G. Hinshaw, N. Jarosik, D. Larson, M.R. Nolta, L. Page, D.N. Spergel, M. Halpern, R.S. Hill, A. Kogut, M. Limon, S.S. Meyer, N. Odegard, G.S. Tucker, J.L. Weiland, E. Wollack, and E.L. Wright. Seven-year Wilkinson Microwave Anisotropy Probe (WMAP) Observations: Cosmological Interpretation. *The Astrophysical Journal Supplement Series*, 192:18, 2011.

[48] M. Kramer, I.H. Stairs, R.N. Manchester, M.A. McLaughlin, A.G. Lyne, R.D. Ferdman, M. Burgay, D.R. Lorimer, A. Possenti, N. D'Amico, J.M. Sarkissian, G.B. Hobbs, J.E. Reynolds, P.C.C. Freire, and F. Camilo. Tests of General Relativity from Timing the Double Pulsar. *Science*, 314:97–102, 2006.

[49] A. Krasiński. *Inhomogeneous Cosmological Models*. Cambridge University Press, 2006.

[50] A. Krasiński, C. Hellaby, M.-N. Célérier, and K. Bolejko. Imitating Accelerated Expansion of the Universe by Matter Inhomogeneities — Corrections of Some Misunderstandings. *General Relativity and Gravitation*, 45:2453–2475, 2010.

[51] J. Kristian and R.K. Sachs. Observations in Cosmology. *Astrophysical Journal*, 143:379, 1966.

[52] H. Kurki-Suonio. Lecturer Notes in Cosmology and Relativity I & II. University of Helsinki, 2011.

[53] O. Lahav. Observational tests for the cosmological principle and world models. *Structure Formation in the Universe, Part II: Proceedings of the NATO Advanced Study Institute on Structure Formation in the Universe, Isaac Newton Institute, Cambridge, U.K. 26 July 6 August 1999, eds R.G. Crittenden and N.G. Turok*, 565:131–142, 2002.

[54] O. Lahav. Observational tests of FRW world models. *Classical and Quantum Gravity*, 19:3517–3526, 2002.

[55] K. Lake. Testing the ΛCDM Model (and More) with the Time Evolution of Redshift. *Physical Review D*, 76:063508, 2007.

[56] G. Lemaître. L'univers en expansion [the expanding universe]. *Ann. Soc. Sci. Bruxelles*, A53:51, 1933. English translation, with historical comments, in *General Relativity and Gravitation*. 29:637, 1997.

[57] A.R. Liddle and D.H. Lyth. *Cosmological Inflation and Large-Scale Structure*. Cambridge University Press, 2000.

[58] T.H.-C. Lu. Obtaining the Spacetime Metric from Cosmological Observations. Master's thesis, University of Cape Town, 2006.

[59] T.H.-C. Lu and C. Hellaby. Obtaining the spacetime metric from cosmological observations. *Classical and Quantum Gravity*, 24(16):4107–4131, 2007.

[60] R. Maartens. *Ideal Observations in Relativistic Cosmology*. Phd thesis, University of Cape Town, 1980.

[61] R. Maartens, N.P. Humphreys, D.R. Matravers, and W.R. Stoeger. Inhomogeneous universes in observational coordinates. *Classical and Quantum Gravity*, 13(6):1689, 1995.

[62] R. Maartens and D.R. Matravers. Isotropic and semi-isotropic observations in cosmology. *Classical and Quantum Gravity*, 11(11):2693+, 1999.

[63] M.L. McClure and C. Hellaby. Determining the metric of the Cosmos: stability, accuracy, and consistency. *Physical Review D*, 78(4), 2008.

[64] W.H. McCrea. Observable Relations in Relativistic Cosmology. I. *Zeitschrift für Astrophysik*, 9:290, 1935.

[65] W.H. McCrea. Observable Relations in Relativistic Cosmology. II. *Zeitschrift für Astrophysik*, 18:98, 1939. Reprinted, with historical comments, in *Gen. Relativ. Gravit*, 30:315, 1998.

[66] C.W. Misner and D.H. Sharp. Relativistic Equations for Adiabatic, Spherically Symmetric Gravitational Collapse. *Physical Review Online Archive (Prola)*, 136(2B):B571–B576, 1964.

[67] J.W. Moffat. Inhomogeneous Cosmology, Inflation and Late-Time Accelerating Universe. *ArXiv Astrophysics e-prints*, 2006.

[68] N. Mustapha and C. Hellaby. Clumps into Voids. *General Relativity and Gravitation* , 33:455–77, 2001.

[69] N. Mustapha, C. Hellaby, and G.F.R. Ellis. Large Scale Inhomogeneity Versus Source Evolution – Can We Distinguish Them Observationally?, 1997.

[70] W.J. Percival, B.A. Reid, D.J. Eisenstein, N.A. Bahcall, T. Budavari, J.A. Frieman, M. Fukugita, J.E. Gunn, Ž. Ivezić, G.R. Knapp, R.G. Kron, J. Loveday, R.H. Lupton, T.A. McKay, A. Meiksin, R.C. Nichol, A.C. Pope, D.J. Schlegel, D.P. Schneider, D.N. Spergel, C. Stoughton, M.A. Strauss, A.S. Szalay, M. Tegmark, M.S. Vogeley, D.H. Weinberg, D.G. York, and I. Zehavi. Baryon acoustic oscillations in the Sloan Digital Sky Survey Data Release 7 galaxy sample. *Notices of the Royal Astronomical Society*, 401:2148–2168, 2010.

[71] J. Plebanski and A. Krasinski. *An Introduction to General Relativity and Cosmology*. Cambridge University Press, 2006.

[72] M.A. Podurets. On One Form of Einstein's Equations for a Spherically Symmetrical Motion of a Continuous Medium. *Astronomicheskii Zhurnal*, 41:28–32, 1964. English translation, in *Soviet Astronomy-AJ*. 8:19-22, 1964.

[73] R.V. Pound and G.A. Rebka. Gravitational red-shift in nuclear resonance. *Physical Review Letters*, 3:439–441, 1959.

[74] M.B. Ribeiro and W.R. Stoeger. Relativistic Cosmology Number Counts and the Luminosity Function. *The Astrophysical Journal*, 592(1):1–16, 2003.

[75] A.G. Riess, L. Macri, S. Casertano, M. Sosey, H. Lampeitl, H.C. Ferguson, A.V. Filippenko, S.W. Jha, W. Li, R. Chornock, and D. Sarkar. A Redetermination of the Hubble Constant with the Hubble Space Telescope from a Differential Distance Ladder. *Astrophys. J*, 699:539–563, 2009.

[76] W. Rindler and D. Suson. How to Determine a Tolman-Bondi Universe from Ideal Observable and Theoretical Relations. *Astronomy and Astrophysics*, 218:15–8, 1989.

[77] H.P. Robertson. On the Foundations of Relativistic Cosmology. *Proceedings of the National Academy of Science*, 15:822–829, 1929.

[78] K. Rudnicki. *The cosmological principles*. Uniwersytet Jagielloński, 1995.

[79] B.S. Ryden. *Introduction to cosmology*. Addison-Wesley, 2003.

[80] I.I. Shapiro, M.E. Ash, R.P. Ingalls, W.B. Smith, D.B. Campbell, R.B. Dyce, R.F. Jurgens, and G.H. Pettengill. Fourth test of general relativity: New radar result. *Physical Review Letters*, 26:1132–1135, 1971.

[81] D.N. Spergel, L. Verde, H.V. Peiris, E. Komatsu, M.R. Nolta, C.L. Bennett, M. Halpern, G. Hinshaw, N. Jarosik, A. Kogut, M. Limon, S.S. Meyer, L. Page, G.S. Tucker, J.L. Weiland, E. Wollack, and E. L. Wright. First-Year Wilkinson Microwave Anisotropy Probe (WMAP) Observations: Determination of Cosmological Parameters. *The Astrophysical Journal Supplement Series*, 148(1):175–194, 2008.

[82] W. R. Stoeger, S. J. Stanley, D. Nel, and G. F. R. Eillis. Observational cosmology. IV. Perturbed spherically symmetric dust solutions. *Classical and Quantum Gravity*, 9(7):1711+, 1999.

[83] W.R. Stoeger, G.F.R. Ellis, and S.D. Nel. Observational cosmology. III. Exact spherically symmetric dust solutions. *Classical and Quantum Gravity*, 9(2):509+, 1999.

[84] W.R. Stoeger, S.D. Nel, R. Maartens, and G.F.R. Ellis. The fluid-ray tetrad formulation of Einstein's field equations. *Classical and Quantum Gravity*, 9(2):493+, 1999.

[85] W.R. Stoeger, S.J. Stanley, D. Nel, and G.F.R. Ellis. Observational cosmology. V. Solution of the first-order general perturbation equations. *Classical and Quantum Gravity*, 9(7):1725+, 1999.

[86] D.A. Szafron. Inhomogeneous cosmologies: new exact solutions and their evolution. *Journal of Mathematical Physics*, 18:1673–1677, 1977.

[87] P. Szekeres. A class of inhomogeneous cosmological models. *Communications in Mathematical Physics*, 41:55–64, 1975. 10.1007/BF01608547.

[88] P. Szekeres. Quasispherical gravitational collapse. *Physical Review D*, 12:2941–2948, 1975.

[89] M. Tanimoto and Y. Nambu. Luminosity distanceredshift relation for the LTB solution near the centre. *Classical and Quantum Gravity*, 24(15):3843–3857, 2007.

[90] G. Temple. New Systems of Normal Co-ordinates for Relativistic Optics. *Royal Society of London Proceedings Series A*, 168:122–148, 1938.

[91] R.C. Tolman. Effect of inhomogeneity on cosmological models. *Proc. Nat. Acad. Sci. USA*, 20:169, 1934. Reprinted, with historical comments, in *General Relativity and Gravitation*. 29:935, 1997.

[92] R.A. Vanderveld, E.E. Flanagan, and I. Wasserman. Mimicking Dark Energy with Lemaître-TolmanBondi Models: Weak Central Singularities and Critical Points. *Physical Review D*, 74:023506, 2006.

[93] A.G. Walker. On Riemannian Space with Spherical Symmetry about a line and The Conditions for Isotropy in General Relativity. *The Quarterly Journal of Mathematics*, 6:81–93, 1938.

[94] J.M. Weisberg, D.J. Nice, and J.H. Taylor. Timing Measurements of the Relativistic Binary Pulsar PSR B1913+16. *The Astrophysical Journal*, 722(2):1030+, 2010.

[95] C.-M. Yoo. A Note on the Inverse Problem with LTB Universes. *Prog.Theor. Phys*, 124:645–665, 2010.

[96] C.-M. Yoo, T. Kai, and K.-I. Nakao. Solving Inverse Problem with Inhomogeneous Universe. *Prog.Theor.Phys.*, 120:937–960, 2008.

Appendix A

The Transformation of Lemaître to Null-Comoving Coordinates

The Lemaître metric [56] is discussed in chapter 2, but we here pull together the equations needed for the transformation. Its metric is given in (2.1),

$$ds^2 = -e^{2\sigma}\,dt^2 + e^{\lambda}\,dr^2 + R^2\,d\Omega^2 \ , \tag{A.1}$$

where

$$d\Omega^2 = d\theta^2 + \sin^2\theta d\phi^2 \ , \tag{A.2}$$

$R = R(t, r)$ and $R' = \partial R/\partial r$. Equation (2.15) gives its evolution,

$$\dot{R} = \pm e^{\sigma}\sqrt{\frac{2M}{R} + f + \frac{\Lambda R^2}{3}} \ , \tag{A.3}$$

where $\dot{R} = \partial R/\partial t$, f is defined by (2.16)

$$f = e^{-\lambda}R'^2 - 1 \qquad \leftrightarrow \qquad e^{\lambda} = \frac{R'^2}{1+f} \ , \tag{A.4}$$

and the mass density and pressure are given by (2.13) & (2.14),

$$\kappa\rho = \frac{2M'}{R^2R'} \ , \tag{A.5}$$

$$\kappa p = -\frac{2\dot{M}}{R^2\dot{R}} \ . \tag{A.6}$$

The metric variables σ and λ have been calculated from the conservation equations to obey (2.7) and (2.8),

$$\dot{\lambda} = -\frac{2\dot{\rho}}{(\rho+p)} - \frac{4\dot{R}}{R} \ . \tag{A.7}$$

$$\sigma' = -\frac{p'}{p+\rho} \ . \tag{A.8}$$

We wish to transforms this metric into the observer coordinate form (4.1)

$$ds^2 = -A(w,y)^2\,dw^2 + 2A(w,y)B(w,y)\,dw\,dy + C(w,y)^2\,d\Omega^2 \ . \tag{A.9}$$

As in section 4.3, we introduce the transformation

$$t = t(w,y)\ , \qquad r(w,y) = y \qquad \to \qquad J = \frac{\partial(t,r)}{\partial(w,y)} = \begin{pmatrix} t_w & t_y \\ r_w & r_y \end{pmatrix} = \begin{pmatrix} t_w & t_y \\ 0 & 1 \end{pmatrix}\ , \tag{A.10}$$

which retains y as a comoving coordinate, so the metric becomes

$$ds^2 = -e^{2\sigma}\,(t_w\,dw + t_y\,dy)^2 + e^{\lambda}\,(r_w\,dw + r_y\,dy)^2 + R^2\,d\Omega^2 \tag{A.11}$$

$$= -t_w^2\,e^{2\sigma}\,dw^2 - 2\,t_w\,t_y\,e^{2\sigma}dw\,dy + \left(-t_y^2\,e^{2\sigma} + e^{\lambda}\right)dy^2 + R^2\,d\Omega^2\ . \tag{A.12}$$

We want w to be an incoming null coordinate, i.e. $dw = 0 = d\theta = d\phi$ must give $ds = 0$, and $t_y < 0$, which leads to, using (A.4),

$$g_{yy} = 0 \qquad \to \qquad t_y^2 = \frac{e^{\lambda}}{e^{2\sigma}} \qquad \to \qquad t_y e^{\sigma} = \frac{-R'}{\sqrt{1+f}} \tag{A.13}$$

$$\to \qquad ds^2 = -t_w^2\,e^{2\sigma}\,dw^2 + 2\,t_w e^{\sigma}\,\frac{R'}{\sqrt{1+f}}\,dw\,dy + R^2\,d\Omega^2\ . \tag{A.14}$$

Applying this transformation to the Lemaître evolution equation (A.3), i.e.

$$R_w = \dot{R}\,t_w + R'\,r_w = \dot{R}\,t_w\ , \tag{A.15}$$

we find the new evolution equation in the new coordinates is,

$$R_w = \pm t_w\,e^{\sigma}\,\sqrt{\frac{2M}{R} + f + \frac{\Lambda R^2}{3}}\ . \tag{A.16}$$

Similarly, by transforming R_y we obtain

$$R_y = \dot{R}\,t_y + R'\,r_y = -\dot{R}\left(\frac{R'}{e^{\sigma}\sqrt{1+f}}\right) + R' \qquad \to$$

$$R' = R_y\left(\frac{\sqrt{1+f}}{\sqrt{1+f}\ \mp\sqrt{\frac{2M}{R} + f + \frac{\Lambda R^2}{3}}}\right)\ , \tag{A.17}$$

where (A.13), (A.3) and (A.10) were used. The metric now becomes

$$ds^2 = -t_w^2\,e^{2\sigma}\,dw^2 + \frac{2\,R_y\,t_w e^{\sigma}}{\left(\sqrt{1+f}\ \mp\sqrt{\frac{2M}{R} + f + \frac{\Lambda R^2}{3}}\right)}\,dw\,dy + R^2\,d\Omega^2\ . \tag{A.18}$$

Now, comparing (A.18) with (A.9) it is clear that

$$B = \frac{R_y}{\left(\sqrt{1+f}\ \mp\sqrt{\frac{2M}{R} + f + \frac{\Lambda R^2}{3}}\right)} = -t_y\,e^{\sigma} = e^{\lambda/2}\ ,$$

$$A = e^{\sigma} t_w \ , \qquad \frac{t_y}{t_w} = -\frac{B}{A} \ . \tag{A.19}$$

Similarly, by transforming M_y we obtain

$$M_y = \dot{M}\, t_y + M'\, r_y = M' - \frac{\dot{M}\, R'}{e^{\sigma}\sqrt{1+f}} \tag{A.20}$$

Since $\dot{M} = M_w/t_w$, we use (A.5), (A.17) to substitute for M', and R',

$$M_y = \frac{\kappa\rho W R^2 R_y}{2\left(\sqrt{1+f} \ \mp \sqrt{\frac{2M}{R} + f + \frac{\Lambda R^2}{3}}\right)} - \frac{(M_w/t_w e^{\sigma})\, R_y}{\left(\sqrt{1+f} \ \mp \sqrt{\frac{2M}{R} + f + \frac{\Lambda R^2}{3}}\right)} \ , \tag{A.21}$$

and therefore, rearranging this equation, the mass density is

$$\kappa\rho = \frac{2M_y}{C^2 BW} + \frac{2M_w}{C^2 AW} \ , \tag{A.22}$$

which is in agreement with (4.28). On the other hand, M_w transform as

$$M_w = \dot{M}\, t_w + M'\, r_w = \dot{M}\, t_w \ , \tag{A.23}$$

Using (A.6) and (A.15) this leads to

$$M_w = -\frac{\kappa p}{2} R^2\, \dot{R}\, t_w = -\frac{\kappa p}{2} R^2\, R_w \ , \tag{A.24}$$

which can be arranged for p, so that

$$\kappa p = -\frac{2M_w}{R^2\, R_w} \ . \tag{A.25}$$

Again this exactly as (4.24). On the other hand the λ transformation is given by the following:

$$\lambda_w = \dot{\lambda}\, t_w + \lambda'\, r_w = \dot{\lambda}\, t_w + 0 \ , \tag{A.26}$$

and substituting the value of $\dot{\lambda}$ from (A.7), this is

$$\lambda_w = -\frac{2\dot{\rho} t_w}{(\rho + p)} - \frac{4\dot{R} t_w}{R} \ . \tag{A.27}$$

Since $\rho_w = \dot{\rho} t_w$ and $R_w = \dot{R} t_w$, we arrive at

$$\lambda_w = -\frac{2\rho_w}{(\rho + p)} - \frac{4R_w}{R} \ . \tag{A.28}$$

differentiate B in (A.19) we get

$$B_w = -\frac{\rho_w}{(\rho + p)} - \frac{2R_w}{R} \ . \tag{A.29}$$

which is the same as (4.14). The σ' transformation can be obtained as follows

$$\sigma_y = \dot{\sigma}\, t_y + \sigma' = \dot{\sigma}\, t_y - \frac{p'}{(\rho + p)} \ , \tag{A.30}$$

where (A.8) has been used to substitute for the value of σ'. Since $p' = p_y - \dot{p} t_y$ therefore,

$$\begin{aligned} \sigma_y &= \dot{\sigma}\, t_y - \frac{p_y}{(\rho + p)} + \frac{\dot{p} t_y}{(\rho + p)} \ , \\ &= \sigma_w \frac{t_y}{t_w} - \frac{p_y}{(\rho + p)} + \frac{p_w}{(\rho + p)} \frac{t_y}{t_w} \ . \end{aligned} \tag{A.31}$$

Using (A.19) gives

$$\sigma_y A + \sigma_w B = -\frac{B p_w + p_y A}{(\rho + p)} \ , \tag{A.32}$$

Using (A.19) integrability condition $(t_w)_y = (t_y)_w$ gives

$$A_y - \sigma_y A = -B_w + \sigma_w$$

Then the left hand side of equation (A.32) can be replaced by

$$A_y + B_w = -\frac{B p_w}{(\rho + p)} - \frac{p_y A}{(\rho + p)} \ . \tag{A.33}$$

which is the same as (4.10).

Finally, using (A.19) the matter tensor transforms to

$$\tilde{T}^{ab} = T^{cd} \, (J^{-1})^a_c \, (J^{-1})^b_d = \begin{pmatrix} \rho/A^2 + p/A^2 & p/A\,B & 0 & 0 \\ p/A\,B & p/B^2 & 0 & 0 \\ 0 & 0 & p/R^2 & 0 \\ 0 & 0 & 0 & p/R^2\, sin^2\theta \end{pmatrix} \ , \tag{A.34}$$

and

$$\tilde{T}_{ab} = T_{cd} \, J^c_a \, J^d_b = \begin{pmatrix} \rho\, A^2 & \rho\, A\, B & 0 & 0 \\ \rho\, A\, B & \rho\, B^2 + p\, B & 0 & 0 \\ 0 & 0 & p\, R^2 & 0 \\ 0 & 0 & 0 & p\, R^2 \sin^2\theta \end{pmatrix} \ . \tag{A.35}$$

Appendix B

The Near-Maximum Series for A barotropic equation of state on the PNC

As working with a general equation of state implies a heavy computing load, and in order to test the near-maximum series solution for a simpler case, we often used a barotropic equation of state $p(\rho) = \chi\rho$ (where χ is the equation of the state parameter). We apply our Taylor series expansion about $z = z_m$, to the system of DEs (5.2), (5.3) and (5.4), and solve them. Writing $\xi = (1 + \chi)$, we obtain the following.

$$\varphi_m = y_1 = \frac{-4C_mC_2\left(1+z_m\right)}{\xi K_m}\ , \tag{B.1}$$

$$\varphi_1 = y_2 = \left(\left\{\frac{K_1}{K_m} - \frac{3}{\left(1+z_m\right)}\right\}C_2 - 3C_3\right)\frac{C_m\left(1+z_m\right)}{\xi K_m}\ , \tag{B.2}$$

$$\begin{aligned}\varphi_2 = y_3 = &\left(\left\{\frac{4K_2}{9K_m} - \frac{K_1^2}{3K_m^2} + \frac{10K_1}{9K_m\left(1+z_m\right)} - \frac{1}{3\left(1+z_m\right)^2}\right\}C_2\right.\\ &\left.+\left\{\frac{K_1}{K_m} - \frac{3}{\left(1+z_m\right)}\right\}\frac{C_3}{2} - \frac{8C_4}{3} - \frac{4C_2^2}{9C_m}\right)\frac{C_m\left(1+z_m\right)}{\xi K_m}\ ,\end{aligned} \tag{B.3}$$

$$\begin{aligned}\varphi_3 = y_4 = &\left(\left\{\frac{K_3}{4K_m} - \frac{K_1K_2}{3K_m^2} + \frac{K_1^3}{8K_m^3} + \frac{7K_2}{12K_m\left(1+z_m\right)} - \frac{11K_1^2}{24K_m^2\left(1+z_m\right)}\right.\right.\\ &\left.+\frac{5K_1}{24K_m\left(1+z_m\right)^2} + \frac{1}{8\left(1+z_m\right)^3}\right\}C_2\\ &+\left\{\frac{K_2}{2K_m} - \frac{3K_1^2}{8K_m^2} + \frac{5K_1}{4K_m\left(1+z_m\right)} - \frac{3}{8\left(1+z_m\right)^2}\right\}C_3 + \left\{\frac{K_1}{K_m} - \frac{3}{1+z_m}\right\}\frac{C_4}{2}\\ &\left.-\frac{5C_5}{2} + \left\{\frac{K_1}{K_m} - \frac{7}{\left(1+z_m\right)}\right\}\frac{C_2^2}{12C_m} - \frac{3C_2C_3}{4C_m}\right)\frac{C_m\left(1+z_m\right)}{\xi K_m}\ .\end{aligned} \tag{B.4}$$

$$M_m = \left\{1 - \frac{\Lambda C_m^2}{3}\right\}\frac{C_m}{2}\ , \tag{B.5}$$

$$M_1 = M_1 \ , \qquad \text{i.e. undetermined} \tag{B.6}$$

$$M_2 = \left\{ \frac{K_1}{K_m} + \frac{1}{(1+z_m)} \right\} \frac{M_1}{2} - \frac{\lambda_m C_2}{2} + \frac{(\xi-2)\xi K_m^2}{8C_m} \ , \tag{B.7}$$

$$\begin{aligned} M_3 = & \left\{ \frac{K_2}{K_m} + \frac{K_1}{K_m(1+z_m)} - \frac{C_2}{C_m} \right\} \frac{M_1}{3} \\ & - \left\{ \frac{K_1}{K_m} + \frac{1}{(1+z_m)} \right\} \frac{\lambda_m C_2}{4} - \frac{\lambda_m C_3}{4} - \frac{(2-\xi)\xi K_m K_1}{8C_m} \ , \end{aligned} \tag{B.8}$$

$$\begin{aligned} M_4 = & \left\{ \frac{K_3}{K_m} + \frac{K_2}{K_m(1+z_m)} - \frac{K_1 C_2}{K_m C_m} - \frac{C_3}{C_m} - \frac{C_2}{C_m(1+z_m)} \right\} \frac{M_1}{4} \\ & - \left\{ \frac{5K_1}{36K_m(1+z_m)} + \frac{2K_2}{9K_m} - \frac{K_1^2}{24K_m^2} - \frac{C_2}{18C_m} - \frac{1}{24(1+z_m)^2} \right\} \lambda_m C_2 \\ & - \left\{ \left(\frac{K_1}{K_m} + \frac{1}{(1+z_m)} \right) \frac{C_3}{8} + \frac{C_4}{6} \right\} \lambda_m \\ & + \left\{ \frac{K_1^2}{32} + \frac{K_2 K_m}{12} + \frac{K_m^2}{96(1+z_m)^2} - \frac{K_m^2 C_2}{24} \right\} \frac{(2-\xi)\xi}{C_m} \ . \end{aligned} \tag{B.9}$$

and

$$W_m = \frac{M_1}{\xi K_m} \ , \tag{B.10}$$

$$W_1 = \frac{2M_1}{\xi K_m(1+z_m)} - \frac{2\lambda_m C_2}{\xi K_m} - \frac{K_m}{2C_m} \ , \tag{B.11}$$

$$W_2 = -\frac{2C_2 M_1}{\xi C_m K_m} + \left\{ \frac{K_1}{2K_m} - \frac{3}{2(1+z_m)} \right\} \frac{\lambda_m C_2}{\xi K_m} - \frac{3\lambda_m C_3}{2\xi K_m} - \frac{K_1}{4C_m} + \frac{(\xi-1)K_m}{4(1+z_m)C_m} \ , \tag{B.12}$$

$$\begin{aligned} W_3 = & -\left\{ C_3 + \frac{C_2}{(1+z_m)} \right\} \frac{M_1}{\xi C_m K_m} \\ & + \left\{ \frac{4C_2}{9C_m} + \frac{2K_2}{9K_m} - \frac{K_1^2}{6K_m^2} + \frac{7K_1}{18K_m(1+z_m)} + \frac{1}{3(1+z_m)^2} \right\} \frac{\lambda_m C_2}{\xi K_m} \\ & + \left\{ \frac{K_1 C_3}{2K_m} - \frac{C_3}{(1+z_m)} - \frac{4C_4}{3} \right\} \frac{\lambda_m}{\xi K_m} - \frac{K_2}{6C_m} \\ & + \frac{(\xi-1)K_1}{12C_m(1+z_m)} - \frac{4C_2^2}{3\xi C_m K m} - \frac{(\xi-3)C_2 K m}{6C_m^2} - \frac{(2\xi-1)K_m}{12C_m(1+z_m)^2} \ . \end{aligned} \tag{B.13}$$

Where $\xi = (1+w)$. The density coefficients near the maximum are

$$\hat{\rho}_m = -\frac{\xi K_m^2}{4 C_m^3 C_2} \ , \tag{B.14}$$

$$\hat{\rho}_1 = \left\{ \frac{3C_3}{C_2} - \frac{3K_1}{K_m} + \frac{1}{(1+z_m)} \right\} \frac{\xi K_m^2}{8C_2 C_m^3} \ ,$$

$$\hat{\rho}_2 = \left\{ -\frac{C_4}{2} - \frac{9C_3^2}{16C_2} + \left(\frac{9K_1}{K_m} - \frac{3}{(1+z_m)} \right) \frac{C_3}{16} \right.$$

$$+\frac{7C_2^2}{12C_m}+\left(-\frac{K_1^2}{8K_m^2}+\frac{K_1}{6K_m\left(1+z_m\right)}-\frac{K_2}{3K_m^2}-\frac{1}{8\left(1+z_m\right)^2}\right)C_2\Bigg\}\frac{\xi K_m}{C_m^3C_2}\ . \quad \text{(B.15)}$$

Appendix C

Artificial Data Generation Models

The artificial data used in the thesis was generated by Matlab, written for other purposes by C Hellaby. The datasets consist of tables of $(z, \hat{R}, \kappa\mu n)$ values at z intervals of 0.001, starting at $z = 0.0005$. They are all generated from LT models (which have zero pressure), because the L version of the PNC data generation program is not yet complete. Each of the 3 arbitrary functions M, f and a, was given definitions 'A', 'B', 'C', etc, and the functional form of each definition sometimes allowed a few free parameters. Below we describe just the models used.

`AAA1` This is an FLRW model with $H_0 = 0.72$, $q_0 = 0.22$, $\Omega_\Lambda = 0$.

`AAA8` This is a highly inhomogeneous model; M/r^3 varies from high to low to high; f/r^2 increases from negative to positive; a decreases gently. At the origin, the behaviour is that of an FLRW model with $H_0 = 0.72$, $\Omega_\Lambda = 0$, $q_0 = 0.6$.

`ACA1` This is an inhomogeneous model in which only the geometry/energy function f is inhomogeneous, while M and a are similar to their FLRW forms. Here f/r^2 drop rapidly from zero, and then approaches a constant value. At the origin, the behaviour is that of an FLRW model with $H_0 = 0.72$, $\Omega_\Lambda = 0$, $q_0 = 0.52$.